



Cite this: *Phys. Chem. Chem. Phys.*,  
2018, 20, 5435

# Untangling the methane chemistry in interstellar and solar system ices toward ionizing radiation: a combined infrared and reflectron time-of-flight analysis†

Matthew J. Abplanalp,<sup>ab</sup> Brant M. Jones<sup>ab</sup> and Ralf I. Kaiser<sup>id</sup> \*<sup>ab</sup>

Pure methane (CH<sub>4</sub>/CD<sub>4</sub>) ices were exposed to three ionizing radiation sources at 5.5 K under ultrahigh vacuum conditions to compare the complex hydrocarbon spectrum produced across several interstellar environments. These irradiation sources consisted of energetic electrons to simulate secondary electrons formed in the track of galactic cosmic rays (GCRs), Lyman α (10.2 eV; 121.6 nm) photons simulated the internal VUV field in a dense cloud, and broadband (112.7–169.8 nm; 11.0–7.3 eV) photons which mimic the interstellar ultra-violet field. The *in situ* chemical evolution of the ices was monitored *via* Fourier transform infrared spectroscopy (FTIR) and during heating *via* mass spectrometry utilizing a quadrupole mass spectrometer with an electron impact ionization source (EI-QMS) and a reflectron time-of-flight mass spectrometer with a photoionization source (PI-ReTOF-MS). The FTIR analysis detected six small hydrocarbon products from the three different irradiation sources: propane [C<sub>3</sub>H<sub>8</sub>(C<sub>3</sub>D<sub>8</sub>)], ethane [C<sub>2</sub>H<sub>6</sub>(C<sub>2</sub>D<sub>6</sub>)], the ethyl radical [C<sub>2</sub>H<sub>5</sub>(C<sub>2</sub>D<sub>5</sub>)], ethylene [C<sub>2</sub>H<sub>4</sub>(C<sub>2</sub>D<sub>4</sub>)], acetylene [C<sub>2</sub>H<sub>2</sub>(C<sub>2</sub>D<sub>2</sub>)], and the methyl radical [CH<sub>3</sub>(CD<sub>3</sub>)]. The sensitive PI-ReTOF-MS analysis identified a complex array of products with different products being detected between experiments with general formulae: C<sub>n</sub>H<sub>2n+2</sub> (*n* = 4–8), C<sub>n</sub>H<sub>2n</sub> (*n* = 3–9), C<sub>n</sub>H<sub>2n–2</sub> (*n* = 3–9), C<sub>n</sub>H<sub>2n–4</sub> (*n* = 4–9), and C<sub>n</sub>H<sub>2n–6</sub> (*n* = 6–7) from electron irradiation and C<sub>n</sub>H<sub>2n+2</sub> (*n* = 4–8), C<sub>n</sub>H<sub>2n</sub> (*n* = 3–10), C<sub>n</sub>H<sub>2n–2</sub> (*n* = 3–11), C<sub>n</sub>H<sub>2n–4</sub> (*n* = 4–11), C<sub>n</sub>H<sub>2n–6</sub> (*n* = 5–11), and C<sub>n</sub>H<sub>2n–8</sub> (*n* = 6–11) from broadband photolysis and Lyman α photolysis. These experiments show that even the simplest hydrocarbon can produce important complex hydrocarbons such as C<sub>3</sub>H<sub>4</sub> and C<sub>4</sub>H<sub>6</sub> isomers. Distinct isomers from these groups have been shown to be important reactants in the synthesis of polycyclic aromatic hydrocarbons like indene (C<sub>9</sub>H<sub>8</sub>) and naphthalene (C<sub>10</sub>H<sub>8</sub>) under interstellar conditions.

Received 29th August 2017,  
Accepted 26th September 2017

DOI: 10.1039/c7cp05882a

rsc.li/pccp

## 1. Introduction

The New Horizons Mission to Pluto confirmed the presence of methane – along with molecular nitrogen – as a major constituent on Pluto's surface.<sup>1–7</sup> The relatively volatile ice constituents, including methane, of Pluto play a major role in Pluto's geological processes<sup>8,9</sup> as Pluto likely carries complex molecules such as polycyclic aromatic hydrocarbons (PAHs), which accumulate at the poles from seasonal cycling of methane on the surface.<sup>7,10–14</sup> Also, Makemake – the largest known Kuiper Belt Object (KBO) after Pluto – has the most methane-dominated spectrum.<sup>15–18</sup>

Charon, a moon of Pluto, has been proposed as a possible sink for methane escaping Pluto's atmosphere that can be photolyzed to produce complex molecules up to PAHs that are less volatile and deposit on the moon's surface.<sup>7,10,19</sup> Methane has further been tentatively detected throughout our solar system on Earth's moon<sup>20</sup> and Mars,<sup>21</sup> as well as on small bodies such as Orcus,<sup>22–24</sup> Triton,<sup>2,25–29</sup> 2007 OR10,<sup>30</sup> Eris,<sup>1,2,31</sup> Quaoar,<sup>32–34</sup> Sedna,<sup>35</sup> and Titan.<sup>36</sup> Mixed methane and ethane lakes are also likely to be present on Titan.<sup>37</sup> It was suggested that ice clouds containing methane may also be present on Uranus and Neptune.<sup>38</sup> Comets have also been identified having methane as a constituent including C/1996 B2 Hyakutake,<sup>39</sup> C/1995 O1 Hale-Bopp, C/1999 H1 Lee, C/1991 T1 McNaught–Hartley, C/2002 C1 153/P Ikeya–Zhang, C/1994 S4 LINEAR,<sup>40</sup> C/2000 WM1 LINEAR, C/2001 A2 LINEAR,<sup>41</sup> C/2007 N3 Lulin,<sup>42</sup> C/2004 Q2 Machholz,<sup>43</sup> and 2P/Encke.<sup>44</sup> These detections are very important as comets have been thought to be carriers of (part of) the pristine material that was present during our solar system's formation.<sup>45</sup>

<sup>a</sup> W. M. Keck Research Laboratory in Astrochemistry, University of Hawaii at Manoa, Honolulu, Hawaii, HI, 96822, USA. E-mail: ralfk@hawaii.edu

<sup>b</sup> Department of Chemistry, University of Hawaii at Manoa, Honolulu, Hawaii, HI, 96822, USA

† Electronic supplementary information (ESI) available. See DOI: 10.1039/c7cp05882a

Besides our solar system, methane's detection was reported throughout the interstellar medium in the gas phase as well as in its solid form on interstellar grains at fractions of a few per cent; furthermore, non-polar interstellar ices are suggested to have higher methane abundances up to a few tens of percent.<sup>46</sup> The detection of methane in molecular clouds and toward young stellar objects has been repeatedly substantiated.<sup>47–50</sup> In the interstellar medium (ISM), methane (CH<sub>4</sub>), the simplest saturated hydrocarbon, has been suggested to form on dust grains *via* hydrogen atom addition to carbon atoms.<sup>51</sup> Interstellar ices typically consist of water (H<sub>2</sub>O) as the main constituent with smaller fractions of carbon monoxide (CO), carbon dioxide (CO<sub>2</sub>), methanol (CH<sub>3</sub>OH), and methane (CH<sub>4</sub>) with abundances of the latter of up to 11% of water.<sup>50</sup>

These distinct, methane-carrying environments are exposed to a complex array of ionizing radiation, such as ultraviolet photons mainly in the form of Lyman  $\alpha$  (10.2 eV) and charged particles from the solar wind or in the form of galactic cosmic rays (GCRs), which are able to chemically modify the methane ices. In the ISM these ices are processed by GCRs (98% protons; 2%  $\alpha$ -particles), which have kinetic energies as high as GeV.<sup>52</sup> Furthermore, GCRs are able to produce an internal ultraviolet radiation field as they penetrate deep into molecular clouds, producing a flux of  $10^3$  photons cm<sup>-2</sup> s<sup>-1</sup>.<sup>53</sup> The processing of these ices produces complex species starting from simple ices.

Laboratory processing of pure methane ices has been studied by several groups over the last few years. High energy experiments using  $\gamma$ -rays were among the very first investigations of methane irradiation. Previous experiments used a cobalt-60  $\gamma$ -ray source to irradiate pure methane at 4.2 K and analyzed the ice exploiting electron spin resonance (ESR) to detect methyl radicals (CH<sub>3</sub>) and hydrogen atoms in nearly equivalent ratios;<sup>54</sup> further this detection was confirmed by several other studies.<sup>55–58</sup> Solid methane was also irradiated at 77 K utilizing cobalt-60  $\gamma$ -rays and detected products, as large as heptane (C<sub>7</sub>H<sub>16</sub>), using gas chromatography.<sup>59</sup> Four of these products matched calibrations of straight chain hydrocarbons of propane, butane, hexane, and heptane. However, the authors were unsure if these products were truly formed in the solid methane or in the gas above the methane sample. Also, they suggested the rapid 'polymerization' of the solid methane by the detection of 'viscous oil' that could have only formed from the solid methane. The oil was determined to contain both saturated straight-chain and branched hydrocarbons with a typical length of 20 carbon atoms per molecule.<sup>60</sup>

The irradiation of methane with ions has also been previously studied. Previous studies on the irradiation of pure methane ice at 10–15 K with 10–20 MeV protons (H<sup>+</sup>) and helium ions (<sup>3</sup>He<sup>2+</sup>) were performed and detected the production of acetylene (C<sub>2</sub>H<sub>2</sub>), ethylene (C<sub>2</sub>H<sub>4</sub>), ethane (C<sub>2</sub>H<sub>6</sub>), and hydrocarbons up to C<sub>12</sub> during heating of the processed ice *via* a quadrupole mass spectrometer (QMS).<sup>61</sup> These experiments also resulted in a residue forming, which was analyzed with scanning electron microscopy, Rutherford backscattering spectroscopy, elastic recoil detection analysis, infrared spectroscopy in transmission, hydrogen nuclear magnetic resonance, high performance liquid

chromatography, and gas chromatography-mass spectrometry with the detection of long aliphatic and unsaturated hydrocarbons as the primary products including PAHs.<sup>62</sup> Other experiments also used this irradiation source to study the formation of atomic and molecular hydrogen formation *via* Fourier transform infrared spectroscopy (FTIR) as well as QMS from 10–50 K and found that, similar to previously cited experiments, the methyl radical and hydrogen atom were primary products while methane can also decompose to carbene (CH<sub>2</sub>).<sup>63</sup> They also detected an "explosive" desorption of the ice after a dose of 90–145 eV was reached and stated that this may be a non-thermal mechanism to transport molecules from the ice into the gas phase. Another study used the same type of irradiation source to process pure methane at 15–77 K to simulate the effects of solar wind interacting with a comet surface, and found that a residue was formed after subliming the irradiated methane ice.<sup>64</sup> Further experiments also discussed the formation mechanisms of hydrocarbons up to coronene by simulating the interaction of GCRs, *via* 9 MeV  $\alpha$ -particles and 7.3 MeV protons, with solid methane, ethylene, and ethane.<sup>65</sup> These mechanisms were determined to be initiated by collision cascades that resulted in suprathreshold chemistry such as the production of carbon atoms that were not in thermal equilibrium with the rest of their 10 K ice. Other experiments investigated the processing of pure methane ice with 30 keV He<sup>+</sup> ions at 10–20 K using infrared absorption spectroscopy and showed that the optical constants were continually altered by the impinging ions, but that these changes did not alter the energy deposition of the ions.<sup>66</sup> The products identified were ethane, propane (C<sub>3</sub>H<sub>8</sub>), and a polymer-like material that after much processing formed a refractory residue. The irradiation of pure methane with 60 keV Ar<sup>2+</sup> ions at a dose of 7 eV per 16 amu was also performed and detected ethane, propane, ethylene, and acetylene as products *via* FTIR.<sup>67</sup> Another study utilizing Raman spectroscopy irradiated pure methane films with 30 keV He<sup>+</sup> and 60 keV Ar<sup>2+</sup> ions with a final dose of 1000 eV per 16 amu and observed a broad stretch that was assigned to the G and D features of amorphous carbon.<sup>68,69</sup> A similar study utilizing 200 keV Ar<sup>+</sup> and 400 keV Ar<sup>2+</sup> ions to irradiate pure methane ices at a dose up to 310 eV per 16 amu showed the formation of a refractory residue *via* diffuse reflectance measurements in the visible and near-IR.<sup>70</sup> The residue was compared to Centaurs and trans-Neptunian objects.<sup>70</sup> The processing of pure methane ices *via* 1 keV He<sup>+</sup> ions showed that new molecules were formed within the ices, but not in the surface layer, and that these newly formed molecules are formed *via* nuclear collisions in the ice.<sup>71</sup> Ion irradiation of pure methane *via* 220 MeV <sup>16</sup>O<sup>7+</sup> at 15 K showed the formation of the methyl radical, acetylene, ethylene, ethane, and propane with ethane being the primary product, but the carbon budget of these products only accounts for 30–50% of the amount of methane destroyed during irradiation and the authors identify the remaining carbon being incorporated in species they were unable to observe such as PAHs.<sup>72</sup> Recently, pure methane ices were irradiated with a suite of heavy ions (6 MeV <sup>16</sup>O<sup>2+</sup>, 220 MeV <sup>16</sup>O<sup>7+</sup>, 267 MeV <sup>56</sup>Fe<sup>22+</sup>, and 606 MeV <sup>70</sup>Zn<sup>26+</sup>) at 15 K and analysis by mid-IR showed the production of molecules with the form

$C_nH_m$  ( $n = 2-4$ ;  $m = 2n - 2$  to  $2n + 2$ ) as well as the radical species  $CH_3$ ,  $C_2H_3$ , and  $C_2H_5$ .<sup>73</sup> Recently the effect of using 15.7 MeV  $^{16}O^{5+}$  ions to process pure methane ice was investigated and detected ethane, ethylene, acetylene, propane, and butene ( $C_4H_8$ ) as the standard products *via* FTIR.<sup>74</sup> Alternatively to the previously discussed experiments, these authors determined propane to be the primary product from this ion irradiation, but FTIR has limited capabilities when determining small concentration differences.

The irradiation of pure methane ices with energetic electrons has also been studied. Experiments which irradiated pure methane ice at 10 K with 5 keV electrons while monitoring the chemical changes *via* FTIR and QMS observed  $CH_3$ ,  $C_2H_2$ ,  $C_2H_3$ ,  $C_2H_4$ ,  $C_2H_5$ , and  $C_2H_6$  production rates and reaction mechanisms were also quantified.<sup>75</sup> The formation of molecular deuterium from the processing of pure deuterated methane ( $CD_4$ ) ices with 5 keV electrons at 10 K has also been detected.<sup>76</sup> Also, the processing of pure methane ice with 500–3000 eV electrons at 20 K was studied and detected the dehydrogenation of methane to form  $CH_3$ ,  $CH_2$ , and  $CH$  radicals with the only other two products identified as being ethane and acetylene.<sup>77</sup> A recent study presented a brief overview of the products detected utilizing reflectron time-of-flight mass spectrometry from the 5 keV irradiation of pure methane ices ( $CH_4$ ;  $CD_4$ ) at doses up to 12.5 eV per molecule, which consisted of hydrocarbons as large as  $C_{22}$  being formed.<sup>78</sup>

Pure methane ice has also been processed by vacuum ultraviolet (VUV) irradiation by several groups. Experiments on photolyzed pure methane ices with krypton and xenon lamps at 20 K produced ethylene, propane, propylene, *i*-butane, *n*-butane, *i*-pentane, and *n*-pentane.<sup>79</sup> The processing of methane ices *via* a microwave discharge hydrogen flow lamp was also investigated, and the changes in the solid were monitored with FTIR, which formed  $CH_3$ ,  $C_2H_4$ ,  $C_2H_6$ , allene ( $C_3H_4$ ), and  $C_3H_8$ . As well as stretching that was assigned to higher-order volatiles and residue.<sup>80</sup> The lack of assignment of acetylene as a product is interesting here as multiple assignments to a generic alkyne (HCC-R) vibration were given. Another study showed that the irradiation of pure methane with 10.2 eV photons at 12.5 K produced ethane, where the column density became constant after the dose of 20 eV per 16 amu, and propane with no other specific products stated.<sup>66</sup> Other experiments measured the photodestruction cross section of pure methane using the 100–200 nm spectral range of their deuterium lamp, but did not report any new products formed.<sup>81</sup> Another study suggested that the processing of pure methane ice with VUV photons (6.0–11.5 eV) does not result in the production of acetylene, but instead the formation of ethane, ethylene, and larger hydrocarbons that are hydrogen-rich.<sup>82</sup> A more recent study detected  $CH_3$ ,  $C_2H_2$ ,  $C_2H_4$ ,  $C_2H_6$ , and an unidentified feature at  $912\text{ cm}^{-1}$  after 121.6 nm irradiation of pure methane at 3 K.<sup>83</sup> Recently the investigation of this system using laser desorption coupled with time-of-flight mass spectrometry has shown that products such as  $C_2H_x$  ( $x = 2, 4, 6$ ) and  $C_3H_y$  ( $y = 4, 6, 8$ ) are formed<sup>84</sup> as well as some masses that are related to  $C_4$ – $C_7$  compounds but with no species able to be assigned.<sup>85</sup>

As outlined above the number of experiments studying pure methane ices under different conditions relative to the ISM is significant, but the information provided by all of these investigations is far from exhaustive. Although any products from pure methane irradiation will have similar hydrocarbon stretching to the reactant, the majority of the previous experiments relied solely on FTIR spectroscopy to determine products formed from pure methane irradiation. Different chain lengths and degrees of unsaturation of hydrocarbons do shift certain possible product hydrocarbons from the dominating methane reactant infrared stretching, but as FTIR can only truly assign functional groups of these complex hydrocarbons or confirm small molecules it is extremely difficult to confirm even slightly larger hydrocarbons as their functional groups will always overlap with other possible products. Therefore, the product assignment of large hydrocarbons in a pure methane ice irradiation experiment by only FTIR is difficult and very tentative. Typically a complimentary method of product detection, such as QMS, is also utilized to validate the FTIR assignments. The QMS is able to detect the subliming molecules when the products are warmed up and the products' detection *via* the QMS can also be correlated with the change of the FTIR signal to confirm assignments. However, this traditional method, QMS, also has introduced another problem of product assignment with the use of a hard ionization source – typically electron ionization of up to 100 eV – which causes severe fragmentation and limits the product assignments' validity. In fact, in all the previously discussed types of irradiation experiments typically the products were limited to hydrocarbons of  $C_2$ , sometimes  $C_3$ , and extremely rarely larger than  $C_3$  chain lengths.

However, a few of the investigations suggested that the products were much more diverse than previously assigned<sup>65,80,85</sup> and that by using advanced analytical techniques such as photoionization coupled with reflectron time-of-flight mass spectrometry (PI-ReTOF-MS) that the product list is in fact extremely diverse, including hydrocarbons with carbon chains as long as  $C_{22}$ .<sup>78</sup> The PI-ReTOF-MS technique provides product analysis upon sublimation, typically without fragmentation, to analyze the molecular ion of the molecule, which results in a confident product assignment based on the mass-to-charge ratio. Multiple isomers that contribute to one molecular ion signal can be discriminated *via* their ionization energies as the isomers above the photon energy used to ionize the products will not be detectable, and we are able to vary this ionization energy. The product analysis of pure methane ice irradiation *via* PI-ReTOF-MS shows that diverse hydrocarbon chemistry is clearly taking place across multiple forms of processing; in the present manuscript we are providing the very first comparison of the complex products formed from Lyman  $\alpha$  photons, broadband photolysis, and energetic electron irradiated pure methane ices exploiting PI-ReTOF-MS detection of the products.

## 2. Experimental details

The pure methane irradiation experiments were all carried out in a stainless steel chamber under ultra high vacuum (UHV)

conditions with a typical pressure of  $3 \times 10^{-11}$  Torr, which is able to be achieved using magnetically suspended turbo molecular pumps backed by oil free scroll pumps. Within the UHV chamber, a cold head target constructed of oxygen-free high conductivity copper is connected to a UHV-compatible closed cycle helium compressor (Sumitomo Heavy Industries, RDK-415E). Mounted to the cold head, *via* indium foil for thermal conductivity, is a silver substrate which is cooled as low as  $5.0 \pm 0.1$  K. This substrate is able to be translated in the vertical direction as well as rotated  $360^\circ$  utilizing a UHV-compatible bellow (McAllister, BLT106) and a differentially pumped rotary feedthrough (Thermoionics Vacuum Products, RNN-600/FA/MCO), respectively.<sup>86–88</sup> To deposit the methane ice, methane gas (Specialty Gases of America, 99.999%) was directed to the silver substrate using a glass capillary array, which was positioned approximately 30 mm from the substrate, at UHV chamber background pressures of about  $5 \times 10^{-8}$  Torr for several minutes. During this deposition, the thickness was monitored online and *in situ* *via* a HeNe laser ( $\lambda = 632.8$  nm; CVI MellesGriot; 25-LHP-230) which was reflected off of the silver substrate and into a photodiode. By recording the interference pattern that the growing ice produces and knowing the refractive index ( $n$ ) of solid methane,  $n = 1.280 \pm 0.008$ ,<sup>89</sup> the thickness of the ice is able to be determined.<sup>90,91</sup> The thickness of the ice was determined to be  $590 \pm 50$  nm *via* laser interferometry and  $490 \pm 100$  nm by using a modified Lambert–Beer relationship by applying the absorption coefficients  $3.95 \times 10^{-19}$ ,  $1.40 \times 10^{-17}$ ,  $1.29 \times 10^{-20}$ ,  $3.89 \times 10^{-19}$ ,  $8.15 \times 10^{-19}$ , and  $8.76 \times 10^{-20}$  cm molecule<sup>-1</sup> (ref. 89) to the integrated areas of the respective infrared bands at  $2814$  cm<sup>-1</sup> ( $\nu_2 + \nu_4$ ),  $3010$  cm<sup>-1</sup> ( $\nu_3$ ),  $4114$  cm<sup>-1</sup> ( $\nu_2 + 2\nu_4$ ),  $4202$  cm<sup>-1</sup> ( $\nu_1 + \nu_4$ ),  $4301$  cm<sup>-1</sup> ( $\nu_3 + \nu_4$ ), and  $4528$  cm<sup>-1</sup> ( $\nu_2 + \nu_3$ ), which shows agreement within the error bars of each method of thickness determination. To verify assignments of products, both in the solid and gas phase, isotopic ices of D4-methane (CDN Isotopes, 99.9% D) were also investigated. Once the ice has been deposited it is monitored without interruption online and *in situ* before, during, and after irradiation using a FTIR spectrometer (Nicolet 6700) in absorption–reflection–absorption setup at an angle of  $45^\circ$  to the normal of the silver substrate.<sup>92–95</sup> The spectrum is monitored from  $6000$  to  $500$  cm<sup>-1</sup> at a resolution of  $4$  cm<sup>-1</sup> by averaging spectra over 2 minute periods, which resulted in 30 irradiation spectra during an hour-long irradiation experiment with 5 keV electrons. Alternatively, when the methane ice was processed with VUV photons, the infrared spectrum was collected at well-defined intervals as the substrate was oriented normal to the incident photons to minimize reflection (ESI†, Fig. S1).

During the electron irradiation experiment, an area of  $1.0 \pm 0.1$  cm<sup>2</sup> of methane ice was subjected to 5 keV electrons striking at an incidence angle of  $70^\circ$  relative to the surface normal of the substrate for 1 hour with a current of 30 nA.<sup>96</sup> Monte Carlo simulations *via* CASINO 2.42 software<sup>97</sup> determined the average penetration depth of the impinging electrons to be  $410 \pm 20$  nm in methane and  $310 \pm 20$  nm in deuterated methane (Table 1a). Using a density of  $0.47$  g cm<sup>-3</sup> and  $0.68$  g cm<sup>-3</sup> for methane and deuterated methane, respectively, it was determined

that the average energy deposited into the methane ice was  $3.5 \pm 1.1$  eV molecule<sup>-1</sup> of methane and  $4.4 \pm 1.3$  eV molecule<sup>-1</sup> of D4-methane.<sup>98,99</sup> Pure methane ices were also processed using VUV photons solely at Lyman  $\alpha$  (121.6 nm; 10.2 eV) as well as a broadband photolysis (112.7–169.8 nm; 11.0–7.3 eV). These VUV photolysis experiments utilized a 30 W deuterium lamp (McPherson Model 632) coupled to a UHV compatible monochromator (McPherson Model 302UHV), which is equipped with a 1200 grooves per mm grating.<sup>100</sup> In both photolysis experiments the ice surface was aligned normal to the incident photons during irradiation and was irradiated for 115 hours at a constant temperature of  $5.5 \pm 0.1$  K. The Lyman  $\alpha$  processed ice was irradiated with  $7.25 \times 10^{12}$  photons cm<sup>-2</sup> s<sup>-1</sup> while the broadband processed ice was irradiated with  $7.16 \times 10^{13}$  photons cm<sup>-2</sup> s<sup>-1</sup>, which were determined *via* a NIST calibrated photodiode (International Radiation Detectors AXUV-100G). It was calculated, using the same ice parameters as discussed for the electron irradiation, that these photolysis experiments deposited an average energy of  $230 \pm 60$  eV molecule<sup>-1</sup> (Table 1b) and  $150 \pm 20$  eV molecule<sup>-1</sup> (Table 1c) into the broadband and Lyman  $\alpha$  processed methane ices, respectively. The photolysis doses are relatively larger when compared to the electron irradiation experiments as the number of methane molecules processed is smaller due to the limited penetration depth of the Lyman  $\alpha$  photons (120 nm) and broadband photons (55 nm)<sup>66,101</sup> compared to the energetic electrons (410 nm) (Table 1a). The penetration depth of the photons was calculated utilizing the absorption cross section of methane at Lyman  $\alpha$  ( $1.4 \times 10^{-17}$  cm<sup>2</sup>) in the VUV experiment assuming 95% absorption of the impinging photons.<sup>102</sup> The broadband penetration depth was calculated in a similar fashion using the complete VUV absorption spectrum of methane ice and averaging *via* the output measured for the deuterium lamp (ESI†).

Once the irradiation step was completed the ice was then heated at a controlled rate, also known as temperature programmed desorption (TPD), from 5 to 300 K at  $0.5$  K min<sup>-1</sup> while monitoring the subliming molecules with PI-ReTOF-MS and electron-impact QMS (EI-QMS; Extrel-5221). The EI-QMS data were recorded in residual-gas analyzer (RGA) mode using a mass range of 4–500 amu, electron impact energy of 100 eV, and an emission current of 1 mA.<sup>103–105</sup> However, the PI-ReTOF-MS method is also employed, which is a far more sensitive analytical tool than the RGA that is commonly used in astrophysical simulation chambers. Details of the PI-ReTOF-MS setup have been previously described.<sup>78,106</sup> Briefly, this technique utilizes pulsed coherent VUV light at 10.49 eV ( $\lambda = 118.2$  nm) to ionize the subliming molecules during TPD.<sup>107–113</sup> These ions are then detected *via* a modified reflectron time-of-flight mass spectrometer (Jordan TOF Products, Inc.) utilizing a multichannel plate (MCP) in the dual chevron configuration. The ion signals from the MCP were then amplified *via* a fast pre-amplifier (Ortec 9305) and shaped with a 100 MHz discriminator (Advanced Research Instruments Corporation; F-100TD). Finally, the signals are then recorded by a computer based multichannel scaler (FAST ComTec, P7888-1 E) in 4 ns bins that are triggered at 30 Hz *via* a pulse delay generator (Quantum Composers 9518). The software is

**Table 1** (a) Data applied to calculate the average dose per molecule in the methane (CH<sub>4</sub>) and D4-methane (CD<sub>4</sub>) ice. (b) Data applied to calculate the broadband dose per molecule in the methane (CH<sub>4</sub>) ice. (c) Data applied to calculate the Lyman  $\alpha$  dose per molecule in the methane (CH<sub>4</sub>) ice

(a)	CH <sub>4</sub>	CD <sub>4</sub>
Initial kinetic energy of the electrons, $E_{\text{init}}$	5 keV	5 keV
Irradiation current, $I$	$30 \pm 2$ nA	$30 \pm 2$ nA
Total number of electrons	$(6.7 \pm 0.5) \times 10^{14}$	$(6.7 \pm 0.5) \times 10^{14}$
Average kinetic energy of backscattered electrons, $E_{\text{bs}}^a$	$3.0 \pm 0.3$ keV	$3.0 \pm 0.3$ keV
Fraction of backscattered electrons, $f_{\text{bs}}^a$	$0.27 \pm 0.03$	$0.27 \pm 0.03$
Average kinetic energy of transmitted electrons, $E_{\text{trans}}^a$	$2.0 \pm 0.3$ keV	$1.1 \pm 0.3$ keV
Fraction of transmitted electrons, $f_{\text{trans}}^a$	$0.19 \pm 0.01$	$0.02 \pm 0.01$
Average penetration depth, $l^a$	$410 \pm 20$ nm	$310 \pm 20$ nm
Density of the ice, $\rho$	$0.47 \pm 0.07$ g cm <sup>-3</sup>	$0.68 \pm 0.09$ g cm <sup>-3</sup>
Irradiated area, $A$	$1.0 \pm 0.1$ cm <sup>2</sup>	$1.0 \pm 0.1$ cm <sup>2</sup>
Total molecules processed	$(7.3 \pm 1.2) \times 10^{17}$	$(6.42 \pm 1.2) \times 10^{17}$
Dose per molecule	$3.5 \pm 1.1$ eV	$4.4 \pm 1.3$ eV
(b)		
Photon energies	$7.3\text{--}11.0 \pm 0.1$ eV	
Total photon current	$670 \pm 0.01$ nA	
Total photon fluence	$(2.9 \pm 0.5) \times 10^{19}$ photons cm <sup>-2</sup>	
Ice density	$0.47 \pm 0.07$ g cm <sup>-3</sup>	
Molecular weight	16 amu	
Penetration depth <sup>b</sup>	$55 \pm 10$ nm	
Molecules processed	$(1.7 \pm 0.4) \times 10^{18}$	
Dose per molecule	$230 \pm 60$ eV	
(c)		
Photon energy	$10.20 \pm 0.01$ eV	
Photon current	$81 \pm 1$ nA	
Photon fluence	$(3.0 \pm 0.2) \times 10^{18}$ photons cm <sup>-2</sup>	
Ice density	$0.47 \pm 0.07$ g cm <sup>-3</sup>	
Molecular weight	16 amu	
Penetration depth <sup>c</sup>	$120 \pm 20$ nm	
Molecules processed	$(2.1 \pm 0.5) \times 10^{17}$	
Dose per molecule	$150 \pm 20$ eV	

<sup>a</sup> CASINO values. <sup>b</sup> The weighted average penetration depth at which 95% of the energy is absorbed. <sup>c</sup> The penetration depth at which 95% of the photons are absorbed.

optimized so that 3600 sweeps per mass spectrum corresponds to a 1 K increase in the temperature of the substrate.<sup>114–119</sup>

### 3. Results

#### 3.1. Infrared spectroscopy

Multiple new infrared bands were detected utilizing FTIR *in situ* analysis as well the broadening of the reactant methane infrared absorptions suggesting that products may overlap with the reactant spectrum. Infrared absorptions corresponding to the products propane [C<sub>3</sub>H<sub>8</sub>(C<sub>3</sub>D<sub>8</sub>)], ethane [C<sub>2</sub>H<sub>6</sub>(C<sub>2</sub>D<sub>6</sub>)], ethyl radical [C<sub>2</sub>H<sub>5</sub>(C<sub>2</sub>D<sub>5</sub>)], ethylene [C<sub>2</sub>H<sub>4</sub>(C<sub>2</sub>D<sub>4</sub>)], acetylene [C<sub>2</sub>H<sub>2</sub>(C<sub>2</sub>D<sub>2</sub>)], and the methyl radical [CH<sub>3</sub>(CD<sub>3</sub>)] were detected in the electron irradiation experiments as well as both photolysis experiments (Fig. 1 and 2; Table 2). These detections agree well with the previous experiments processing pure methane ice while monitoring changes with FTIR (1. Introduction). Fig. 2 displays the methane FTIR spectrum before and after processing in each experiment showing that several new infrared stretches are clearly visible in the typical hydrocarbon stretching region near 3000 cm<sup>-1</sup>. Although these stretches can be assigned to the above products these stretches are still present, but less

intense, even after their assigned product molecule has been observed to have sublimed *via* mass spectrometry showing that these infrared bands are contributed to by a suite of other complex hydrocarbons.<sup>120,121</sup>

#### 3.2. Mass spectrometry

As a complimentary method to the FTIR analysis the products formed within the processed ices were also monitored with both an RGA as well as PI-ReTOF-MS. Although two mass spectrometry techniques were employed, data analysis of the RGA spectra revealed no additional information that was not already present from the PI-ReTOF-MS data analysis with the exception of the detection of propane in the deuterated methane experiments. In the non-deuterated experiments the corresponding mass-to-charge ratio of propane overlaps with carbon dioxide and, as previously stated, this hard ionization technique leads to extensive fragmentation. Therefore, it is only useful to look at the molecular ions of alkanes as they will not overlap with fragments from other species. Fig. S2 (ESI<sup>†</sup>) displays the integrated RGA profiles for the molecular ions of ethane ( $m/z = 30$ ), propane ( $m/z = 44$ ), and butane ( $m/z = 58$ ) in each experiment during the TPD phase as well as the C<sub>3</sub>H<sub>7</sub><sup>+</sup> fragment which is associated

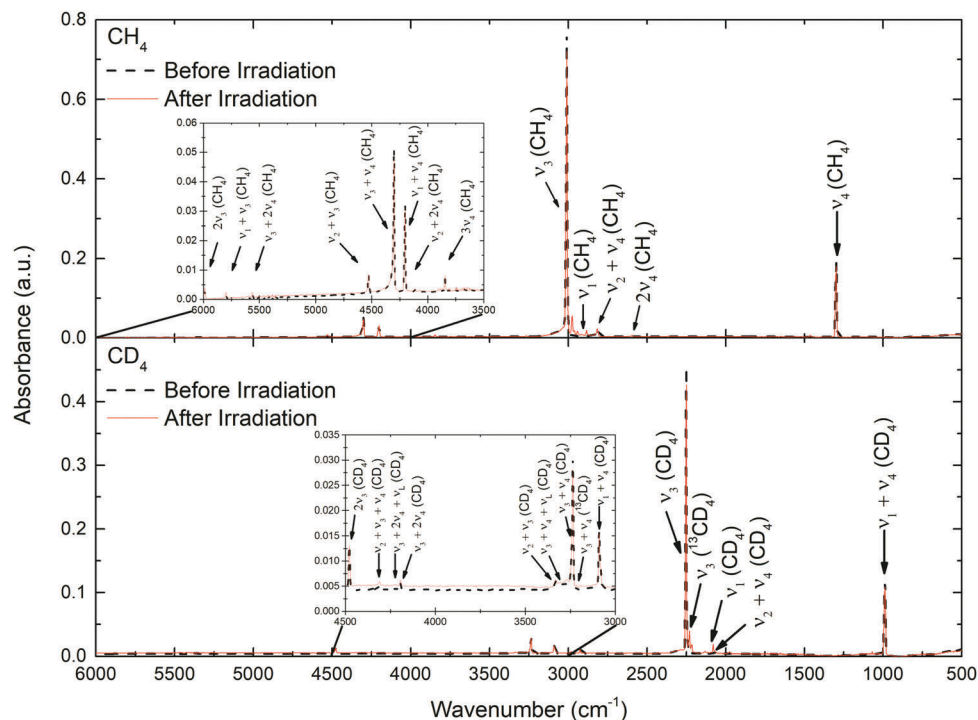


Fig. 1 Infrared spectra from 6000–500  $\text{cm}^{-1}$  for methane ( $\text{CH}_4$ ; top) and D4-methane ( $\text{CD}_4$ ; bottom) ices before (black-dotted) and after (red-solid) the electron irradiation with a zoom of the overtones in the inset box along with assignments (Tables 2a and b).

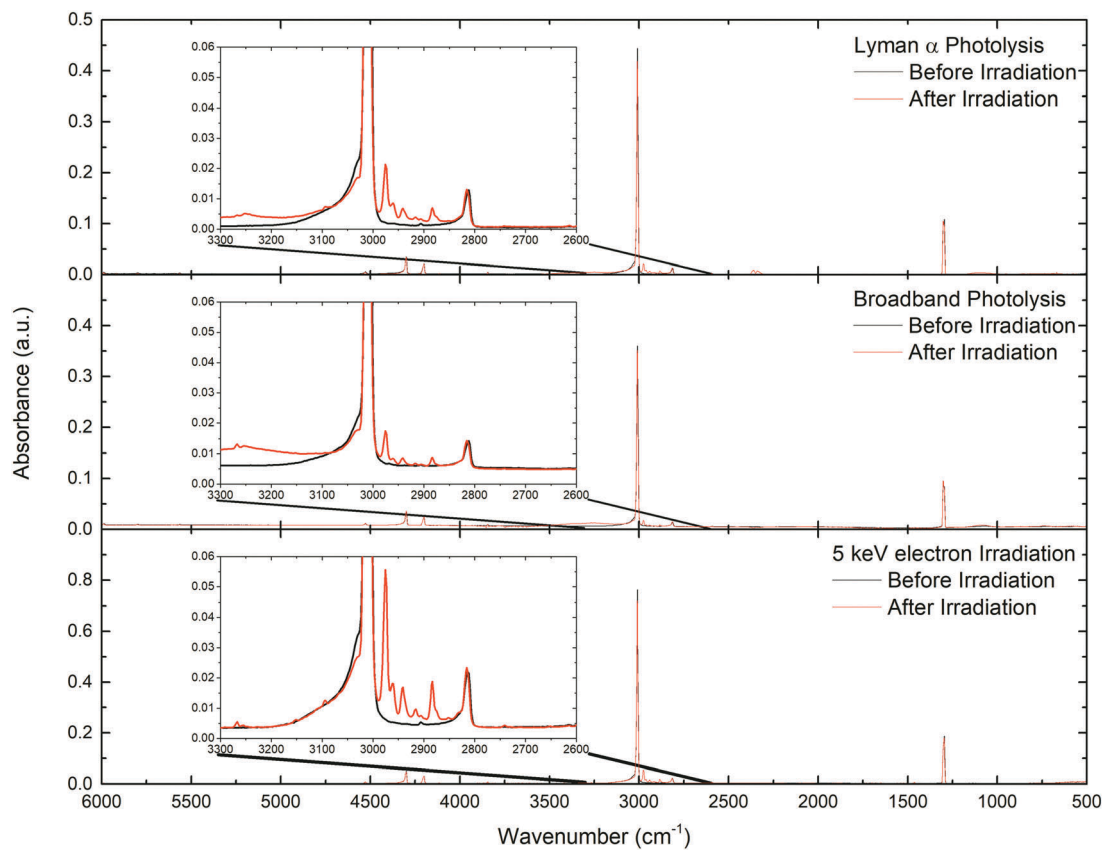


Fig. 2 Infrared spectra from 6000–500  $\text{cm}^{-1}$  for methane ( $\text{CH}_4$ ) ices before (black) and after (red) the (top panel) Lyman  $\alpha$  photolysis, (middle panel) broadband photolysis, and (bottom panel) electron irradiation with a zoom of the primary CH vibration region in the inset box showing multiple new infrared bands at the end of processing before heating (Table 2).



Table 2 (continued)

(b)		Absorptions after irradiation (cm <sup>-1</sup> )		Assignment		Carrier	Ref.
Absorptions before irradiation (cm <sup>-1</sup> )		Absorptions after irradiation (cm <sup>-1</sup> )		Assignment		Carrier	Ref.
		2415		$\nu_3(\text{C}_2\text{D}_2)$		CD stretch	<i>e</i>
		2372		$\nu_3(\text{CD}_3)$		CD stretch	<i>p,s</i>
		2333		$\nu_9(\text{C}_2\text{D}_4)$		CD <sub>2</sub> asymmetric stretch	
2289				$\nu_3 + \nu_4(\text{CD}_4)$		Degenerate stretch	<i>y</i>
2249				$\nu_3(\text{CD}_4)$			
2239				$\nu_3(^{13}\text{CD}_4)$			
		2230		$\nu_{10}(\text{C}_2\text{D}_6)/\nu_{\text{as}}(\text{C}_3\text{D}_8)$		CD <sub>3</sub> degenerate stretch/CD <sub>3</sub> asymmetric stretch	<i>e,u,ac,ad</i>
		2215		$\nu_2 + \nu_6(\text{C}_2\text{D}_6)$		Combination	<i>ad</i>
		2195		$\nu_{11}(\text{C}_2\text{D}_4)$		CD <sub>2</sub> symmetric stretch	<i>p,s</i>
2135				$\nu_1(\text{CHD}_3)$		Combination	<i>u</i>
		2130		$\nu_6 + \nu_{11}(\text{C}_2\text{D}_6)$		CD <sub>3</sub> symmetric stretch	<i>y</i>
		2115		$\nu_8(\text{C}_3\text{D}_8)$		Symmetric stretch	
2092				$\nu_1(\text{CD}_4)$			
2071				$\nu_2 + \nu_4(\text{CD}_4)$		Combination	<i>ab</i>
		2032		$\nu_6 + \nu_9(\text{C}_2\text{D}_6)$			<i>v</i>
		2019		$\nu_8 + \nu_9(\text{C}_2\text{D}_6)$		Combination	<i>v</i>
1975				$2\nu_4(\text{CD}_4)$			<i>ab</i>
1284				$\nu_2(\text{CHD}_3)$		CD <sub>3</sub> degenerate stretch	<i>v</i>
		1070		$\nu_{11}(\text{C}_2\text{D}_6)$		CD <sub>3</sub> symmetric stretch	<i>v</i>
1028				$\nu_6(\text{C}_2\text{D}_6)$			<i>ab</i>
987				$\nu_4(\text{CHD}_3)$			
				$\nu_4(\text{CD}_4)$			
		721		$\nu_7(\text{C}_2\text{D}_4)$		CD <sub>2</sub> wag	<i>e,s</i>

(c)		Absorptions after irradiation intervals (cm <sup>-1</sup> )		Assignment		Carrier	Ref.					
Absorptions before irradiation (cm <sup>-1</sup> )		Absorptions after irradiation intervals (cm <sup>-1</sup> )		Assignment		Carrier	Ref.					
5989, 5789,		34 eV	46 eV	52 eV	84 eV	92 eV	104 eV	150 eV	185 eV	230 eV		
5564, 4528,		—	—	—	—	—	—	—	—	—		
4301, 4202,		—	—	—	—	—	—	—	—	—		
4114, 3844		—	—	—	—	—	—	—	—	—		
—	4164	—	—	—	—	—	—	—	—	—		
—	—	—	—	—	—	—	—	—	—	—		
—	—	3266	—	—	—	3317	—	—	—	—		
—	—	3256	—	—	—	—	—	—	—	—		
—	—	3153	—	—	—	—	—	—	—	—		
—	—	—	—	—	—	—	—	—	—	—		
—	—	—	—	—	—	—	—	—	—	—		
—	—	—	3093	—	—	—	—	—	—	—		
3008	2975	—	—	—	—	—	—	—	—	—		
—	—	—	—	—	—	—	—	—	—	—		
—	—	2961	—	—	—	—	—	—	—	—		

Table 2 (continued)

Absorptions before irradiation (cm <sup>-1</sup> )		Absorptions after irradiation intervals (cm <sup>-1</sup> )										Carrier	Ref.
		34 eV	46 eV	52 eV	84 eV	92 eV	104 eV	150 eV	185 eV	230 eV			
		molecule <sup>-1</sup>	molecule <sup>-1</sup>	molecule <sup>-1</sup>	molecule <sup>-1</sup>	molecule <sup>-1</sup>	molecule <sup>-1</sup>	molecule <sup>-1</sup>	molecule <sup>-1</sup>	molecule <sup>-1</sup>	Assignment		
—	2942	—	—	—	—	—	—	—	—	—	$\nu_8 + \nu_{11}(\text{C}_2\text{H}_6)/\nu_{22}(\text{C}_4\text{H}_{10})$		<i>g</i>
—	2918	—	—	—	—	—	—	—	—	—	$\nu_8 + \nu_{11}(\text{C}_2\text{H}_6)/\nu_5(\text{C}_4\text{H}_8)$		<i>v,w</i>
2905	—	—	2851	—	—	—	—	—	—	—	$\nu_1(\text{CH}_4)$		<i>e,g</i>
—	—	—	—	—	—	—	—	—	—	—	$\nu_5(\text{C}_2\text{H}_6)/\nu_{23}(\text{C}_4\text{H}_{10})$		<i>b,j,x</i>
2814	—	—	—	—	—	2744	—	—	—	—	$\nu_2 + \nu_4 + \nu_{12}(\text{C}_2\text{H}_6)$		<i>g</i>
—	—	—	—	—	—	—	—	—	—	2651	$\nu_2 + \nu_4 + \nu_{12}(\text{C}_2\text{H}_6)$		<i>e,g</i>
—	—	—	—	—	—	—	—	—	—	—	$\nu_2 + \nu_6(\text{C}_2\text{H}_6)$		<i>g,j</i>
—	—	—	—	—	—	—	—	—	—	—	$\nu_6 + \nu_{12}(\text{C}_2\text{H}_4)/\nu_8 + \nu_{12}(\text{C}_2\text{H}_6)$		<i>g,p</i>
2591	—	—	—	—	—	—	—	—	—	—	$2\nu_4(\text{CH}_4)$		<i>a</i>
1297	—	—	—	—	—	—	—	—	—	—	$\nu_4(\text{CH}_4)$		<i>g,x</i>
—	—	—	—	—	—	—	—	—	—	950	$\nu_7(\text{C}_2\text{H}_4)$		<i>n,p,s</i>
—	—	—	—	—	—	821	—	—	—	—	$\nu_{10}(\text{C}_2\text{H}_4)$		<i>l,n,p,s,t</i>
—	—	—	—	—	—	—	—	—	—	—	$\nu_2(\text{CH}_3)$		<i>a,e,f,w</i>

Absorptions before irradiation (cm <sup>-1</sup> )		Absorptions after irradiation intervals (cm <sup>-1</sup> )										Carrier	Ref.
		24 eV	30 eV	33 eV	34 eV	55 eV	61 eV	86 eV	119 eV	146 eV			
		molecule <sup>-1</sup>	molecule <sup>-1</sup>	molecule <sup>-1</sup>	molecule <sup>-1</sup>	molecule <sup>-1</sup>	molecule <sup>-1</sup>	molecule <sup>-1</sup>	molecule <sup>-1</sup>	molecule <sup>-1</sup>	Assignment		
5989, 5789, 5564, 4528, 4301, 4202, 4114, 3844	—	—	—	—	—	—	—	—	—	—	$2\nu_3, \nu_1 + \nu_3, \nu_3 + 2\nu_4, \nu_2 + \nu_3, \nu_3 + \nu_4, \nu_1 + \nu_4, \nu_2 + 2\nu_4, 3\nu_4(\text{CH}_4)$		<i>a,b</i>
—	4164	—	—	—	—	—	—	—	—	—	$\nu_7 + \nu_{12}(\text{C}_2\text{H}_6)$		<i>c</i>
—	—	—	—	—	—	—	—	—	—	—	$\nu_3 + \nu_4 + \nu_5(\text{C}_2\text{H}_2)$		<i>d</i>
—	—	3266	—	—	—	—	3317	—	—	—	$\nu_3(\text{C}_2\text{H}_2)$		<i>e,f</i>
—	—	3256	—	—	—	—	—	—	—	—	$\nu_4 + \nu_7(\text{C}_2\text{H}_6)$		<i>g</i>
—	3153	—	—	—	—	—	—	—	—	—	$\nu_3(\text{CH}_3)$		<i>e,h,i</i>
—	—	—	—	—	—	3108	—	—	—	—	$\nu_{10}(\text{C}_2\text{H}_5)$		<i>j,k</i>
—	—	—	—	—	—	—	—	—	—	—	$\nu_9(\text{C}_2\text{H}_4)$		<i>l,m,n,o,p</i>
—	—	—	—	—	—	—	—	—	—	—	$\nu_3(\text{CH}_4)$		<i>a,e,g,r</i>
3008	—	—	—	—	—	—	—	—	—	—	$\nu_{11}(\text{C}_2\text{H}_4)/\nu_{10}(\text{C}_2\text{H}_6)$		<i>l,n,p,s,t,u</i>
—	2975	—	—	—	—	—	—	—	—	—	$\nu_{4s}(\text{C}_3\text{H}_8)$		
—	—	—	—	—	—	—	—	—	—	—	stretch/ $\text{CH}_3$ asymmetric stretch		
—	—	—	—	—	—	—	—	—	—	—	Degenerate stretch		
—	—	—	—	—	—	—	—	—	—	—	$\text{CH}_2$ symmetric stretch/ $\text{CH}_3$ degenerate stretch/ $\text{CH}_3$ asymmetric stretch		
—	—	—	—	—	—	—	—	—	—	—	$\nu_1(\text{C}_2\text{H}_6)/\nu_8(\text{C}_3\text{H}_8)$		<i>u,v</i>
—	2691	—	—	—	—	—	—	—	—	—	$\nu_6 + \nu_{11}(\text{C}_2\text{H}_6)$		<i>g</i>
—	2942	—	—	—	—	—	—	—	—	—	$\nu_{22}(\text{C}_4\text{H}_{10})$		
—	—	—	—	—	—	—	—	—	—	—	$\nu_8 + \nu_{11}(\text{C}_2\text{H}_6)$		<i>v,w</i>
—	2918	—	—	—	—	—	—	—	—	—	$\nu_5(\text{C}_4\text{H}_8)$		
—	—	—	—	—	—	—	—	—	—	—	$\nu_1(\text{CH}_4)$		<i>e,g</i>

Table 2 (continued)

Absorptions before irradiation (cm <sup>-1</sup> )	Absorptions after irradiation intervals (cm <sup>-1</sup> )								Assignment	Carrier	Ref.		
	8 eV	24 eV	30 eV	33 eV	34 eV	55 eV	61 eV	86 eV				119 eV	146 eV
—	—	—	2851	—	—	—	—	—	—	—	1/5(C <sub>2</sub> H <sub>6</sub> )/1/23(C <sub>3</sub> H <sub>10</sub> ) 1/2 + 1/4 + 1/12(C <sub>2</sub> H <sub>6</sub> ) Combination	CH <sub>3</sub> symmetric stretch Combination Combination	<i>b,j,x</i> <i>g</i>
2814	2744	—	2652	—	—	—	—	—	—	—	1/2 + 1/4(C <sub>2</sub> H <sub>4</sub> ) 1/2 + 1/6(C <sub>2</sub> H <sub>6</sub> ) Combination	Combination	<i>g,j</i>
—	—	—	—	—	—	—	—	—	—	—	1/6 + 1/12(C <sub>2</sub> H <sub>4</sub> )/1/8 + 1/12(C <sub>2</sub> H <sub>6</sub> ) 2 1/4(C <sub>2</sub> H <sub>4</sub> ) 1/4(CH <sub>4</sub> ) Overtone	Combinations	<i>g,p</i>
2591	—	—	—	—	—	—	—	—	—	—	1/7(C <sub>2</sub> H <sub>4</sub> ) 1/10(C <sub>2</sub> H <sub>4</sub> ) 1/12(C <sub>2</sub> H <sub>6</sub> ) 1/2(CH <sub>3</sub> ) Degenerate deformation	Out of plane	<i>a</i> <i>q,x</i>
1297	—	950	—	—	—	—	—	—	—	—	1/7(C <sub>2</sub> H <sub>4</sub> ) 1/10(C <sub>2</sub> H <sub>4</sub> ) 1/12(C <sub>2</sub> H <sub>6</sub> ) 608	CH <sub>2</sub> wag CH <sub>2</sub> rock CH <sub>3</sub> rock	<i>n,p,s</i> <i>l,n,p,s,t</i> <i>a,g,j,n</i> <i>a,e,f,w</i>

<sup>a</sup> Bennett *et al.* (2006).<sup>75</sup> <sup>b</sup> Emnis *et al.* (2011).<sup>188</sup> <sup>c</sup> Herman (1998).<sup>189</sup> <sup>d</sup> Wu *et al.* (2014).<sup>190</sup> <sup>e</sup> Kaiser and Roessler (1998).<sup>65</sup> <sup>f</sup> Moore and Hudson (2003).<sup>176</sup> <sup>g</sup> Hepp and Herman (1999).<sup>191</sup> <sup>h</sup> Shelson (1970).<sup>192</sup> <sup>i</sup> Wormhoudt and McCurdy (1989).<sup>193</sup> <sup>j</sup> Kim *et al.* (2010).<sup>164</sup> <sup>k</sup> Pacansky and Dupuis (1982).<sup>194</sup> <sup>l</sup> Brecher and Halford (1961).<sup>195</sup> <sup>m</sup> Brock *et al.* (1994).<sup>196</sup> <sup>n</sup> Comeford and Gould (1961).<sup>197</sup> <sup>o</sup> Hudson *et al.* (2014).<sup>198</sup> <sup>p</sup> Jacox (1962).<sup>99</sup> <sup>q</sup> Chapados and Cabana (1972).<sup>200</sup> <sup>r</sup> Gerakines and Hudson (2015).<sup>89</sup> <sup>s</sup> Dows (1962).<sup>201</sup> <sup>t</sup> Rytter and Gruen (1979).<sup>202</sup> <sup>u</sup> Schachtschneider and Snyder (1963).<sup>203</sup> <sup>v</sup> Abplanalp and Kaiser (2016).<sup>121</sup> <sup>w</sup> Gerakines *et al.* (1996).<sup>80</sup> <sup>x</sup> Kondo and Saeki (1973).<sup>204</sup> <sup>y</sup> Kaiser *et al.* (2014).<sup>91</sup> <sup>z</sup> He *et al.* (2010).<sup>76</sup> <sup>aa</sup> Calvani *et al.* (1994).<sup>205</sup> <sup>ab</sup> Momose *et al.* (2004).<sup>206</sup> <sup>ac</sup> Bell *et al.* (2000).<sup>207</sup> <sup>ad</sup> Tejada and Eggers (1976).<sup>208</sup> Note: once a peak was detected it remained detectable through the end of irradiation, while a – means there was nothing detected at that dose.

with propane and butane *via* a hydrogen loss and a methyl group (CH<sub>3</sub>) loss from the molecular ion, respectively (ESI<sup>+</sup>). The sublimation of ethane is identical in all experiments peaking at 58 K. Propane's mass-to-charge ratio overlaps with that of carbon dioxide (CO<sub>2</sub>; *m/z* 44) which explains the much higher background when compared to the deuterated experiment which shifts the propane molecular ion to *m/z* = 52. The ion signal for propane is slightly above the CO<sub>2</sub> background in the electron irradiation experiment, but no such signal is visible in either photolysis experiment. However, the shifted mass-to-charge ratio of deuterated propane shows a clear signal in the RGA. To further investigate and confirm the presence of propane its fragment C<sub>3</sub>H<sub>7</sub><sup>+</sup>/C<sub>3</sub>D<sub>7</sub><sup>+</sup> was also analyzed and detected in both the deuterated and non-deuterated electron irradiation experiments. However, these ion signals displayed a bimodal structure where the first peak could be correlated to the sublimation of propane at 71 K while the second peak was attributed to the fragmentation of subliming butane at 89 K. The Lyman  $\alpha$  photolysis data showed a tentative peak corresponding to C<sub>3</sub>H<sub>7</sub><sup>+</sup> which could have been due to propane or butane. The broadband photolysis data displayed no signal at *m/z* = 43 for this fragment. Finally, the molecular ion of butane was tentatively detected in the non-deuterated electron irradiation experiment but not observed in any other experiment most likely due to fragmentation caused by the ionization source of the RGA. Although the RGA was not able to clearly detect the molecular ion of butane this alkane was detected in all of the PI-ReTOF-MS studies. PI-ReTOF-MS is not able to detect propane when using an ionization source of 10.49 eV as it has an ionization energy (I.E.) of 10.95  $\pm$  0.5 eV.<sup>122</sup> Propane was the only additional molecule confirmed *via* RGA (ESI<sup>+</sup>, Fig. S2), and the following is a summary of the PI-ReTOF-MS data analysis (Tables 3a–c; Fig. 3–15 and Fig. S3–S12, ESI<sup>+</sup>). Fig. 3 depicts the ion signals as a function of temperature for each experiment with mass-to-charge ratios approaching *m/z* = 150 in each system and upon further analysis showed hitherto previously undetected hydrocarbons produced in pure methane ices.

### 3.3. Electron irradiation – PI-ReTOF-MS

The TPD of electron irradiated methane and D<sub>4</sub>-methane ice while monitoring with PI-ReTOF-MS revealed five groups of hydrocarbon products with the general formulae: C<sub>*n*</sub>H<sub>2*n*+2</sub> (*n* = 4–8), C<sub>*n*</sub>H<sub>2*n*</sub> (*n* = 3–9), C<sub>*n*</sub>H<sub>2*n*-2</sub> (*n* = 3–9), C<sub>*n*</sub>H<sub>2*n*-4</sub> (*n* = 4–9), and C<sub>*n*</sub>H<sub>2*n*-6</sub> (*n* = 6–7). By utilizing deuterated methane (CD<sub>4</sub>) the non-deuterated assignments are able to be cross-referenced and confirmed by comparison of mass-to-charge ratio shifts and sublimation profiles between the two methane systems.

**3.3.1. C<sub>*n*</sub>H<sub>2*n*+2</sub>.** The most highly saturated group of hydrocarbons, alkanes C<sub>*n*</sub>H<sub>2*n*+2</sub> (*n* = 4–8), were detected utilizing PI-ReTOF-MS (Fig. 4). According to the FTIR analysis, propane (C<sub>3</sub>H<sub>8</sub>) and ethane (C<sub>2</sub>H<sub>6</sub>) were the only alkane products formed, but this was incorrect as multiple larger alkanes were detected upon sublimation. Using a photoionization energy of 10.49 eV, the smallest alkane ionized was *n*-butane (CH<sub>3</sub>CH<sub>2</sub>CH<sub>2</sub>CH<sub>3</sub>; I.E. = 10.5  $\pm$  0.1 eV). The molecular ion of *n*-butane, *m/z* = 58 (C<sub>4</sub>H<sub>10</sub><sup>+</sup>), was observed to have an onset sublimation temperature

**Table 3** (a) Masses correlated to molecules detected in electron irradiated methane and D4-methane ices at a photoionization energy of 10.49 eV. (b) Masses correlated to molecules detected in each methane ice photolysis experiment utilizing a photoionization energy of 10.49 eV. (c) Compilation of hydrocarbons detected in each hydrocarbon group for distinct radiation sources

(a)			
<i>m/z</i>	CH <sub>4</sub>	CD <sub>4</sub>	<i>m/z</i>
40	C <sub>3</sub> H <sub>4</sub>	C <sub>3</sub> D <sub>4</sub>	44
42	C <sub>3</sub> H <sub>6</sub>	C <sub>3</sub> D <sub>6</sub>	48
43	<sup>13</sup> CC <sub>2</sub> H <sub>6</sub>	<sup>13</sup> CC <sub>2</sub> D <sub>6</sub>	49
52	C <sub>4</sub> H <sub>4</sub>	C <sub>4</sub> D <sub>4</sub>	56
54	C <sub>4</sub> H <sub>6</sub>	C <sub>4</sub> D <sub>6</sub>	60
56	C <sub>4</sub> H <sub>8</sub>	C <sub>4</sub> D <sub>8</sub>	64
57	<sup>13</sup> CC <sub>3</sub> H <sub>8</sub>	<sup>13</sup> CC <sub>3</sub> D <sub>8</sub>	65
58	n.d. <sup>a</sup>	C <sub>4</sub> D <sub>10</sub>	68
65	*C <sub>5</sub> H <sub>5</sub>	n.d.	70
66	C <sub>5</sub> H <sub>6</sub>	C <sub>5</sub> D <sub>6</sub>	72
67	*C <sub>5</sub> H <sub>7</sub>	*C <sub>5</sub> D <sub>7</sub>	74
68	C <sub>5</sub> H <sub>8</sub>	C <sub>5</sub> D <sub>8</sub>	76
69	<sup>13</sup> CC <sub>4</sub> H <sub>8</sub>	n.d.	77
70	C <sub>5</sub> H <sub>10</sub>	C <sub>5</sub> D <sub>10</sub>	80
71	<sup>13</sup> CC <sub>4</sub> H <sub>10</sub>	n.d.	81
72	C <sub>5</sub> H <sub>12</sub>	C <sub>5</sub> D <sub>12</sub> /C <sub>6</sub> D <sub>6</sub>	84
78	C <sub>6</sub> H <sub>6</sub>	C <sub>5</sub> D <sub>12</sub> /C <sub>6</sub> D <sub>6</sub>	84
79	*C <sub>6</sub> H <sub>7</sub>	*C <sub>6</sub> D <sub>7</sub>	86
80	C <sub>6</sub> H <sub>8</sub>	C <sub>6</sub> D <sub>8</sub>	88
81	*C <sub>6</sub> H <sub>9</sub>	*C <sub>6</sub> D <sub>9</sub>	90
82	C <sub>6</sub> H <sub>10</sub>	C <sub>6</sub> D <sub>10</sub>	92
83	<sup>13</sup> CC <sub>5</sub> H <sub>10</sub>	n.d.	93
84	C <sub>6</sub> H <sub>12</sub>	C <sub>6</sub> D <sub>12</sub>	96
85	<sup>13</sup> CC <sub>5</sub> H <sub>12</sub>	n.d.	97
86	C <sub>6</sub> H <sub>14</sub>	C <sub>6</sub> D <sub>14</sub> /C <sub>7</sub> D <sub>8</sub>	100
91	*C <sub>7</sub> H <sub>7</sub>	n.d.	98
92	C <sub>7</sub> H <sub>8</sub>	C <sub>6</sub> D <sub>14</sub> /C <sub>7</sub> D <sub>8</sub>	100
94	C <sub>7</sub> H <sub>10</sub>	C <sub>7</sub> D <sub>10</sub>	104
95	*C <sub>7</sub> H <sub>11</sub>	n.d.	106
96	C <sub>7</sub> H <sub>12</sub>	C <sub>7</sub> D <sub>12</sub>	108
98	C <sub>7</sub> H <sub>14</sub>	C <sub>7</sub> D <sub>14</sub>	112
100	C <sub>7</sub> H <sub>16</sub>	C <sub>7</sub> D <sub>16</sub>	116
108	C <sub>8</sub> H <sub>12</sub>	C <sub>8</sub> D <sub>12</sub>	120
110	C <sub>8</sub> H <sub>14</sub>	C <sub>8</sub> D <sub>14</sub>	124
112	C <sub>8</sub> H <sub>16</sub>	C <sub>8</sub> D <sub>16</sub>	128
114	C <sub>8</sub> H <sub>18</sub>	C <sub>8</sub> D <sub>18</sub>	132
122	C <sub>9</sub> H <sub>14</sub>	C <sub>9</sub> D <sub>14</sub>	136
124	C <sub>9</sub> H <sub>16</sub>	C <sub>9</sub> D <sub>16</sub>	140
126	C <sub>9</sub> H <sub>18</sub>	C <sub>9</sub> D <sub>18</sub>	144

(b)			
<i>m/z</i>	Lyman $\alpha$ photolysis	Broadband photolysis	<i>m/z</i>
40	C <sub>3</sub> H <sub>4</sub>	C <sub>3</sub> H <sub>4</sub>	40
42	C <sub>3</sub> H <sub>6</sub>	C <sub>3</sub> H <sub>6</sub>	42
52	C <sub>4</sub> H <sub>4</sub>	C <sub>4</sub> H <sub>4</sub>	52
54	C <sub>4</sub> H <sub>6</sub>	C <sub>4</sub> H <sub>6</sub>	54
56	C <sub>4</sub> H <sub>8</sub>	C <sub>4</sub> H <sub>8</sub>	56
58	C <sub>4</sub> H <sub>10</sub>	C <sub>4</sub> H <sub>10</sub>	58
64	n.d.	C <sub>5</sub> H <sub>4</sub>	64
65	n.d.	*C <sub>5</sub> H <sub>5</sub>	65
66	C <sub>5</sub> H <sub>6</sub>	C <sub>5</sub> H <sub>6</sub>	66
67	*C <sub>5</sub> H <sub>7</sub>	*C <sub>5</sub> H <sub>7</sub>	67
68	C <sub>5</sub> H <sub>8</sub>	C <sub>5</sub> H <sub>8</sub>	68
70	C <sub>5</sub> H <sub>10</sub>	C <sub>5</sub> H <sub>10</sub>	70
72	C <sub>5</sub> H <sub>12</sub>	C <sub>5</sub> H <sub>12</sub>	72
76	C <sub>6</sub> H <sub>4</sub>	C <sub>6</sub> H <sub>4</sub>	76
77	n.d.	*C <sub>6</sub> H <sub>5</sub>	77
78	C <sub>6</sub> H <sub>6</sub>	C <sub>6</sub> H <sub>6</sub>	78
79	*C <sub>6</sub> H <sub>7</sub>	*C <sub>6</sub> H <sub>7</sub>	79
80	C <sub>6</sub> H <sub>8</sub>	C <sub>6</sub> H <sub>8</sub>	80
81	*C <sub>6</sub> H <sub>9</sub>	*C <sub>6</sub> H <sub>9</sub>	81
82	C <sub>6</sub> H <sub>10</sub>	C <sub>6</sub> H <sub>10</sub>	82

**Table 3** (continued)

(b)			
<i>m/z</i>	Lyman $\alpha$ photolysis	Broadband photolysis	<i>m/z</i>
83	<sup>13</sup> CC <sub>5</sub> H <sub>10</sub>	<sup>13</sup> CC <sub>5</sub> H <sub>10</sub>	83
83	*C <sub>6</sub> H <sub>11</sub>	*C <sub>6</sub> H <sub>11</sub>	83
84	C <sub>6</sub> H <sub>12</sub>	C <sub>6</sub> H <sub>12</sub>	84
86	C <sub>6</sub> H <sub>14</sub>	C <sub>6</sub> H <sub>14</sub>	86
90	C <sub>7</sub> H <sub>6</sub>	C <sub>7</sub> H <sub>6</sub>	90
91	*C <sub>7</sub> H <sub>7</sub>	*C <sub>7</sub> H <sub>7</sub>	91
92	C <sub>7</sub> H <sub>8</sub>	C <sub>7</sub> H <sub>8</sub>	92
93	*C <sub>7</sub> H <sub>9</sub>	*C <sub>7</sub> H <sub>9</sub>	93
94	C <sub>7</sub> H <sub>10</sub>	C <sub>7</sub> H <sub>10</sub>	94
95	*C <sub>7</sub> H <sub>11</sub>	*C <sub>7</sub> H <sub>11</sub>	95
96	C <sub>7</sub> H <sub>12</sub>	C <sub>7</sub> H <sub>12</sub>	96
97	<sup>13</sup> CC <sub>6</sub> H <sub>12</sub>	<sup>13</sup> CC <sub>6</sub> H <sub>12</sub>	97
97	*C <sub>7</sub> H <sub>13</sub>	*C <sub>7</sub> H <sub>13</sub>	97
98	C <sub>7</sub> H <sub>14</sub>	C <sub>7</sub> H <sub>14</sub>	98
100	C <sub>7</sub> H <sub>16</sub>	C <sub>7</sub> H <sub>16</sub>	100
104	C <sub>8</sub> H <sub>8</sub>	C <sub>8</sub> H <sub>8</sub>	104
106	C <sub>8</sub> H <sub>10</sub>	C <sub>8</sub> H <sub>10</sub>	106
108	C <sub>8</sub> H <sub>12</sub>	C <sub>8</sub> H <sub>12</sub>	108
110	C <sub>8</sub> H <sub>14</sub>	C <sub>8</sub> H <sub>14</sub>	110
112	C <sub>8</sub> H <sub>16</sub>	C <sub>8</sub> H <sub>16</sub>	112
114	C <sub>8</sub> H <sub>18</sub>	C <sub>8</sub> H <sub>18</sub>	114
118	C <sub>9</sub> H <sub>10</sub>	C <sub>9</sub> H <sub>10</sub>	118
120	C <sub>9</sub> H <sub>12</sub>	C <sub>9</sub> H <sub>12</sub>	120
122	C <sub>9</sub> H <sub>14</sub>	C <sub>9</sub> H <sub>14</sub>	122
124	C <sub>9</sub> H <sub>16</sub>	C <sub>9</sub> H <sub>16</sub>	124
126	C <sub>9</sub> H <sub>18</sub>	C <sub>9</sub> H <sub>18</sub>	126
132	C <sub>10</sub> H <sub>12</sub>	C <sub>10</sub> H <sub>12</sub>	132
134	C <sub>10</sub> H <sub>14</sub>	C <sub>10</sub> H <sub>14</sub>	134
136	C <sub>10</sub> H <sub>16</sub>	C <sub>10</sub> H <sub>16</sub>	136
138	C <sub>10</sub> H <sub>18</sub>	C <sub>10</sub> H <sub>18</sub>	138
140	C <sub>10</sub> H <sub>20</sub>	C <sub>10</sub> H <sub>20</sub>	140
146	C <sub>11</sub> H <sub>14</sub>	C <sub>11</sub> H <sub>14</sub>	146
148	C <sub>11</sub> H <sub>16</sub>	C <sub>11</sub> H <sub>16</sub>	148
150	C <sub>11</sub> H <sub>18</sub>	C <sub>11</sub> H <sub>18</sub>	150
152	C <sub>11</sub> H <sub>20</sub>	C <sub>11</sub> H <sub>20</sub>	152

(c)			
Generic formula	Electrons	Broadband photolysis	Lyman $\alpha$ photolysis
C <sub><i>n</i></sub> H <sub>2<i>n</i>+2</sub>	<i>n</i> = 4–8	<i>n</i> = 4–8	<i>n</i> = 4–8
C <sub><i>n</i></sub> H <sub>2<i>n</i></sub>	<i>n</i> = 3–9	<i>n</i> = 3–10	<i>n</i> = 3–10
C <sub><i>n</i></sub> H <sub>2<i>n</i>-2</sub>	<i>n</i> = 3–9	<i>n</i> = 3–11	<i>n</i> = 3–11
C <sub><i>n</i></sub> H <sub>2<i>n</i>-4</sub>	<i>n</i> = 4–9	<i>n</i> = 4–11	<i>n</i> = 4–11
C <sub><i>n</i></sub> H <sub>2<i>n</i>-6</sub>	<i>n</i> = 6–7	<i>n</i> = 5–11	<i>n</i> = 6–11
C <sub><i>n</i></sub> H <sub>2<i>n</i>-8</sub>	—	<i>n</i> = 6–11	<i>n</i> = 6–11

Notes: n.d. – not detected; \* – fragment; italics – small/tentative signal.  
<sup>a</sup> Due to the close ionization energy of butane (10.5 ± 0.1 eV) to the photoionization energy used in this study (10.49 eV) butane is not always detectable *via* PI-ReTOF-MS.

of 95 K, which corresponds very well to recent hydrocarbon irradiation experiments also observing *n*-butane as a product.<sup>120,121</sup>

Larger alkane molecular ions were also detected at *m/z* = 72 (C<sub>5</sub>H<sub>12</sub><sup>+</sup>, 98 K), *m/z* = 86 (C<sub>6</sub>H<sub>14</sub><sup>+</sup>, 110 K), *m/z* = 100 (C<sub>7</sub>H<sub>16</sub><sup>+</sup>, 124 K), and *m/z* = 114 (C<sub>8</sub>H<sub>18</sub><sup>+</sup>, 130 K). For each unit of CH<sub>2</sub> added the onset temperature increases by 6–14 K (Fig. 15).<sup>120,121</sup>

Although these alkanes' ion signals have relatively low intensities it is not accurate to attribute this to a low yield product as each isomer has a unique photoionization cross section. Therefore, as the contribution of each of these isomers is not known in the current experiment the signal intensities cannot be extrapolated to quantification in the current manuscript. The ability of this technique to determine specific isomers being

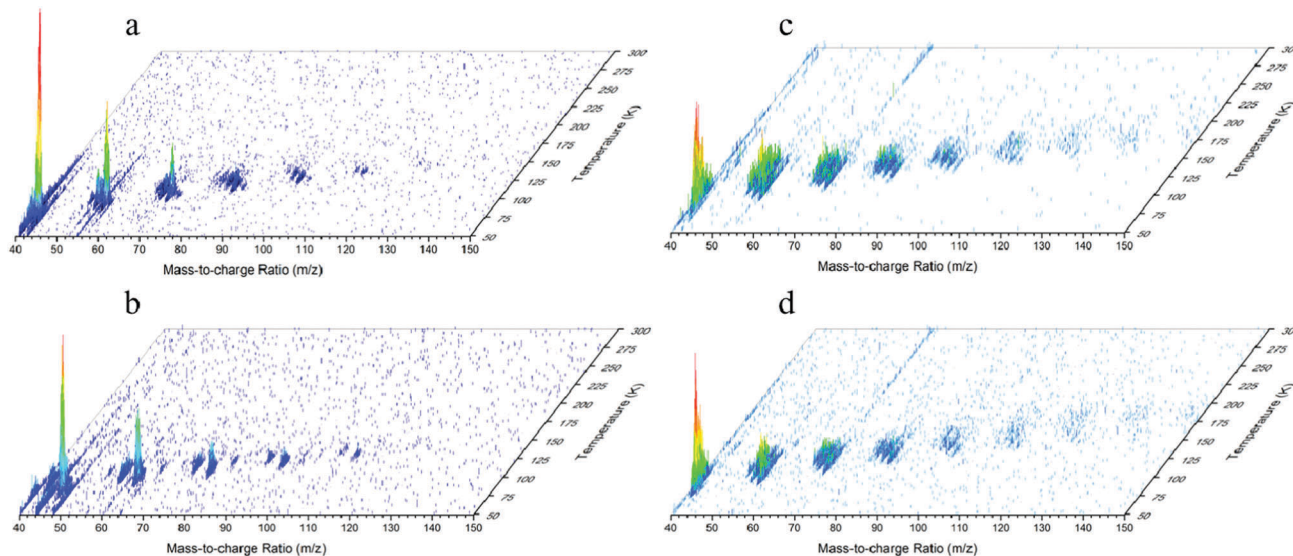


Fig. 3 PI-ReTOF-MS data reporting the temperature dependent mass spectra at a photoionization energy of 10.49 eV for (a) electron irradiated methane ( $\text{CH}_4$ ), (b) electron irradiated D4-methane ( $\text{CD}_4$ ), (c) Lyman  $\alpha$  irradiated methane ( $\text{CH}_4$ ), and (d) broadband irradiated methane ( $\text{CH}_4$ ).

formed within the ice is easily displayed using the example of the  $\text{C}_4\text{H}_{10}$  alkane which has two possible isomers *n*-butane ( $\text{CH}_3\text{CH}_2\text{CH}_2\text{CH}_3$ ; I.E. =  $10.5 \pm 0.1$  eV) and *i*-butane ( $(\text{CH}_3)_2\text{CHCH}_3$ ; I.E. =  $10.68 \pm 0.11$  eV).<sup>123</sup> While *i*-butane has an ionization energy greater than 10.49 eV its isomer, *n*-butane, has an ionization energy at the threshold of our experimental energy. Therefore, if any signal was observed at  $m/z = 58$  then this can be directly used to confirm the presence of *n*-butane production. This method can be applied to other isomers using our tunable VUV system to selectively photoionize and discriminate what isomers are being formed.

**3.3.2.  $\text{C}_n\text{H}_{2n}$ .** Ions corresponding to alkenes ( $\text{C}_n\text{H}_{2n}$ ) or possibly their double-bond equivalent (D.B.E.) (cycloalkanes) with  $n = 3-9$  were also detected (Fig. 5). While FTIR confirmed the alkene molecule ethylene, it was not able to confirm the presence of several larger alkenes on its own. These larger alkene molecular ions were detected at  $m/z = 42$  ( $\text{C}_3\text{H}_6^+$ , 68 K),  $m/z = 56$  ( $\text{C}_4\text{H}_8^+$ , 84 K),  $m/z = 70$  ( $\text{C}_5\text{H}_{10}^+$ , 95 K),  $m/z = 84$  ( $\text{C}_6\text{H}_{12}^+$ , 103 K),  $m/z = 98$  ( $\text{C}_7\text{H}_{14}^+$ , 117 K),  $m/z = 112$  ( $\text{C}_8\text{H}_{16}^+$ , 125 K), and  $m/z = 126$  ( $\text{C}_9\text{H}_{18}^+$ , 138 K). As the size of the ion increases by  $\text{CH}_2$  the sublimation temperature onset increases from 8–16 K. It should be pointed out that the difference in intensity between the deuterated ion signal and the non-isotopic ion signal is due to the difference in photon flux of the ionizing laser used for the PI-ReTOF-MS analysis and not due to a difference in relative yield. The largest alkane detected in this study, from electron irradiation *via* PI-ReTOF-MS, was  $\text{C}_8\text{H}_{18}$  while the largest alkene detected contained one additional carbon atom ( $\text{C}_9\text{H}_{18}$ ).

**3.3.3.  $\text{C}_n\text{H}_{2n-2}$ .** The next hydrocarbon group detected corresponded to alkynes ( $\text{C}_n\text{H}_{2n-2}$ ;  $n = 3-9$ ) or their D.B.E. (dienes or cycloalkenes) (Fig. 6). The FTIR study was able to detect this group *via* acetylene ( $\text{C}_2\text{H}_2$ ), but was unable to definitively assign several larger alkynes that were detected in the PI-ReTOF-MS analysis. Alkyne ion signals were detected at  $m/z = 40$  ( $\text{C}_3\text{H}_4^+$ , 76 K),  $m/z = 54$  ( $\text{C}_4\text{H}_6^+$ , 86 K),  $m/z = 68$  ( $\text{C}_5\text{H}_8^+$ , 95 K),  $m/z = 82$  ( $\text{C}_6\text{H}_{10}^+$ , 110 K),

$m/z = 96$  ( $\text{C}_7\text{H}_{12}^+$ , 124 K),  $m/z = 110$  ( $\text{C}_8\text{H}_{14}^+$ , 131 K), and  $m/z = 124$  ( $\text{C}_9\text{H}_{16}^+$ , 142 K). The addition of each  $\text{CH}_2$  unit resulted in a sublimation temperature increase of 7–15 K.

**3.3.4.  $\text{C}_n\text{H}_{2n-4}$ .** The PI-ReTOF-MS analysis also detected the generic hydrocarbon group  $\text{C}_n\text{H}_{2n-4}$  ( $n = 4-7$ ) corresponding to trienes, cyclodialkenes, bicycloalkenes, and yne-enes (Fig. 7). Further, this hydrocarbon was not able to be discretely detected *via* FTIR showing the power of the PI-ReTOF-MS technique to detect these elusive hydrocarbon products from methane. The  $\text{C}_n\text{H}_{2n-4}$  molecular ions were detected at  $m/z = 52$  ( $\text{C}_4\text{H}_4^+$ , 92 K),  $m/z = 66$  ( $\text{C}_5\text{H}_6^+$ , 106 K),  $m/z = 80$  ( $\text{C}_6\text{H}_8^+$ , 115 K),  $m/z = 94$  ( $\text{C}_7\text{H}_{10}^+$ , 127 K),  $m/z = 108$  ( $\text{C}_8\text{H}_{12}^+$ , 134 K), and  $m/z = 122$  ( $\text{C}_9\text{H}_{14}^+$ , 140 K). For this hydrocarbon group, each additional  $\text{CH}_2$  unit corresponded to a sublimation increase of 6–14 K. It is interesting to point out that the largest molecules detected in this study so far all contained 9 carbon atoms. This similarity in carbon chain length is able to be explained quite readily *via* the proposed reaction mechanism (Section 4.8).

**3.3.5.  $\text{C}_n\text{H}_{2n-6}$ .** The most highly unsaturated hydrocarbon group detected *via* PI-ReTOF-MS after electron irradiation was  $\text{C}_n\text{H}_{2n-6}$  ( $n = 6-7$ ) which corresponds to yne-diene, diynes, tetraenes, cyclotrialkenes, and tricycloalkenes (Fig. 8). The molecular ions corresponding to this group were detected at  $m/z = 78$  ( $\text{C}_6\text{H}_6^+$ , 126 K), and  $m/z = 92$  ( $\text{C}_7\text{H}_8^+$ , 134 K). Here, the addition of the  $\text{CH}_2$  unit corresponded to a sublimation increase of 8 K. The astrophysically important molecule benzene is a possible isomer of the molecular ion  $\text{C}_6\text{H}_6^+$  detected in this group. Also, the lack of detection of several smaller ( $\text{C}_5\text{H}_4$ ) and larger ( $\text{C}_8\text{H}_{10}$ ,  $\text{C}_9\text{H}_{12}$ ) hydrocarbons in this group may be a result of preferential formation routes and provide insight into the complex formation mechanism producing these species (Section 4.8).

### 3.4. Broadband VUV photolysis – PI-ReTOF-MS

The TPD study of broadband photolyzed methane ice while monitoring with PI-ReTOF-MS revealed six groups of hydrocarbon

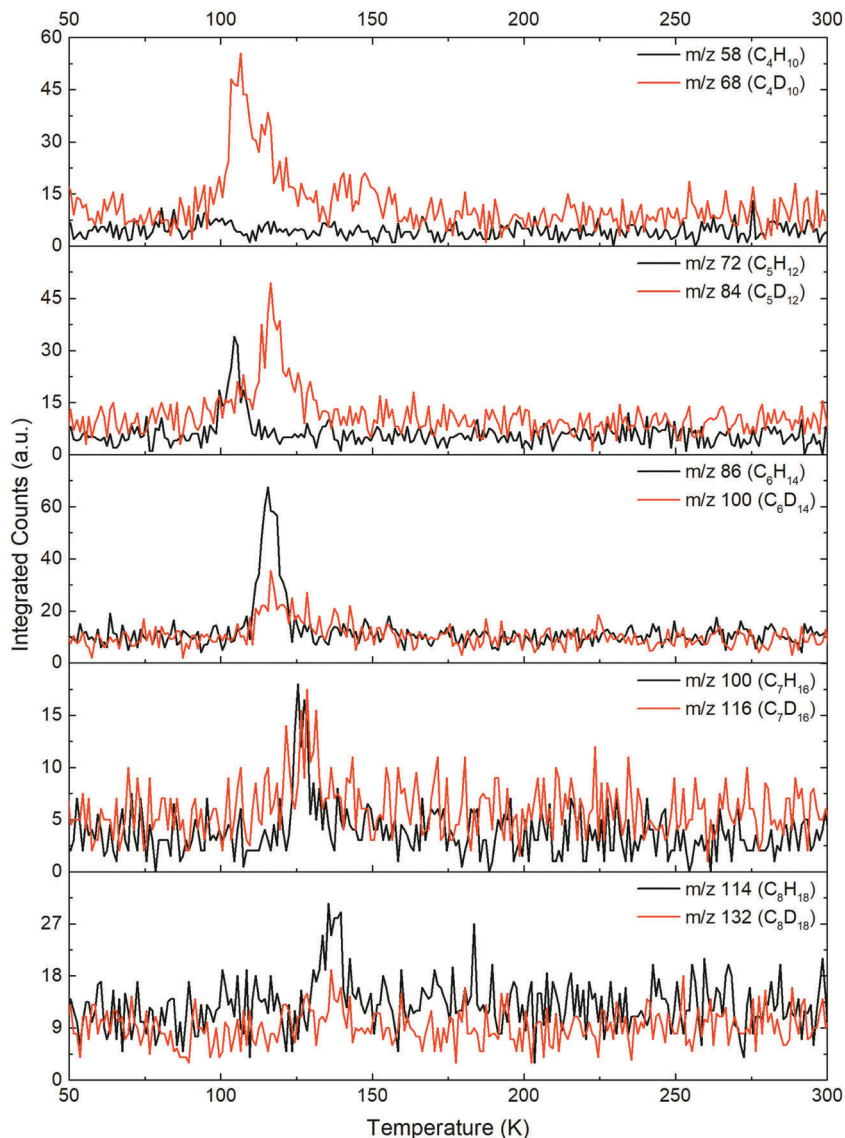


Fig. 4 TPD profiles recorded after electron irradiation via PI-ReTOF-MS for masses with the generic formula of  $C_nH_{2n+2}/C_nD_{2n+2}$  (alkanes).

products with the general formulae:  $C_nH_{2n+2}$  ( $n = 4-8$ ),  $C_nH_{2n}$  ( $n = 3-10$ ),  $C_nH_{2n-2}$  ( $n = 3-11$ ),  $C_nH_{2n-4}$  ( $n = 4-11$ ),  $C_nH_{2n-6}$  ( $n = 5-11$ ), and  $C_nH_{2n-8}$  ( $n = 6-11$ ). Here, the same groups that were detected from electron radiolysis were also present from the broadband photolysis experiment and an even more unsaturated hydrocarbon group ( $C_nH_{2n-8}$ ) was also detected.

**3.4.1.  $C_nH_{2n+2}$ .** The alkanes detected in the broadband photolysis experiment utilizing PI-ReTOF-MS were consistent with those detected in the electron irradiation experiment ( $C_nH_{2n+2}$ ;  $n = 4-8$ ) (Fig. 9). The smallest detectable alkane with PI-ReTOF-MS at 10.49 eV is *n*-butane which corresponded to  $m/z = 58$  ( $C_4H_{10}^+$ , 125 K). Also, FTIR was able to detect the alkane ethane ( $C_2H_6$ ) which has an ionization energy larger than 10.49 eV and will not be detected in this PI-ReTOF-MS experimental setup. Several other low intensity ion signals were detected at  $m/z = 72$  ( $C_5H_{12}^+$ , 129 K),  $m/z = 86$  ( $C_6H_{14}^+$ , 132 K),  $m/z = 100$  ( $C_7H_{16}^+$ , 134 K), and, tentatively,  $m/z = 114$  ( $C_8H_{18}^+$ , 139 K).

Again, an increase in sublimation temperatures was observed from 3–5 K to the next largest alkane. Each of these alkane ion signals are quite low and this makes their true sublimation onset difficult to determine. However, their overall peak lies near to previously detected stronger signals corresponding to these alkanes.<sup>120,121</sup> The relatively stronger ion signals detected for alkanes in the electron irradiation experiment may be a clue to the reaction mechanism for the formation of the more highly unsaturated hydrocarbon group ( $C_nH_{2n-8}$ ) detected in the photolysis experiments (Section 4.8).

**3.4.2.  $C_nH_{2n}$ .** Ions corresponding to alkenes and/or cycloalkanes ( $C_nH_{2n}$ ;  $n = 3-10$ ) were also detected at  $m/z = 42$  ( $C_3H_6^+$ , 73 K),  $m/z = 56$  ( $C_4H_8^+$ , 90 K),  $m/z = 70$  ( $C_5H_{10}^+$ , 103 K),  $m/z = 84$  ( $C_6H_{12}^+$ , 115 K),  $m/z = 98$  ( $C_7H_{14}^+$ , 129 K),  $m/z = 112$  ( $C_8H_{16}^+$ , 136 K),  $m/z = 126$  ( $C_9H_{18}^+$ , 141 K), and  $m/z = 140$  ( $C_{10}H_{20}^+$ , 156 K) (Fig. 10). Here, the typical trend of increasing sublimation temperature was also observed with increases of

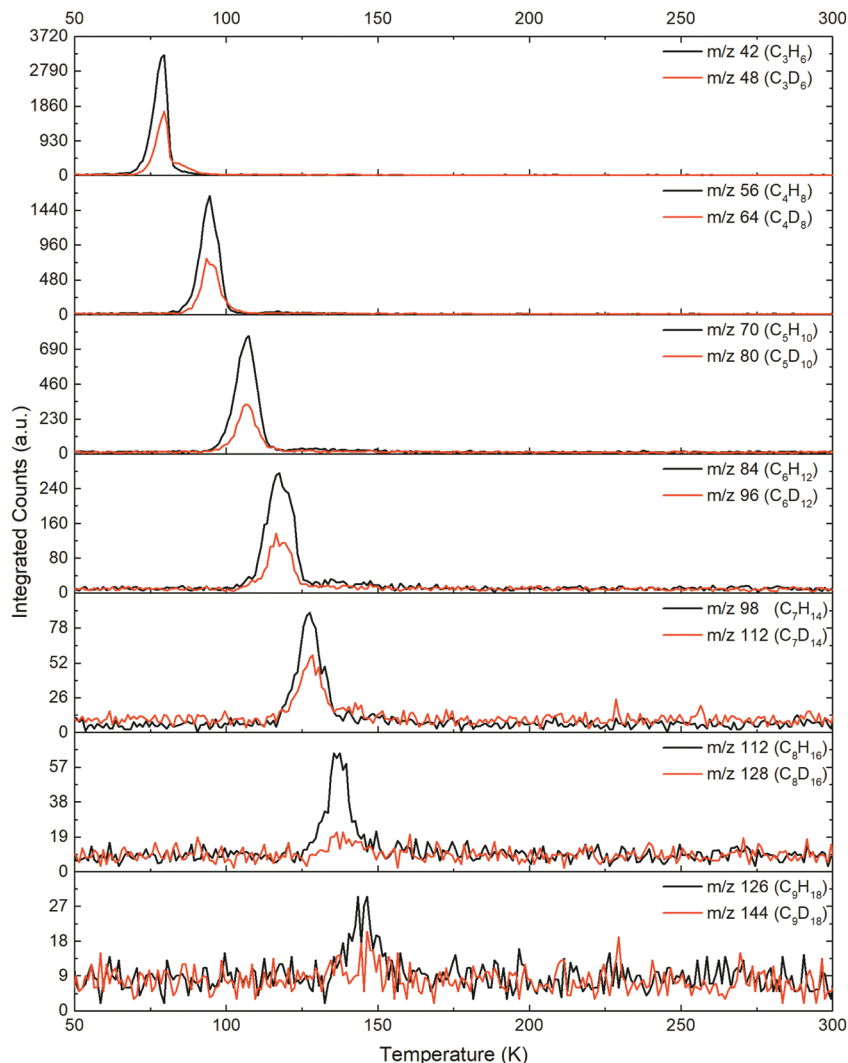


Fig. 5 TPD profiles recorded after electron irradiation via PI-ReTOF-MS for masses with the generic formula of  $C_nH_{2n}/C_nD_{2n}$ , which may correspond to alkenes and/or cycloalkanes.

5–24 K per additional  $CH_2$  unit. It should be noted that the ion signals for  $m/z = 126$  ( $C_9H_{18}^+$ , 141 K) and  $m/z = 140$  ( $C_{10}H_{20}^+$ , 156 K) are only a tentative detection (Table 3b). However, the sublimation temperatures correlate well with the observed increase from the smaller hydrocarbons of this group. The smallest alkene, ethylene ( $C_2H_4$ ), was able to be confirmed *via* FTIR.

**3.4.3.  $C_nH_{2n-2}$ .** The following PI-ReTOF-MS detected hydrocarbon group corresponds to those of alkynes ( $C_nH_{2n-2}$ ;  $n = 3-11$ ) or the D.B.E. (dienes and cycloalkenes) (Fig. 11). The FTIR analysis of the processed ice was able to confirm the production of the simplest alkyne, acetylene ( $C_2H_2$ ), which will not be detected by the PI-ReTOF-MS method. However, multiple ions corresponding to larger hydrocarbons in this group were detected at  $m/z = 40$  ( $C_3H_4^+$ , 79 K),  $m/z = 54$  ( $C_4H_6^+$ , 94 K),  $m/z = 68$  ( $C_5H_8^+$ , 108 K),  $m/z = 82$  ( $C_6H_{10}^+$ , 119 K),  $m/z = 96$  ( $C_7H_{12}^+$ , 132 K),  $m/z = 110$  ( $C_8H_{14}^+$ , 137 K),  $m/z = 124$  ( $C_9H_{16}^+$ , 144 K), and tentatively both  $m/z = 138$  ( $C_{10}H_{18}^+$ , 156 K) and  $m/z = 152$  ( $C_{11}H_{20}^+$ , 165 K). The increase in sublimation temperature observed was 5–15 K for the increase of a  $CH_2$  unit in the

molecular formula. This group displays the longest carbon chain detected yet from these experiments with the molecule containing 11 carbon atoms.

**3.4.4.  $C_nH_{2n-4}$ .** Next, the hydrocarbon group belonging to the generic formulae  $C_nH_{2n-4}$  ( $n = 4-11$ ) was detected *via* PI-ReTOF-MS (Fig. 12). This group, like that detected in the electron irradiation analysis, was the first hydrocarbon group unable to be discretely detected *via* FTIR. Ions corresponding to this group were detected *via*  $m/z = 52$  ( $C_4H_4^+$ , 98 K),  $m/z = 66$  ( $C_5H_6^+$ , 111 K),  $m/z = 80$  ( $C_6H_8^+$ , 125 K),  $m/z = 94$  ( $C_7H_{10}^+$ , 133 K),  $m/z = 108$  ( $C_8H_{12}^+$ , 143 K),  $m/z = 122$  ( $C_9H_{14}^+$ , 151 K), and tentatively  $m/z = 136$  ( $C_{10}H_{16}^+$ , 159 K), and  $m/z = 150$  ( $C_{11}H_{18}^+$ , 163 K). Here the sublimation increase was observed to be 4–14 K as the hydrocarbon grew *via* a  $CH_2$  unit. As in the previous group ( $C_nH_{2n-2}$ ) the longest carbon group detected contained 11 carbon atoms.

**3.4.5.  $C_nH_{2n-6}$ .** The most highly unsaturated hydrocarbon group detected *via* PI-ReTOF-MS after electron irradiation was  $C_nH_{2n-6}$ . Similarly, the analysis of broadband photolysis products

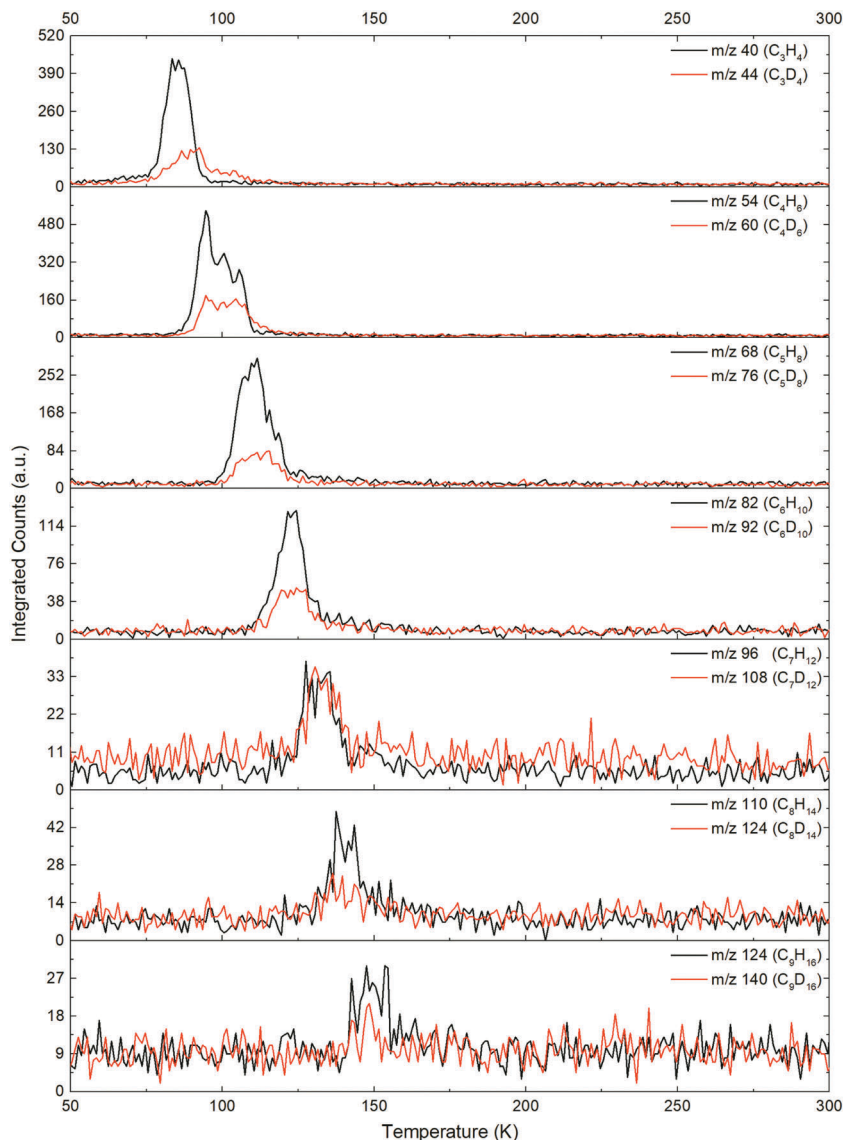


Fig. 6 TPD profiles recorded after electron irradiation via PI-ReTOF-MS for masses with the generic formula of  $C_nH_{2n-2}/C_nD_{2n-2}$ , which may correspond to alkynes, dienes, and/or cycloalkenes.

revealed several corresponding ions for this group ( $n = 5-11$ ; Fig. 13). These ions were detected at  $m/z = 64$  ( $C_5H_4^+$ , 118 K),  $m/z = 78$  ( $C_6H_6^+$ , 123 K),  $m/z = 92$  ( $C_7H_8^+$ , 138 K),  $m/z = 106$  ( $C_8H_{10}^+$ , 149 K),  $m/z = 120$  ( $C_9H_{12}^+$ , 155 K),  $m/z = 136$  ( $C_{10}H_{14}^+$ , 159 K), and  $m/z = 150$  ( $C_{11}H_{16}^+$ , 168 K). This group displayed an increasing sublimation temperature from 4–15 K for each  $CH_2$  unit added. Here, multiple ion signals were detected from broadband photolyzed pure methane ice while only 2 ions ( $C_6H_6$  and  $C_7H_8$ ) were detected in the electron irradiated ice (Section 4.8).

**3.4.6.  $C_nH_{2n-8}$ .** Although  $C_nH_{2n-6}$  was the most unsaturated group detected from electron irradiation the broadband photolysis PI-ReTOF-MS analysis revealed a hydrocarbon group of even greater unsaturation,  $C_nH_{2n-8}$  ( $n = 6-11$ ). These ions were detected at  $m/z = 76$  ( $C_6H_4^+$ , 131 K),  $m/z = 90$  ( $C_7H_6^+$ , 136 K),  $m/z = 104$  ( $C_8H_8^+$ , 148 K),  $m/z = 118$  ( $C_9H_{10}^+$ , 157 K),  $m/z = 132$

( $C_{10}H_{12}^+$ , 159 K), and  $m/z = 146$  ( $C_{11}H_{14}^+$ , 172 K) (Fig. 14). Each additional  $CH_2$  unit resulted in a sublimation increase of 2–13 K. This highly unsaturated group is most likely formed during the broadband photolysis experiment and not in the electron irradiation because of the difference in doses of energy deposited into the methane ices (Section 4.8).

### 3.5. Lyman $\alpha$ photolysis – PI-ReTOF-MS

Finally, the PI-ReTOF-MS analysis during TPD of the Lyman  $\alpha$  photolyzed methane ice detected six hydrocarbon groups, of varying degrees of saturation, with the general formulae:  $C_nH_{2n+2}$  ( $n = 4-8$ ),  $C_nH_{2n}$  ( $n = 3-10$ ),  $C_nH_{2n-2}$  ( $n = 3-11$ ),  $C_nH_{2n-4}$  ( $n = 4-11$ ),  $C_nH_{2n-6}$  ( $n = 6-11$ ), and  $C_nH_{2n-8}$  ( $n = 6-11$ ). Here, the products resemble those observed in the broadband photolysis experiment much more closely than the electron irradiation experiment the highly unsaturated group  $C_nH_{2n-8}$  was

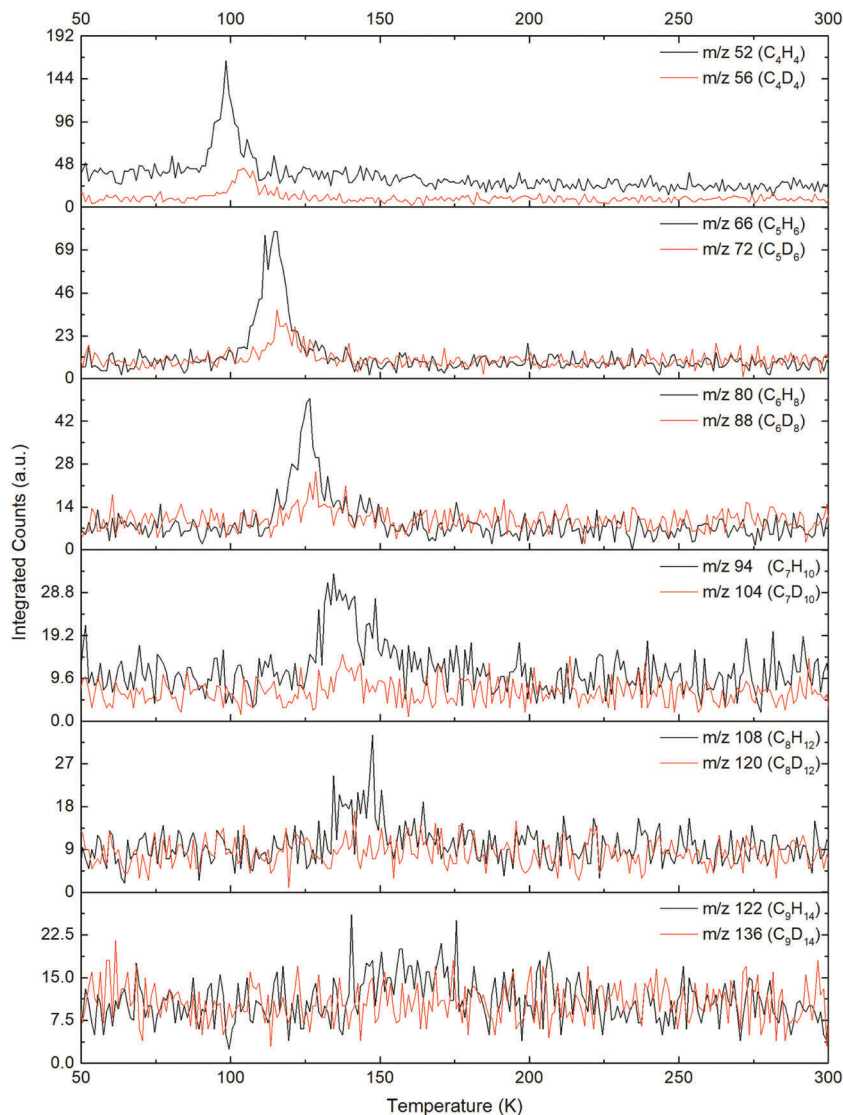


Fig. 7 TPD profiles recorded after electron irradiation via PI-ReTOF-MS for masses with the generic formula of  $C_nH_{2n-4}/C_nD_{2n-4}$  (yne-ene, trienes, cycloalkenes, bi-cycloalkenes).

detected in both photolysis experiments, but not after the electron irradiation.

**3.5.1.  $C_nH_{2n+2}$ .** The completely saturated hydrocarbon group, alkanes ( $C_nH_{2n+2}$ ), was also detected *via* PI-ReTOF-MS from the Lyman  $\alpha$  photolyzed methane ice (ESI,† Fig. S3;  $n = 4-8$ ). The ions corresponding to this group were detected at  $m/z = 58$  ( $C_4H_{10}^+$ , 123 K),  $m/z = 72$  ( $C_5H_{12}^+$ , 100 K),  $m/z = 86$  ( $C_6H_{14}^+$ , 118 K), and tentatively  $m/z = 100$  ( $C_7H_{16}^+$ , 128 K), and  $m/z = 114$  ( $C_8H_{18}^+$ , 147 K). These signals all had relatively low intensities which made their onset temperature difficult to determine, but similar to the previous experiments an increase in the sublimation temperature of 10–19 K was observed for each additional  $CH_2$  unit. The only exception to this trend was that of the *n*-butane ion signal, which is most likely due to it being trapped within the ice and subliming later with another product or possibly it was due to the photo-ionization energy used in these experiments (10.49 eV) being very close to the ionization threshold of the *n*-butane isomer.

**3.5.2.  $C_nH_{2n}$ .** The next group detected from the TPD of Lyman  $\alpha$  photolyzed methane ice corresponded to the general formula  $C_nH_{2n}$  (ESI,† Fig. S4;  $n = 3-10$ ). The ion signals were recorded at  $m/z = 42$  ( $C_3H_6^+$ , 69 K),  $m/z = 56$  ( $C_4H_8^+$ , 88 K),  $m/z = 70$  ( $C_5H_{10}^+$ , 100 K),  $m/z = 84$  ( $C_6H_{12}^+$ , 113 K),  $m/z = 98$  ( $C_7H_{14}^+$ , 121 K),  $m/z = 112$  ( $C_8H_{16}^+$ , 135 K),  $m/z = 126$  ( $C_9H_{18}^+$ , 141 K), and, tentatively,  $m/z = 140$  ( $C_{10}H_{20}^+$ , 148 K). Here, the detected ions grew to the same size of those observed in the broadband photolysis experiment. The increase in sublimation temperature for each larger alkene, or D.B.E., was determined to be 6–19 K. As in the previous experiments the smallest alkene, ethylene ( $C_2H_4$ ), was confirmed *via* the FTIR analysis.

**3.5.3.  $C_nH_{2n-2}$ .** As previously described in the FTIR results of Lyman  $\alpha$  photolyzed methane ice the simplest alkyne, acetylene ( $C_2H_2$ ), was detected, however, several other hydrocarbons corresponding to this general formula ( $C_nH_{2n-2}$ ;  $n = 3-11$ ) were detected utilizing PI-ReTOF-MS (ESI,† Fig. S5). These ions were

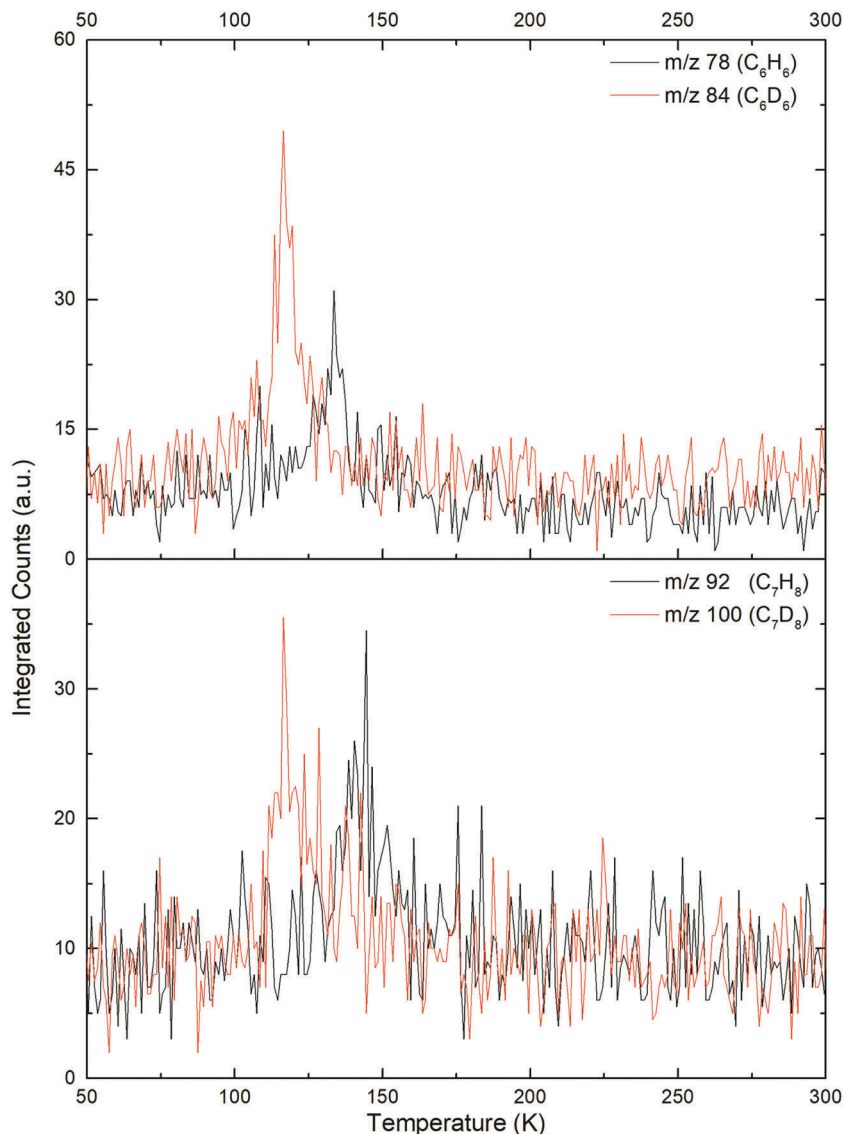


Fig. 8 TPD profiles after electron irradiation recorded via PI-ReTOF-MS for masses with the generic formula of  $C_nH_{2n-6}/C_nD_{2n-6}$  (yne-diene, diynes, tetraenes, cyclotrialkenes, tri-cycloalkenes).

observed at  $m/z = 40$  ( $C_3H_4^+$ , 80 K),  $m/z = 54$  ( $C_4H_6^+$ , 91 K),  $m/z = 68$  ( $C_5H_8^+$ , 106 K),  $m/z = 82$  ( $C_6H_{10}^+$ , 118 K),  $m/z = 96$  ( $C_7H_{12}^+$ , 128 K),  $m/z = 110$  ( $C_8H_{14}^+$ , 135 K),  $m/z = 124$  ( $C_9H_{16}^+$ , 147 K),  $m/z = 138$  ( $C_{10}H_{18}^+$ , 155 K), and, tentatively,  $m/z = 152$  ( $C_{11}H_{20}^+$ , 168 K). The increasing size of these ions corresponded in a sublimation temperature increase of 7–15 K.

**3.5.4.  $C_nH_{2n-4}$ .** The next hydrocarbon group detected corresponds to the generic formula  $C_nH_{2n-4}$  ( $n = 4$ –11) and ions were detected at  $m/z = 52$  ( $C_4H_4^+$ , 95 K),  $m/z = 66$  ( $C_5H_6^+$ , 113 K),  $m/z = 80$  ( $C_6H_8^+$ , 118 K),  $m/z = 94$  ( $C_7H_{10}^+$ , 133 K),  $m/z = 108$  ( $C_8H_{12}^+$ , 138 K),  $m/z = 122$  ( $C_9H_{14}^+$ , 148 K),  $m/z = 136$  ( $C_{10}H_{16}^+$ , 161 K), and  $m/z = 150$  ( $C_{11}H_{18}^+$ , 166 K) (ESI,† Fig. S6). Here, an increase of 5–18 K was observed as the ions increased in size.

**3.5.5.  $C_nH_{2n-6}$ .** The Lyman  $\alpha$  photolysis of methane also produced hydrocarbons that can be classified as yne-diene, diynes, tetraenes, cyclotrialkenes, or tri-cycloalkenes ( $C_nH_{2n-6}$ ;  $n = 6$ –11).

The smallest ion detected in this group was  $m/z = 78$  ( $C_6H_6^+$ , 126 K) which has multiple isomers, but one of these is the astrophysically important benzene molecule. Larger ions were also recorded at  $m/z = 92$  ( $C_7H_8^+$ , 134 K),  $m/z = 106$  ( $C_8H_{10}^+$ , 146 K),  $m/z = 120$  ( $C_9H_{12}^+$ , 156 K),  $m/z = 136$  ( $C_{10}H_{14}^+$ , 164 K), and  $m/z = 150$  ( $C_{11}H_{16}^+$ , 173 K) (ESI,† Fig. S7). Each additional  $CH_2$  unit resulted in the sublimation temperature increasing by 8–12 K. Interestingly the ion signal corresponding to  $C_5H_4^+$  was not detected in this experiment, which matches that of the electron irradiation, but was detected in the broadband experiment. Until this non-detection the ion signals between the broadband photolysis and Lyman  $\alpha$  photolysis experiments have been qualitatively identical.

**3.5.6.  $C_nH_{2n-8}$ .** As observed in the broadband photolysis experiment the most highly unsaturated hydrocarbon group was  $C_nH_{2n-8}$  ( $n = 6$ –11) which can be described as yne-triene,

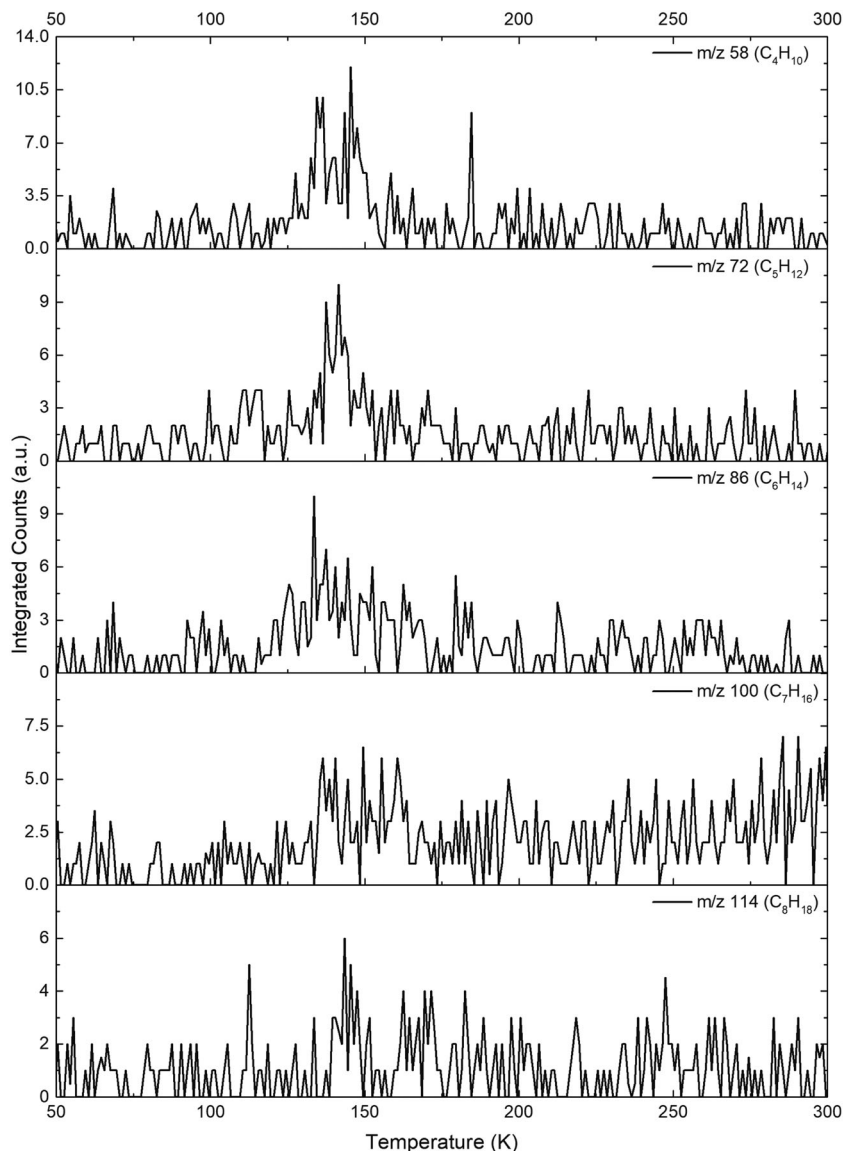


Fig. 9 TPD profiles recorded after broadband photolysis via PI-ReTOF-MS for masses with the generic formula of  $C_nH_{2n+2}$  (alkanes).

diyne-ene, pentaenes, or tri-cyclobialkenes (ESI,† Fig. S8). These ions were detected at  $m/z = 76$  ( $C_6H_4^+$ , 127 K),  $m/z = 90$  ( $C_7H_6^+$ , 138 K),  $m/z = 104$  ( $C_8H_8^+$ , 151 K),  $m/z = 118$  ( $C_9H_{10}^+$ , 165 K),  $m/z = 132$  ( $C_{10}H_{12}^+$ , 171 K), and  $m/z = 146$  ( $C_{11}H_{14}^+$ , 181 K). The increase in ion size corresponded to a sublimation temperature increase of 11–13 K.

### 3.6. Other masses: fragments & isotopes

Ions corresponding to larger hydrocarbon-fragments as well as natural isotopic shifts, odd valued mass-to-charge ratios, were also detected across all three experiments. Fig. S9–S12 (ESI†) display the overlay of the odd valued ion signals, due to either natural isotopic substitution or fragmentation of a larger hydrocarbon, with their non-substituted parent or their most likely molecular ion parent, respectively (ESI†). The odd ions due to natural carbon-13 isotopic substitution in the electron irradiation PI-ReTOF-MS analysis were at  $m/z = 43$  ( $^{13}CC_2H_6^+$ , 64 K),

$m/z = 57$  ( $^{13}CC_3H_8^+$ , 86 K),  $m/z = 69$  ( $^{13}CC_4H_{10}^+$ , 105 K),  $m/z = 71$  ( $^{13}CC_4H_{10}^+$ , 110 K),  $m/z = 83$  ( $^{13}CC_5H_{12}^+$ , 112 K), and  $m/z = 85$  ( $^{13}CC_5H_{12}^+$ , 117 K). Fig. S9 (ESI†) depicts the sublimation event of these odd ions overlaid with their carbon-12 containing isotopologue. Several of these ions' identities were also able to be confirmed with the deuterated methane experiments (ESI,† Fig. S9). However, not all of the odd valued ions were able to be explained *via* carbon-13 substitution and are much more readily explained as fragments of larger hydrocarbons even with the low ionization energy used in these experiments (10.49 eV) (ESI,† Fig. S10–S12).<sup>120,121,123</sup> Fragments in all three irradiation experiments were detected at  $m/z = 65$  ( $C_5H_5^+$ ),  $m/z = 67$  ( $C_5H_7^+$ ),  $m/z = 79$  ( $C_6H_7^+$ ),  $m/z = 81$  ( $C_6H_9^+$ ),  $m/z = 91$  ( $C_7H_7^+$ ), and  $m/z = 95$  ( $C_7H_{11}^+$ ). One exception to this was  $m/z = 65$  ( $C_5H_5^+$ ), which was not detected in the Lyman  $\alpha$  photolysis experiment. Additional odd ions were detected in both photolysis studies, but not in the electron irradiation experiment at  $m/z = 83$  ( $C_6H_{11}^+$ ),

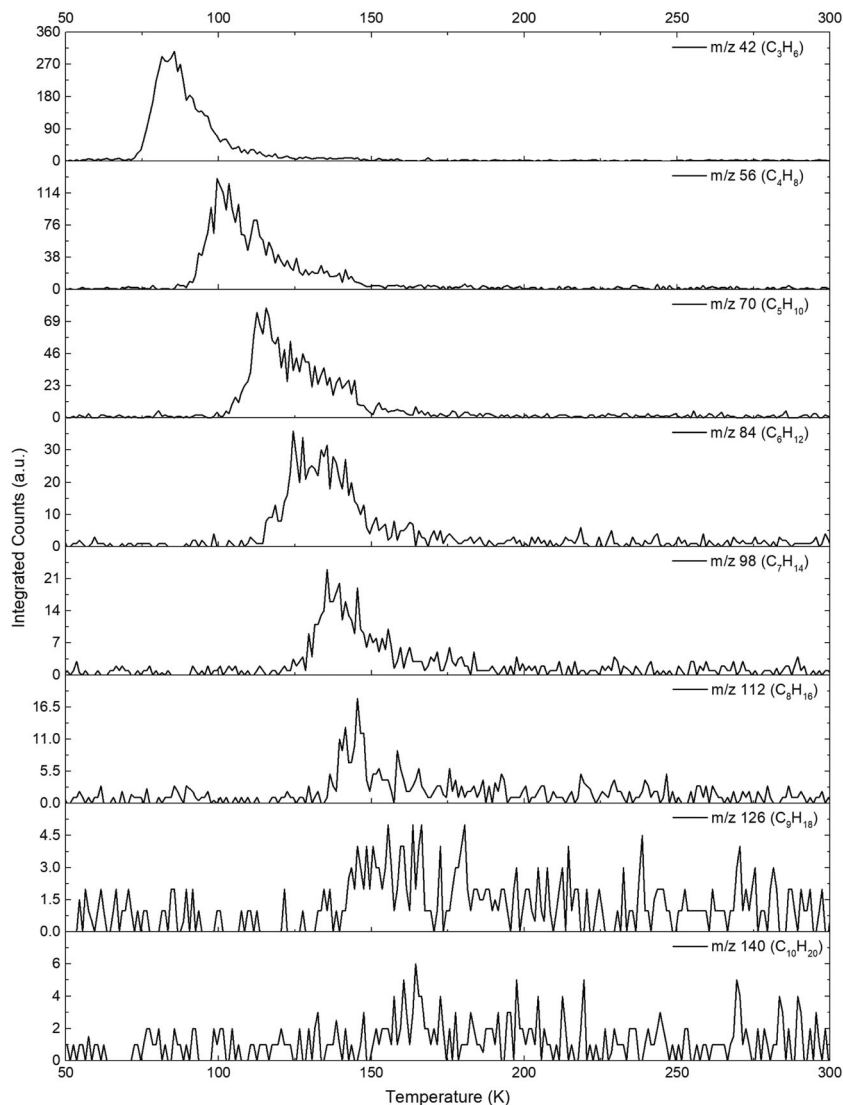


Fig. 10 TPD profiles recorded after broadband photolysis via PI-ReTOF-MS for masses with the generic formula of  $C_nH_{2n}$  (alkenes and/or cycloalkanes).

$m/z = 93$  ( $C_7H_9^+$ ), and  $m/z = 97$  ( $C_7H_{13}^+$ ). Finally,  $m/z = 77$  ( $C_6H_5^+$ ) was only detected in the broadband photolysis experiment.

## 4. Discussion

### 4.1. Summary of results

Compiled here is a brief summary of the results before continuing to the discussion:

1. The FTIR analysis of the processed methane ice was able to detect the same small hydrocarbon products from the three different irradiation sources: propane [ $C_3H_8(C_3D_8)$ ], ethane [ $C_2H_6(C_2D_6)$ ], ethyl radical [ $C_2H_5(C_2D_5)$ ], ethylene [ $C_2H_4(C_2D_4)$ ], acetylene [ $C_2H_2(C_2D_2)$ ], and the methyl radical [ $CH_3(CD_3)$ ].

2. However, the PI-ReTOF-MS analysis identified a diverse group of products with different species being detected in each experiment with the general formulae:

a. Electron irradiation:  $C_nH_{2n+2}$  ( $n = 4-8$ ),  $C_nH_{2n}$  ( $n = 3-9$ ),  $C_nH_{2n-2}$  ( $n = 3-9$ ),  $C_nH_{2n-4}$  ( $n = 4-9$ ), and  $C_nH_{2n-6}$  ( $n = 6-7$ )

b. Broadband photolysis:  $C_nH_{2n+2}$  ( $n = 4-8$ ),  $C_nH_{2n}$  ( $n = 3-10$ ),  $C_nH_{2n-2}$  ( $n = 3-11$ ),  $C_nH_{2n-4}$  ( $n = 4-11$ ),  $C_nH_{2n-6}$  ( $n = 5-11$ ), and  $C_nH_{2n-8}$  ( $n = 6-11$ )

c. Lyman  $\alpha$  photolysis:  $C_nH_{2n+2}$  ( $n = 4-8$ ),  $C_nH_{2n}$  ( $n = 3-10$ ),  $C_nH_{2n-2}$  ( $n = 3-11$ ),  $C_nH_{2n-4}$  ( $n = 4-11$ ),  $C_nH_{2n-6}$  ( $n = 6-11$ ), and  $C_nH_{2n-8}$  ( $n = 6-11$ )

### 4.2. $C_nH_{2n+2}$

Although FTIR only detected the alkanes ( $C_nH_{2n+2}$ ) ethane and propane the PI-ReTOF-MS analysis detected hydrocarbons corresponding to  $n = 4-8$  in all three experiments. For this hydrocarbon group, all three experiments recorded relatively low intensity signals with the electron irradiation products producing the highest ion signals. However, this could be due to a difference in isomers produced between the different experiments. Therefore, as each isomer has a different photoionization cross section at the present photoionization energy (10.49 eV) quantitative measurements are not possible. From this group, the  $n$ -butane

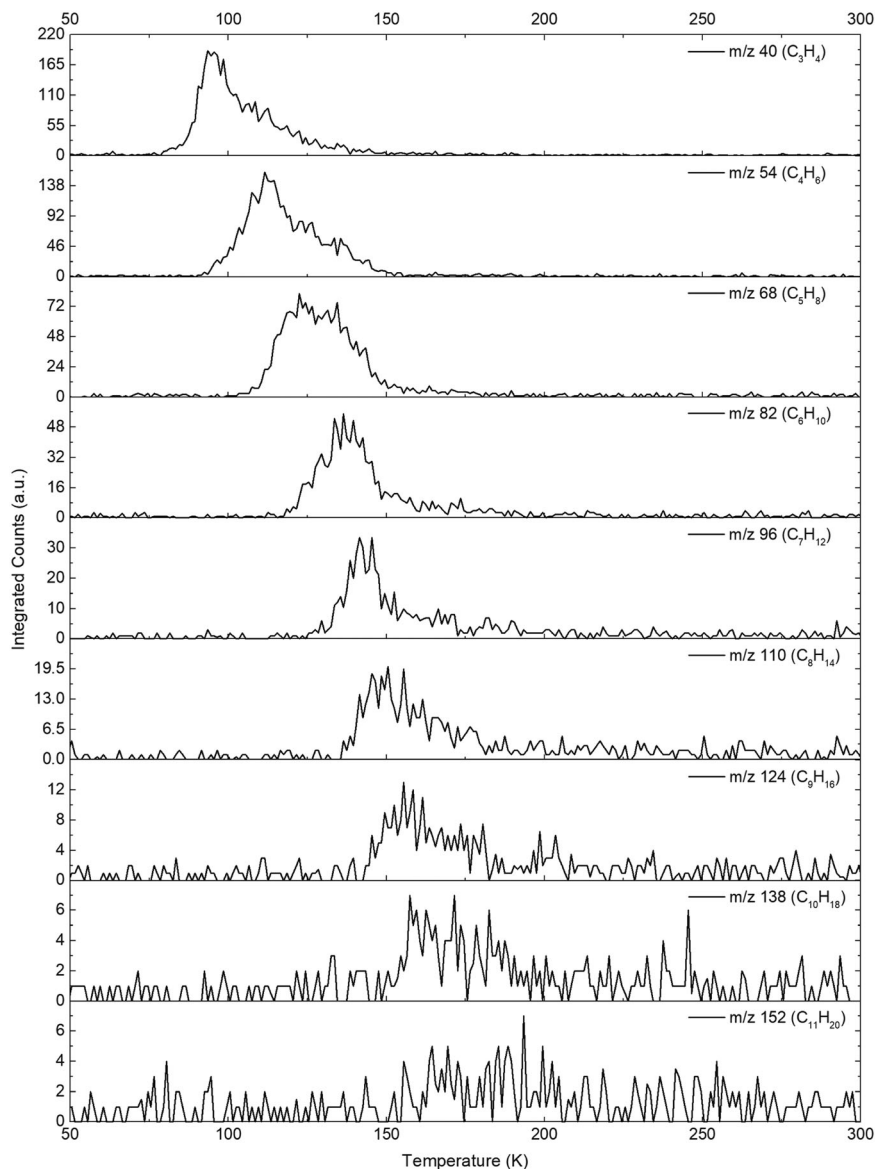


Fig. 11 TPD profiles recorded after broadband photolysis via PI-ReTOF-MS for masses with the generic formula of  $C_nH_{2n-2}$  (alkynes, dienes, and/or cycloalkenes).

isomer ( $CH_3CH_2CH_2CH_3$ ; I.E. =  $10.5 \pm 0.1$  eV) can be confirmed as a product in all three experiments, because its only other isomer, *i*-butane ( $(CH_3)_2CHCH_3$ ; I.E. =  $10.68 \pm 0.11$  eV), has a higher ionization energy than used in the experiments. The detection of alkanes from  $n = 4-8$  shows that complex hydrocarbons are readily formed from pure methane even though only a few previous studies detected any hydrocarbons containing more than seven carbon atoms.<sup>60,61,78</sup> A recent study showed that the ethyl radical ( $C_2H_5$ ) was an important building block for the complex hydrocarbons formed in electron irradiated ethane ices as the hydrocarbons with an even number of carbons had a stronger signal.<sup>121</sup> However, in the methane processing both the methyl radical ( $CH_3$ ) and ethyl radical ( $C_2H_5$ ) were detected and the trend observed in irradiated ethane and ethylene ice products<sup>120,121</sup> was not detected in the methane product signals (*cf.* 4.8).

#### 4.3. $C_nH_{2n}$

The detected alkenes ( $C_nH_{2n}$ ) or D.B.E.s (cycloalkanes) displayed a slightly different trend between the three experiments as the electron irradiation PI-ReTOF-MS analysis detected  $n = 3-9$  while both photolysis experiments detected hydrocarbon ions with  $n = 3-10$ . The difference in the total number of carbon atoms incorporated is easily explained by the higher doses for the photolysis experiments, respectively, when compared to the electron irradiation dose of  $3.5$  eV molecule<sup>-1</sup>. Interestingly neither the  $C_9H_{18}$  nor  $C_{10}H_{20}$  saturated alkane relatives ( $C_9H_{20}/C_{10}H_{22}$ ) of this group were detected. Recent experiments irradiating pure ethane ices with 5 keV electrons were only able to detect up to  $C_{10}H_{20}$  for this group,<sup>121</sup> but irradiated ethylene ices produced alkenes, or their D.B.E.s, up to  $C_{16}H_{32}$ . Also,

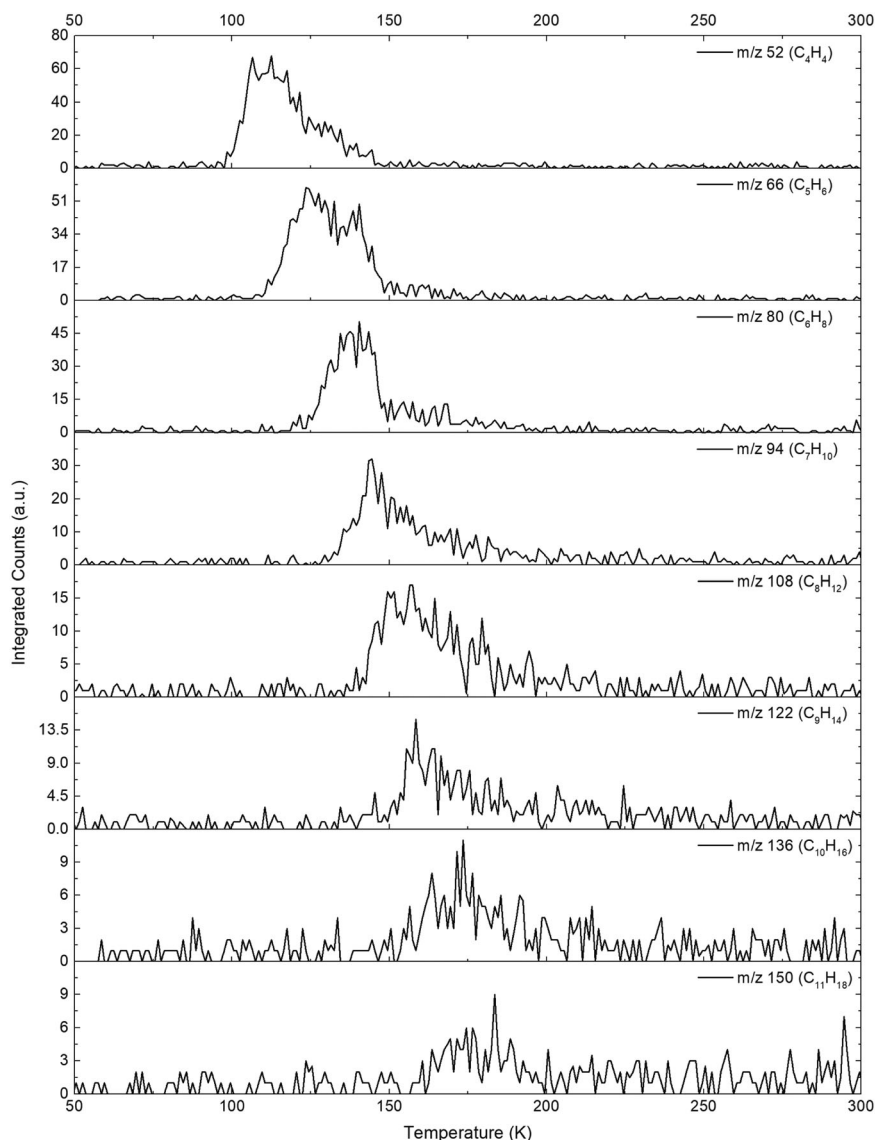


Fig. 12 TPD profiles recorded after broadband photolysis *via* PI-ReTOF-MS for masses with the generic formula of  $C_nH_{2n-4}$  (yne-ene, trienes, cycloalkenes, bi-cycloalkenes).

the detection of  $C_3H_6$  ions is very interesting here as there are only two possible isomers and one of these, propylene ( $CH_2CHCH_3$ ; I.E. = 9.73 eV), has been detected in the ISM<sup>124</sup> and its astrophysical formation route has been investigated.<sup>125,126</sup> The second  $C_3H_6$  isomer, cyclopropane (I.E. = 9.86 eV), is the simplest cyclic alkane that can be produced. Here, the identity of the ion signal at 10.49 eV is ambiguous, as both isomers are ionized if they were formed, but tunable photoionization experiments are being designed to discriminate which of these isomers are formed from pure methane ice irradiation. Several larger alkenes and cycloalkanes have been studied in the lab to understand how they contribute to astrophysical polymer formation,<sup>127</sup> to determine their contribution of unsaturated products in the ISM,<sup>128</sup> to understand the chemical reactions that occur with PAH formation,<sup>129</sup> and as well with modeling gas phase reactions relevant to Titan's atmosphere.<sup>130</sup>

#### 4.4. $C_nH_{2n-2}$

The ion signals related to alkynes or their D.B.E.s were detected at  $n = 3-9$  for the electron irradiation experiment and  $n = 3-11$  for both photolysis experiments. While the electron irradiation products follow the same trend in size as the previous group the photolysis experiments produced an even larger hydrocarbon with the general formula  $C_{11}H_{20}$ . Although this group has been detected with FTIR *via* acetylene in several previous studies only one study detected another specific molecule relevant to this group: allene ( $H_2CCCH_2$ ).<sup>80</sup> In the present experiment an ion signal corresponding to  $C_3H_4$  was detected, however, this could be due to methyl acetylene ( $CH_3CCH$ ; I.E. = 10.36 eV), allene ( $H_2CCCH_2$ ; I.E. = 9.69 eV), or cyclopropene ( $c-C_3H_4$ ; I.E. = 9.67 eV)<sup>123</sup> and further experiments are needed to understand which isomers are produced as well as their yields.

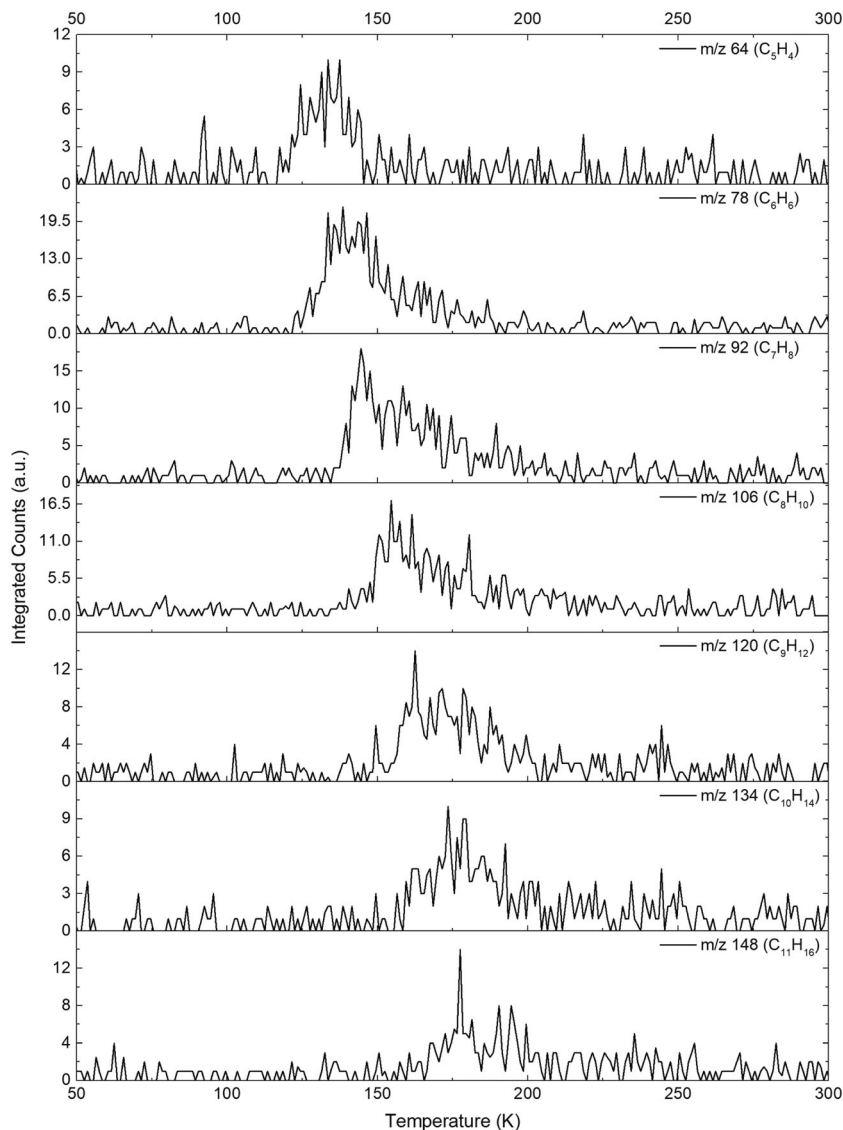


Fig. 13 TPD profiles recorded after broadband photolysis via PI-ReTOF-MS for masses with the generic formula of  $C_nH_{2n-6}$  (yne-diene, diynes, tetraenes, cyclotrialkenes, tri-cycloalkenes).

Methyl acetylene has been observed in several sources SgrB2, PKS 1830-211, and L1544.<sup>131-133</sup> Not only is methyl acetylene a molecule of astrophysical interest due to its interstellar detection, but methyl acetylene and allene have been used to better understand Titan's chemistry.<sup>134-136</sup> In the present experiment though several larger alkynes, or their D.B.E.s, were detected for the first time using PI-ReTOF-MS. One of these larger hydrocarbons was at an ion signal for  $C_4H_6$  which could belong to 1,3-butadiene ( $H_2CCHCHCH_2$ ; I.E. = 9.07 eV), 1,2-butadiene ( $H_2CCCH(CH_3)$ ; I.E. = 9.03 eV), 1-butyne ( $HCCC_2H_5$ ; I.E. = 10.18 eV), and/or 2-butyne ( $CH_3CCCH_3$ ; I.E. = 9.58 eV).<sup>123</sup> This group of isomers is very important as 1,3-butadiene is an essential building block in gas phase growth of prototypical PAHs.<sup>137,138</sup> Other possible molecules detected in this group have also been studied for their relevance to PAH formation such as isoprene ( $CH_2C(CH_3)CHCH_2$ ;

I.E. = 8.86 eV) with dicarbon ( $C_2$ ) producing the benzyl radical ( $C_6H_5CH_2$ ).<sup>139</sup>

#### 4.5. $C_nH_{2n-4}$

The next unsaturated group can be identified as yne-enes, trienes, cycloalkenes, or bicycloalkenes with  $n = 4-9$  for the electron irradiation product ions and  $n = 4-11$  for the photolysis experiments with all three product groups following the same length trend as the previous group. This hydrocarbon group was recently detected as the most highly unsaturated product group from pure ethane ice irradiation.<sup>121</sup> This group contained the ion signal for  $C_4H_4$  which has the astrophysically important isomer vinyl acetylene ( $H_2CCHCCH$ ; I.E. = 9.58 eV) associated with it.<sup>123</sup> Vinyl acetylene has been studied several times as a possible hydrocarbon important for Titan's chemistry,<sup>136,140,141</sup> as well as a reactant to produce prototype PAHs such as

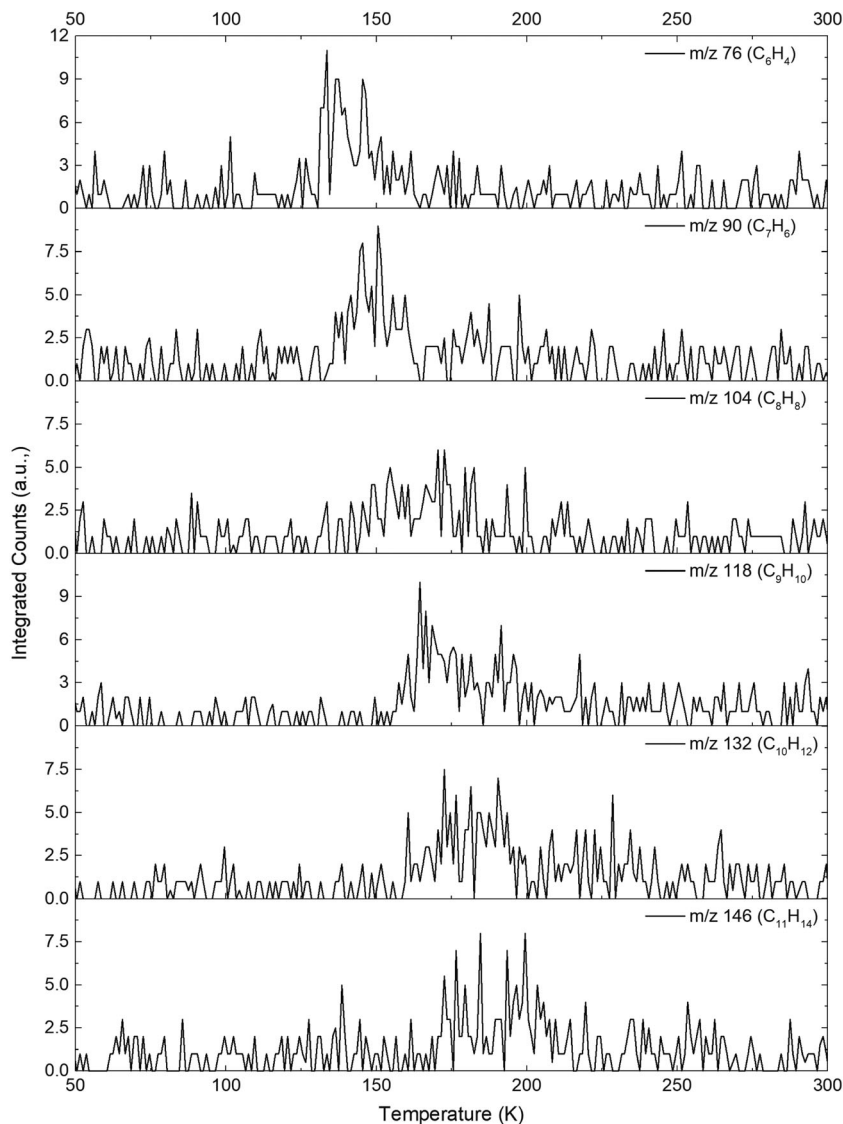


Fig. 14 TPD profiles recorded after broadband photolysis via PI-ReTOF-MS for masses with the generic formula of  $C_nH_{2n-8}$  (yne-triene, diyne-ene, pentaenes, tri-cyclobialkenes).

naphthalene ( $C_{10}H_8$ ),<sup>142</sup> 2-methylnaphthalene ( $C_{11}H_{10}$ ),<sup>143</sup> and 1-methylnaphthalene ( $C_{11}H_{10}$ ).<sup>144</sup>

#### 4.6. $C_nH_{2n-6}$

The electron irradiation products for this group consisted of  $n = 6-7$  and  $n = 5-11$  for the photolysis studies. Although this unsaturated group was not detected in ethane irradiation<sup>121</sup> it was detected in ethylene irradiation.<sup>120</sup> However, the simplest ion formula for this group,  $C_4H_2$ , was not detected in any of the investigations of this manuscript showing that diacetylene is not produced in methane ices by electrons or UV photons. Another astrophysically important molecule, benzene ( $c-C_6H_6$ ), may have been produced though as the ion signal for  $C_6H_6$  was detected in all three of the investigations. Benzene has been detected in several atmosphere's including Titan,<sup>145,146</sup> Jupiter, and Saturn<sup>147</sup> as well as in the proto-planetary nebula CRL 618.<sup>148</sup> Benzene has been shown to be synthesized in the gas phase,<sup>149</sup>

as well as being an important gas phase precursor to PAHs by reacting with phenyl radicals ( $C_6H_5$ ),<sup>150</sup> carbon atoms,<sup>151,152</sup> dicarbon,<sup>153</sup> and tricarbon molecules<sup>154</sup> to produce diphenyl ( $C_6H_5C_6H_5$ ), 1,2-didehydrocycloheptatrienyl radical ( $C_7H_5$ ), phenylethynyl radical ( $C_6H_5CC$ ), and phenyltricarbon ( $C_6H_5CCC$ ), respectively.

#### 4.7. $C_nH_{2n-8}$

For the  $C_nH_{2n-8}$  group a deviation from the previous groups occurred as there were no electron irradiation products detected for this group. However, both photolysis experiments detected product ions at  $n = 6-11$ . As discussed earlier the detection of products belonging to this group only from the photolysis experiments is likely due to these methane ices receiving a much larger energy dose per molecule. This group represents the most highly unsaturated hydrocarbon group detected in any of the three different experiments discussed here. The smallest hydrocarbon

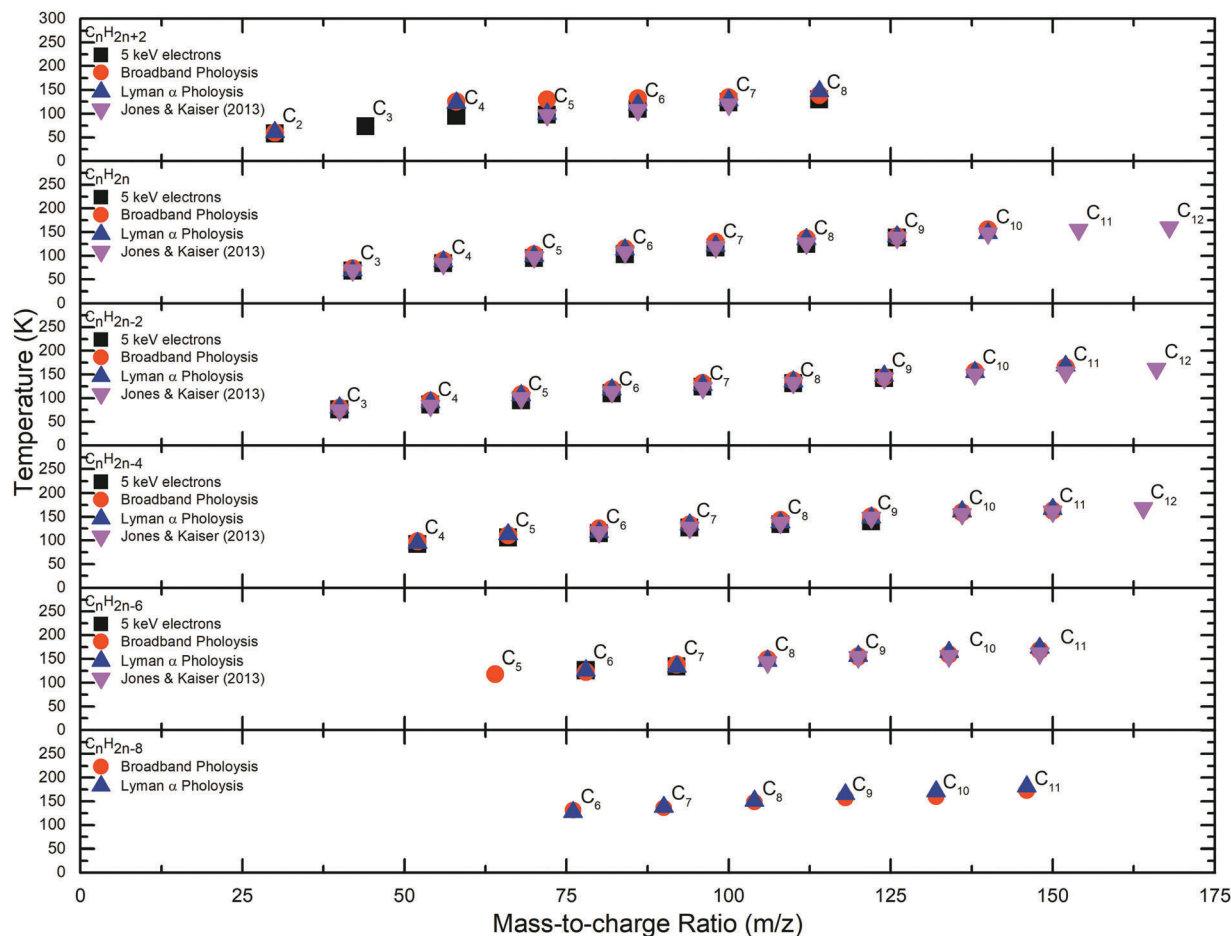


Fig. 15 Sublimation onset temperatures of  $C_nH_{2n+2}$  ( $n = 2-8$ ),  $C_nH_{2n}$  ( $n = 3-12$ ),  $C_nH_{2n-2}$  ( $n = 3-12$ ),  $C_nH_{2n-4}$  ( $n = 4-12$ ),  $C_nH_{2n-6}$  ( $n = 5-11$ ) and  $C_nH_{2n-8}$  ( $n = 6-11$ ) after irradiation with electrons (black squares), broadband photons (red circles), Lyman  $\alpha$  photons (blue triangles), and a higher dose (12.5 eV molecule<sup>-1</sup>) of 5 keV electrons from Jones and Kaiser (2013)<sup>77</sup> (pink triangles).

in this group was identified as  $C_6H_4$  and theoretical studies have been performed to elucidate the pathways to different  $C_6H_4$  isomers from acetylene.<sup>155</sup> One of these isomers, *ortho*-benzynes (*o*- $C_6H_4$ ), has been detected as a gas phase product due to the reaction of ethynyl radical with vinyl acetylene.<sup>156</sup> Another important molecule from this group includes fulvenallene ( $C_7H_6$ ) which was reacted with both atomic carbon<sup>157</sup> and the hydroxyl radical<sup>158</sup> to investigate a PAH precursor, the fulvenallenyl radical. The reaction of ethynyl radicals with styrene ( $C_6H_5C_2H_3$ ), another molecule belonging to this highly unsaturated group, was also studied to investigate PAH growth pathways.<sup>159</sup> Styrene has also been shown to form in the gas phase from the bimolecular collision of ethylene and phenyl radicals.<sup>160</sup>

#### 4.8. Reaction mechanism & carbon budget

The detection of the products propane [ $C_3H_8(C_3D_8)$ ], ethane [ $C_2H_6(C_2D_6)$ ], ethyl radical [ $C_2H_5(C_2D_5)$ ], ethylene [ $C_2H_4(C_2D_4)$ ], acetylene [ $C_2H_2(C_2D_2)$ ], and the methyl radical [ $CH_3(CD_3)$ ] *via* infrared spectroscopy allows for the kinetic fitting *via* the numerical solving of coupled differential equations for each product's column density with code written for the MATLAB platform (Fig. 16–18).<sup>161,162</sup> The reaction scheme used to solve

the kinetic fits is shown in Fig. 19 and the numerically solved rate constants are compiled in Table 4. Although many more complex species than those presented in Fig. 19 were detected only species that could be uniquely identified in the FTIR analysis, and therefore confidently quantified, were used in the reaction scheme, or the possible radical or excited state species related to those detected *via* FTIR. A previous study disclosed that the 5 keV electron irradiation of pure methane ice resulted in multiple decomposition pathways leading to more complex hydrocarbons.<sup>75</sup> Interestingly all three of the different experimental systems described in this manuscript can be explained using the same reaction scheme; however, the rate constants of each reaction vary from one system to the next by orders of magnitude for several of the pathways showing that each irradiation source initiates a unique chemistry within the ice. By kinetically fitting the experimental data, and assuming that methane undergoes a first-order decay, the decomposition of methane upon irradiation produced methyl radicals (reaction (1)). These methyl radicals are then capable of producing internally excited ethane molecules ( $[C_2H_6]^*$ ) (reaction (2)). However, a secondary decomposition pathway of methane, *via* pseudo first-order kinetics of methane dimers, can also produce internally excited ethane molecules *via* two methane molecules

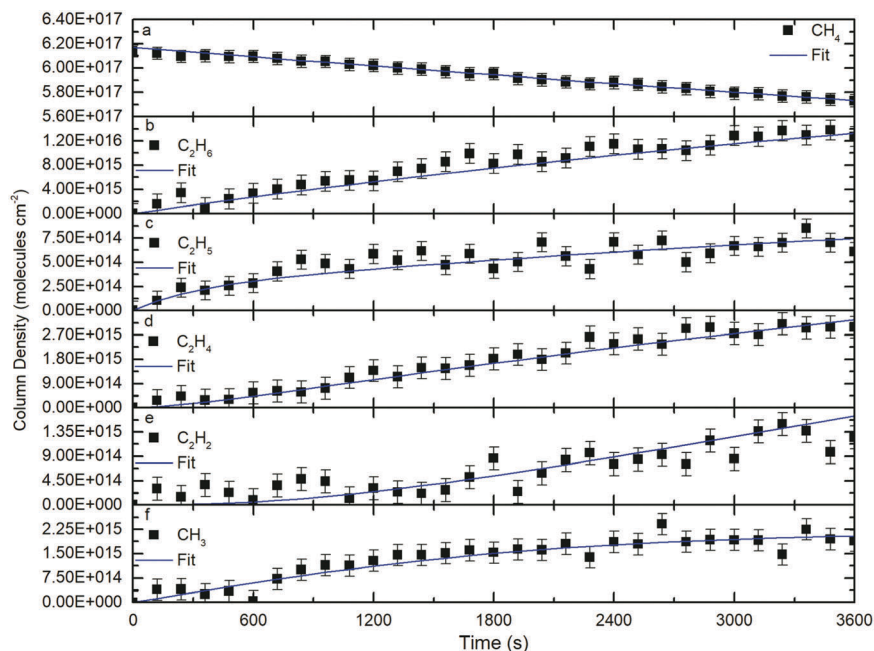


Fig. 16 Temporal evolution during electron irradiation and kinetic fitting of column densities of (a) methane, (b) ethane, (c) ethyl radical, (d) ethylene, (e) acetylene, and the (f) methyl radical. Rate constants derived from the kinetic fitting are compiled in Table 4.

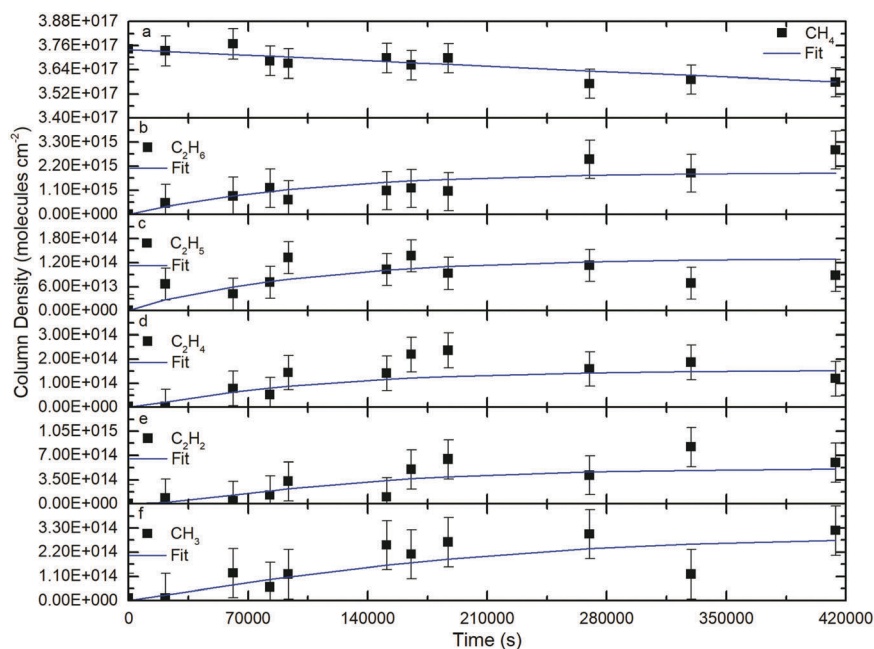
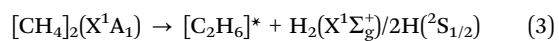
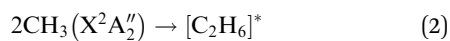
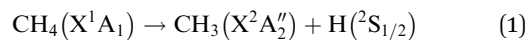


Fig. 17 Temporal evolution during broadband photolysis and kinetic fitting of column densities of (a) methane, (b) ethane, (c) ethyl radical, (d) ethylene, (e) acetylene, and the (f) methyl radical. Rate constants derived from the kinetic fitting are compiled in Table 4.

eliminating molecular hydrogen or two hydrogen atoms in a one-step formation route (reaction (3)).



In reactions (1)–(3) the corresponding rate constants ( $k_1 - k_3$ ) show that the electron irradiated system proceeded faster than either of the photolysis experiments (Table 4). The internally excited ethane was then shown to stabilize by phonon interaction with the matrix (reaction (4)), as well as through decomposition *via* atomic and molecular hydrogen elimination (reactions (5) and (6)). Comparing the rate constants of reactions (4)–(6) revealed that the dominant pathway was reaction (4) across

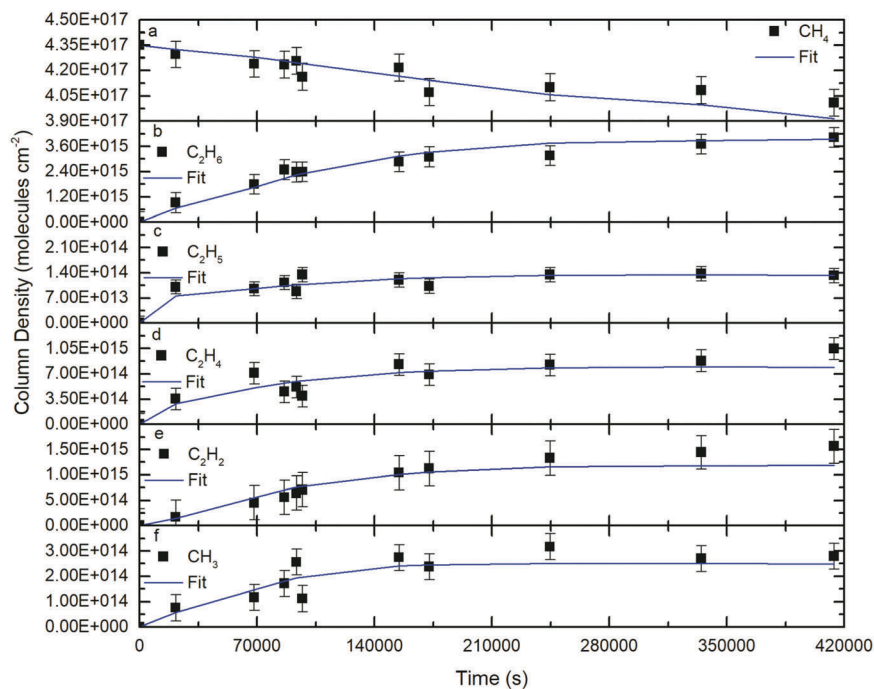


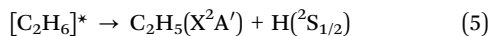
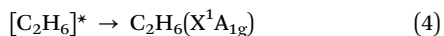
Fig. 18 Temporal evolution during Lyman  $\alpha$  photolysis and kinetic fitting of column densities of (a) methane, (b) ethane, (c) ethyl radical, (d) ethylene, (e) acetylene, and the (f) methyl radical. Rate constants derived from the kinetic fitting are compiled in Table 4.

Table 4 Rate constants calculated *via* the solution of the coupled differential equations for the reaction scheme in Fig. 19

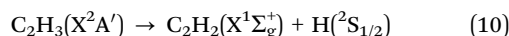
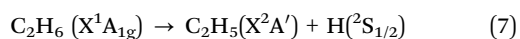
Reaction	Electrons ( $s^{-1}$ )	Broadband photons ( $s^{-1}$ )	Lyman $\alpha$ photons ( $s^{-1}$ )
$CH_4 \rightarrow CH_3 + H$	$k_1 = 6.02 \times 10^{-3}$	$k_1 = 1.15 \times 10^{-5}$	$k_1 = 2.26 \times 10^{-5}$
$2CH_3 \rightarrow C_2H_6^*$	$k_2 = 3.55 \times 10^{-16 a}$	$k_2 = 2.39 \times 10^{-17 a}$	$k_2 = 7.19 \times 10^{-17 a}$
$2CH_4 \rightarrow C_2H_6^* + 2H/H_2$	$k_3 = 5.64 \times 10^{-20 a}$	$k_3 = 5.04 \times 10^{-22 a}$	$k_3 = 1.04 \times 10^{-21 a}$
$C_2H_6^* \rightarrow C_2H_6$	$k_4 = 6.00 \times 10^{+5}$	$k_4 = 9.28 \times 10^{+3}$	$k_4 = 6.66 \times 10^{+1}$
$C_2H_6^* \rightarrow C_2H_5 + H$	$k_5 = 1.20 \times 10^{+5}$	$k_5 = 9.46 \times 10^{+2}$	$k_5 = 4.41 \times 10^{+1}$
$C_2H_6^* \rightarrow C_2H_4 + 2H/H_2$	$k_6 = 2.70 \times 10^{+4}$	$k_6 = 0.53 \times 10^{+1}$	$k_6 = 4.57 \times 10^{-2}$
$C_2H_6 \rightarrow C_2H_5 + H$	$k_7 = 4.85 \times 10^{-1}$	$k_7 = 3.17 \times 10^{-2}$	$k_7 = 2.41 \times 10^{-2}$
$C_2H_5 \rightarrow C_2H_4 + H$	$k_8 = 1.20 \times 10^{+1}$	$k_8 = 5.10 \times 10^{-1}$	$k_8 = 0.12 \times 10^{+1}$
$C_2H_4 \rightarrow C_2H_3 + H$	$k_9 = 0.21 \times 10^{+1}$	$k_9 = 4.33 \times 10^{-1}$	$k_9 = 6.47 \times 10^{-4}$
$C_2H_3 \rightarrow C_2H_2 + H$	$k_{10} = 7.20 \times 10^{+4}$	$k_{10} = 1.32 \times 10^{+3}$	$k_{10} = 5.63 \times 10^{+2}$
$C_2H_2 \rightarrow X$	$k_{11} = 6.00 \times 10^{-1}$	$k_{11} = 1.29 \times 10^{-1}$	$k_{11} = 1.85 \times 10^{-1}$
$C_2H_6 \rightarrow C_2H_4 + 2H/H_2$	$k_{12} = 6.01 \times 10^{-3}$	$k_{12} = 9.06 \times 10^{-8}$	$k_{12} = 2.35 \times 10^{-5}$
$C_2H_4 \rightarrow C_2H_2 + 2H/H_2$	$k_{13} = 6.06 \times 10^{-8}$	$k_{13} = 1.13 \times 10^{-5}$	$k_{13} = 2.04 \times 10^{-1}$

<sup>a</sup> Units  $cm^2 \text{ molecules}^{-1} s^{-1}$ .

all irradiation sources. However, the rate constants of reactions (5) and (6) showed that they were viable pathways in the proposed reaction mechanism as well.

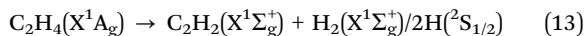
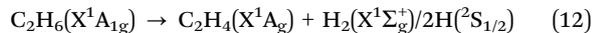


As the rate constants show these reactions take place very fast and the internally excited ethane molecule is rapidly stabilized. Each of these products formed from the internally excited ethane (reactions (4)–(6)) can also continue to produce more highly unsaturated species *via* the successive loss of hydrogen atoms (reactions (7)–(10)).

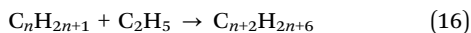
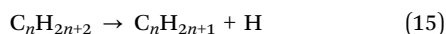
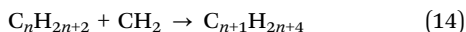


As previously mentioned, the same reaction scheme was used to fit all three experimental systems and the electron irradiation fits produced faster rate constants than either photolysis study, even for reactions (7)–(10). As infrared spectroscopy is not very sensitive and not very useful in determining large molecules we were unable to detect any other products *via* FTIR and therefore using the knowledge obtained from the PI-ReTOF-MS data a pathway to buildup these more complex (unknown) molecules (reaction (11)) must also be included. The production of these more highly unsaturated species from ethane and ethylene

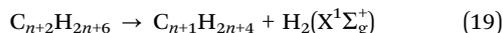
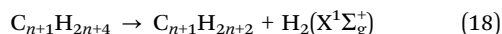
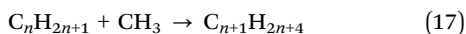
must also be accounted for by molecular hydrogen loss or two hydrogen atom loss in a one-step formation route (reactions (12) and (13)), respectively.<sup>121</sup>



also showed that even more complex hydrocarbons can be produced from pure ethane ices and extrapolated this previous reaction mechanism to account for the build-up of larger molecules. First, carbene ( $\text{CH}_2$ ) presented a pathway to add one carbon unit at a time to produce larger alkanes, but the only alkane with an odd number of carbon atoms detected in those experiments was propane. Therefore, reaction (14) was only observed to occur for carbene insertion into ethane producing propane. However, a generic alkyl radical, formed from radiolysis (reaction (15)), can readily recombine with another alkyl radical (reaction (16)) to produce a larger alkane that has grown by two carbon atoms.



Another recent work showed that ethylene produced complex hydrocarbons and extrapolated the previously determined reaction network<sup>163</sup> to include the production of larger hydrocarbons.<sup>120</sup> Although, reaction pathways (14)–(16) provide a reasonable explanation for the complex products observed in ethane and ethylene irradiation an alternative pathway also exists in methane *via* the reaction of the methyl radical with a neighboring alkyl radical (reaction (17)). This accounts for the production of the odd alkanes along with reaction (14), but was not incorporated into the ethane or ethylene reaction networks as there were no methyl radicals observed from irradiation. Finally, these larger alkanes can produce more highly unsaturated products (reactions (18) and (19)).



Most of these reactions, excluding radical–radical recombination, are endoergic by a few electron volts. But recall that the impinging electrons deposited on average  $3.5 \pm 1.1$  eV into the methane ice while the Lyman  $\alpha$  delivered an average of  $150 \pm 20$  eV and the broadband photolysis supplied an average of  $230 \pm 60$  eV providing the necessary energy to overcome reaction barriers in each of these reactions. The difference in average energy delivered in each experiment likely explains the difference in rate constants as many of the reaction pathways are endoergic and need an energy source to be initiated. Furthermore, the different initial energies of the radiation sources, 5 keV electrons and 7.3–11 eV photons, may also explain the increased values of

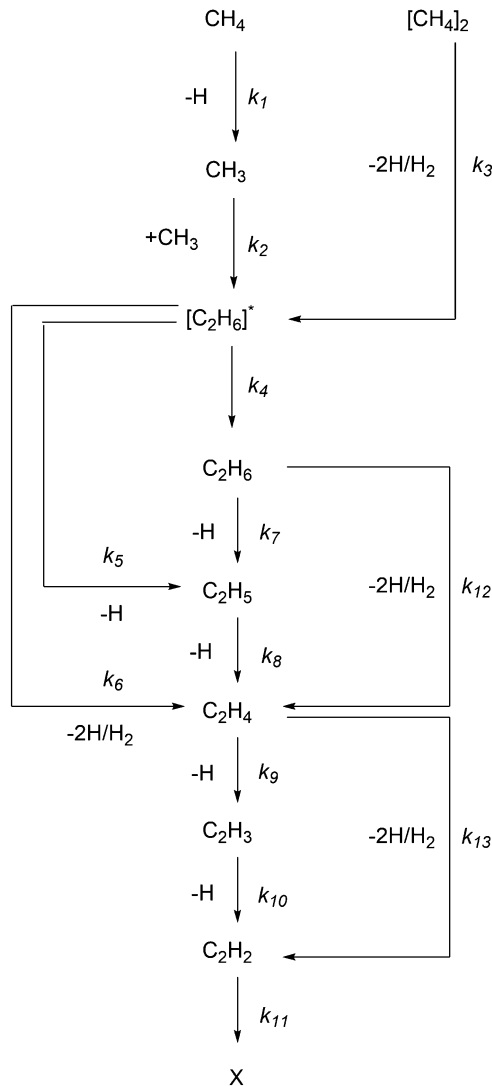


Fig. 19 Chemical reaction scheme utilized in the coupled differential equation fitting for the column densities of methane and the products from its radiolysis.

the electron induced rate constants compared to the photolysis initiated reactions.

A comparison of the temporal profiles (Fig. 16–18) for the electron irradiation, broadband photolysis, and Lyman  $\alpha$  photolysis (Table 5) shows that overall the three experiments discussed have a similar outcome for product abundance with some interesting differences. The most abundant product at the end of irradiation was ethane (23–59%) in all three experiments. Meanwhile, the ethyl radical was the least abundant product across all experiments, and the methyl radical had a nearly similarly low abundance of about 1–4% of the total carbon consumed from methane in each experiment. However, a discrepancy between the three experiments arises when comparing the abundances of ethylene and acetylene. In the electron irradiation, the ethylene product is the second most abundant product (15%) while acetylene is the third (5%); however, broadband photolysis resulted in ethylene being less than 1% of the carbon

Table 5 Carbon mass balance

Species	Change in column density <sup>a</sup>					
	Electrons	% Carbon consumed	Broadband photons	% Carbon consumed	Lyman $\alpha$ photons	% Carbon consumed
CH <sub>4</sub>	$-3.76 \pm 0.68 \times 10^{16}$	—	$-1.66 \pm 0.45 \times 10^{15}$	—	$-3.42 \pm 0.53 \times 10^{16}$	—
CH <sub>3</sub>	$1.50 \pm 0.78 \times 10^{15}$	4	$3.07 \pm 0.89 \times 10^{14}$	2	$2.79 \pm 3.20 \times 10^{14}$	1
C <sub>2</sub> H <sub>2</sub>	$2.03 \pm 0.50 \times 10^{15}$	5	$1.18 \pm 0.29 \times 10^{15}$	7	$3.12 \pm 0.44 \times 10^{15}$	9
C <sub>2</sub> H <sub>4</sub>	$5.44 \pm 1.30 \times 10^{15}$	15	$5.78 \pm 2.37 \times 10^{13}$	0.35	$2.09 \pm 0.60 \times 10^{15}$	6
C <sub>2</sub> H <sub>5</sub>	$1.14 \pm 0.33 \times 10^{15}$	3	$4.40 \pm 2.11 \times 10^{13}$	0.27	$8.32 \pm 2.46 \times 10^{13}$	0.24
C <sub>2</sub> H <sub>6</sub>	$2.22 \pm 0.28 \times 10^{16}$	59	$5.43 \pm 0.89 \times 10^{15}$	33	$7.93 \pm 0.93 \times 10^{15}$	23
Total % carbon in products		86 $\pm$ 20		42 $\pm$ 20 <sup>b</sup>		39 $\pm$ 12 <sup>b</sup>

<sup>a</sup> Only peaks that did not need deconvolution were used to calculate changes in the column densities. <sup>b</sup> The total amount of carbon present in the products does not reach 100% and the remaining carbon can be accounted for by the more complex hydrocarbons as detected in these experiments via PI-ReTOF-MS.

consumed from methane destruction while acetylene was the second most abundant product (7%). Finally, Lyman  $\alpha$  photolysis generated acetylene as its second most abundant product (9%), and ethylene as its third most abundant product (6%). Here, the photolysis experiments both generated more acetylene and less ethylene than the electron irradiation experiment. A possible explanation for this difference is the larger dose introduced into the Lyman  $\alpha$  (150 eV molecule<sup>-1</sup>) and broadband (230 eV molecule<sup>-1</sup>) photolyzed ices compared to the electron irradiated ice (3.5 eV molecule<sup>-1</sup>). This corresponds well with the proposed reaction schemes<sup>75,163,164</sup> for simple hydrocarbons becoming further unsaturated to produce acetylene as well as more complex species. Both of these criteria are met as the VUV photolysis studies both generated more acetylene as well as more highly unsaturated product groups than the electron irradiation experiment.

Although the higher dose is a reasonable justification alternate pathways may exist. Other experiments showed that pure methane at 3 K irradiated with Lyman  $\alpha$  light formed the methyl radical and not the methylidene or carbene radical, but when the methane was dispersed in an inert neon matrix and photolyzed the methyl radical and methylidene radical were detected.<sup>83</sup> It was postulated that carbene was also a product, as the energy needed to produce this molecule was well below that of the impinging Lyman  $\alpha$  photons, but it was not detected. This result shows that although the possible reaction pathway through successive dehydrogenation of methane to produce these radicals is feasible the non-detection of carbene and methylidene does not allow for a useful incorporation into the reaction scheme. It is interesting though that the two most abundant products from the photolysis studies in the present manuscript were ethane and acetylene, which are the result of recombination of two methyl radicals, or methylidene radicals, respectively. Interestingly these were the two radicals detected from the photolyzed methane in neon studies. Meanwhile the recombination of two carbene radicals, a radical which was not detected in the photolyzed methane in neon studies, produces ethylene and in the present photolysis studies was determined to be a minor product. Another interesting prospect is that the VUV photons readily convert the ethylene to acetylene. The photodissociation cross section of ethylene with Lyman  $\alpha$  photons

was determined to be  $2.36 \times 10^{-17}$  cm<sup>2</sup>.<sup>165</sup> The lowest energy channel for the destruction of gaseous ethylene with VUV photons was shown to produce acetylene and molecular hydrogen.<sup>166</sup> This was shown to be true for ethylene ice as well where pure ethylene films were irradiated with 8.4, 10.0, 11.6–11.8, and 21.2 eV photons, and acetylene was detected as the dominant product.<sup>167</sup> Contributing to the validity of this hypothesis is the fact that the abundance of ethylene in the broadband photolysis (0.35%) is much lower than that in the Lyman  $\alpha$  photolysis (6%), which suggests that there is an efficient ethylene destruction and/or conversion of ethylene to acetylene with photons other than at Lyman  $\alpha$  (121.6 nm). However, similar processes should be occurring with the ethane products as well, but the abundance is closer to the electron irradiation abundance and larger than the Lyman  $\alpha$  photolysis amount. Here, the photodissociation cross section of ethane with Lyman  $\alpha$  photons was determined to be  $2.26 \times 10^{-17}$  cm<sup>2</sup>,<sup>165</sup> but the dissociation produces the ethyl radical and atomic hydrogen. Although ethane photolysis can produce ethylene and molecular hydrogen this pathway was shown to be less important as the photon energy increases,<sup>168</sup> and could readily recombine with a hydrogen atom to reform an ethane molecule.

Finally, a recent experiment proposed branching ratios for the photolysis of methane into methyl (95%), carbene (4%), and methylidene radicals (2%), but these were based on indirect measurements<sup>84</sup> from fragmentation patterns in the gas phase after sublimation of a processed methane ice. Another study observed the methyl radical, but not that of the carbene radical and noted it is a known product of gaseous methane UV photolysis.<sup>80</sup> They also reported abundances after irradiation for ethane (8.0%) and ethylene (2.6%) corresponding to a ratio of 3.1 : 1, which is very close to the ratio observed in the Lyman  $\alpha$  experiments of this paper 3.8 : 1 (Table 5). A recent study also attempted to use the product abundance ratios of ethane and ethylene, ignoring secondary photodissociation, to infer the branching ratios of the methane reactant ice to methyl and carbene radicals.<sup>82</sup> However, it is obvious that this is not a safe assumption as ethylene readily takes part in further reactions. Interestingly another experiment also irradiated pure methane ices and found that they could account for the production of ethane and acetylene with neighboring methyl

and methylidene radicals, respectively, formed from methane dehydrogenation after irradiation, but not for ethylene.<sup>77</sup>

## 5. Conclusions

The different radiation sources used in the present manuscript were chosen to provide a representation of the possible ionizing radiation that can process an interstellar ice over its lifetime. Secondary electrons readily form in the track of GCRs as they pass through interstellar ices, and in dense clouds this is a major source of ionizing radiation as the cosmic UV field photons are not able to penetrate deep into the cloud.<sup>169</sup> However, these GCRs do induce an internal UV radiation field ( $\lambda < 13.6$  eV) with a flux of  $10^3$  photons  $\text{cm}^{-2} \text{s}^{-1}$ .<sup>53</sup> The dose imparted by UV photons, at an average photon energy of 10 eV, was estimated for the different regions of interstellar clouds and after  $10^6$  years ices in diffuse clouds receive  $2.36 \times 10^5$  eV molecule<sup>-1</sup> and 0.82 eV molecule<sup>-1</sup> for dense clouds.<sup>101</sup> These UV doses for interstellar ices show a very significant difference between diffuse and dense clouds displaying how ineffectively UV photons process ices within dense clouds. The broadband and Lyman  $\alpha$  photolysis experiments here are able to represent a partially processed diffuse cloud's ice or an ice partially shielded within a dense interstellar cloud. Calculations also suggest that GCRs deliver approximately 1–30 eV molecule<sup>-1</sup> to ices in diffuse clouds and between 1–3 eV molecule<sup>-1</sup> for dense clouds at the same lifetime.<sup>101</sup> In the present experiment the energetic electrons simulate those generated from GCRs and the calculated dose matches very nicely to an ice in a dense cloud or a mildly processed ice in a diffuse cloud. These experimental conditions can also be extrapolated to other environments as well as, for example, Pluto, which is processed with Lyman  $\alpha$  photons,<sup>170</sup> and the solar wind<sup>171</sup> deposits a dose of about 36 eV for each methane molecule per orbital period. These very different environments need to be systematically studied to fully understand the complex hydrocarbon chemistry taking place in the interstellar medium as well as on other objects such as comets and trans-Neptunian objects (TNOs) from the simplest hydrocarbon, methane.

Methane ices have been detected in the interstellar medium with abundances up to 11% with respect to water<sup>50</sup> as well as on several outer solar system objects such as Pluto.<sup>7</sup> These detections, along with the knowledge that simple hydrocarbons (C1 and C2) are important reactants for aromatics from benzene<sup>172</sup> to PAHs,<sup>173</sup> reinforce just how important hydrocarbon chemistry is to astrochemistry. Although several previous studies of pure methane irradiation from different sources did detect products larger than C2 we show for the first time that molecules with very high degrees of unsaturation ( $\text{C}_n\text{H}_{2n-8}$ ) are even able to be produced. Multiple groups contain molecules that have been shown to be very important in other interesting astrochemical pathways as discussed in the previous section. However, a pure methane ice is not a perfect simulation as methane is typically found mixed with other compounds such as water in interstellar ices<sup>50</sup> and this has been previously

studied.<sup>81,82,174</sup> A previous study on a binary mixture of methane diluted in water ice was carried out to better understand the products of cometary ices from the ISM as surveys have detected methane, ethane, and acetylene, but not ethylene in the comets C/1996 B2 Hyakutake<sup>39</sup> and C/1995 O1 Hale-Bopp,<sup>175</sup> and this study also did not detect ethylene in their laboratory ice experiments.<sup>174</sup> The cometary detection of ethane and acetylene along with the lack of detection of ethylene is interesting as these results match very closely to the broadband photolysis results from the current study, which provides further insight into the possible processing that these comets underwent.

Other ice mixtures containing methane have been studied to unravel the chemistry taking place on Pluto<sup>67,176–179</sup> and these studies found several hydrocarbons as well as oxygen bearing species and molecules containing both oxygen and nitrogen. There were also investigations done on unprocessed Pluto analog ices<sup>180–182</sup> to better characterize the spectra and physical properties of the possible ices present. These studies, along with the recent New Horizon mission to Pluto<sup>7</sup> that confirmed the presence of methane, show how important this simple hydrocarbon is not only for the interstellar medium, but within our solar system as well. This recent mission also confirmed the Lyman  $\alpha$  flux available to Pluto, which again directly relates to the results of this manuscript in the event that Pluto's atmosphere collapses. Other TNOs have been studied as well with the hydrocarbons being produced on Triton most likely due to atmospheric processing of methane with Lyman  $\alpha$  photons,<sup>176,183,184</sup> and Charon's solid methane is likely rapidly photolyzed by Lyman  $\alpha$  photons which then evaporates in warmer seasons and can react further to produce tholins<sup>7</sup> or more complex hydrocarbons as shown in this study. Furthermore, hydrocarbons, specifically alkanes, have been shown to react with carbon dioxide in ice mixtures producing carboxylic acids.<sup>185–187</sup> These carboxylic acids are building blocks which can react with glycerol to form the very important biomolecules known as lipids.

As stated above, multiple hydrocarbon groups have been shown to hold important astrophysical implications and isomer-specific experiments are currently being designed to untangle the chemistry and detailed formation pathways of the C3 and C4 hydrocarbons as these have been proven to be a key reactant for the formation of PAHs. Revealing which specific hydrocarbon isomers are produced within simple astrophysical ice analogs will greatly assist in our understanding of the role that ice chemistry plays with PAH formation.

## Conflicts of interest

There are no conflicts to declare.

## Acknowledgements

RIK and MJA thank the US National Science Foundation (AST-1505502) for support to conduct the experiments and data analysis. The experimental setup was financed by the W. M. Keck Foundation through an equipment grant.

## References

- 1 S. C. Tegler, D. M. Cornelison, W. M. Grundy, W. Romanishin, M. R. Abernathy, M. J. Bovyn, J. A. Burt, D. E. Evans, C. K. Maleszewski, Z. Thompson and F. Vilas, *Astrophys. J.*, 2010, **725**, 1296–1305.
- 2 S. C. Tegler, W. M. Grundy, C. B. Olkin, L. A. Young, W. Romanishin, D. M. Cornelison and R. Khodadadkouchaki, *Astrophys. J.*, 2012, **751**, 76–86.
- 3 D. P. Cruikshank, T. L. Roush, J. M. Moore, M. V. Sykes, T. C. Owen, M. J. Bartholomew, R. H. Brown and K. A. Tryka, in *Pluto and Charon*, ed. S. A. Stern and D. J. Tholen, University of Arizona, Arizona, U.S.A., 1997, pp. 221–267.
- 4 S. Douté, B. Schmitt, E. Quirico, T. C. Owen, D. P. Cruikshank, C. de Bergh, T. R. Geballe and T. L. Roush, *Icarus*, 1999, **142**, 421–444.
- 5 V. Lorenzi, N. Pinilla-Alonso, J. Licandro, D. P. Cruikshank, W. M. Grundy, R. P. Binzel and J. P. Emery, *Astron. Astrophys.*, 2016, **585**, A131.
- 6 S. Protopapa, W. M. Grundy, S. C. Tegler and J. M. Bergonio, *Icarus*, 2015, **253**, 179–188.
- 7 W. M. Grundy, R. P. Binzel, B. J. Buratti, J. C. Cook, D. P. Cruikshank, C. M. Dalle Ore, A. M. Earle, K. Ennico, C. J. A. Howett, A. W. Lunsford, C. B. Olkin, A. H. Parker, S. Philippe, S. Protopapa, E. Quirico, D. C. Reuter, B. Schmitt, K. N. Singer, A. J. Verbiscer, R. A. Beyer, M. W. Buie, A. F. Cheng, D. E. Jennings, I. R. Linscott, J. W. Parker, P. M. Schenk, J. R. Spencer, J. A. Stansberry, S. A. Stern, H. B. Throop, C. C. C. Tsang, H. A. Weaver, G. E. Weigle and L. A. Young, *Science*, 2016, **351**, aad9189.
- 8 W. B. McKinnon, F. Nimmo, T. Wong, P. M. Schenk, O. L. White, J. H. Roberts, J. M. Moore, J. R. Spencer, A. D. Howard, O. M. Umurhan, S. A. Stern, H. A. Weaver, C. B. Olkin, L. A. Young, K. E. Smith and the New Horizons Geology, Geophysics and Imaging Theme Team, *Nature*, 2016, **534**, 82–85.
- 9 J. M. Moore, A. D. Howard, O. M. Umurhan, O. L. White, P. M. Schenk, R. A. Beyer, W. B. McKinnon, J. R. Spencer, W. M. Grundy, T. R. Lauer, F. Nimmo, L. A. Young, S. A. Stern, H. A. Weaver, C. B. Olkin and K. Ennico, *Icarus*, 2017, **287**, 320–333.
- 10 W. M. Grundy, D. P. Cruikshank, G. R. Gladstone, C. J. A. Howett, T. R. Lauer, J. R. Spencer, M. E. Summers, M. W. Buie, A. M. Earle, K. Ennico, J. W. Parker, S. B. Porter, K. N. Singer, S. A. Stern, A. J. Verbiscer, R. A. Beyer, R. P. Binzel, B. J. Buratti, J. C. Cook, C. M. Dalle Ore, C. B. Olkin, A. H. Parker, S. Protopapa, E. Quirico, K. D. Retherford, S. J. Robbins, B. Schmitt, J. A. Stansberry, O. M. Umurhan, H. A. Weaver, L. A. Young, A. M. Zangari, V. J. Bray, A. F. Cheng, W. B. McKinnon, R. L. McNutt, J. M. Moore, F. Nimmo, D. C. Reuter, P. M. Schenk and the New Horizons Science Team, *Nature*, 2016, **539**, 65–68.
- 11 W. M. Grundy and M. W. Buie, *Icarus*, 2001, **153**, 248–263.
- 12 C. B. Olkin, E. F. Young, L. A. Young, W. Grundy, B. Schmitt, A. Tokunaga, T. Owen, T. Roush and H. Terada, *Astron. J.*, 2007, **133**, 420.
- 13 W. M. Grundy, C. B. Olkin, L. A. Young, M. W. Buie and E. F. Young, *Icarus*, 2013, **223**, 710–721.
- 14 W. M. Grundy and U. Fink, *Icarus*, 1996, **124**, 329–343.
- 15 A. H. Parker, M. W. Buie, W. M. Grundy and K. S. Noll, *Astrophys. J., Lett.*, 2016, **825**, L9.
- 16 M. E. Brown, K. M. Barkume, G. A. Blake, E. L. Schaller, D. L. Rabinowitz, H. G. Roe and C. A. Trujillo, *Astron. J.*, 2007, **133**, 284–289.
- 17 J. Licandro, N. Pinilla-Alonso, M. Pedani, E. Oliva, G. P. Tozzi and W. M. Grundy, *Astron. Astrophys.*, 2006, **445**, L35–L38.
- 18 S. C. Tegler, W. M. Grundy, F. Vilas, W. Romanishin, D. M. Cornelison and G. J. Consolmagno, *Icarus*, 2008, **195**, 844–850.
- 19 B. J. Buratti, J. D. Hofgartner, M. D. Hicks, H. A. Weaver, S. A. Stern, T. Momary, J. A. Mosher, R. A. Beyer, A. J. Verbiscer, A. M. Zangari, L. A. Young, C. M. Lisse, K. Singer, A. Cheng, W. Grundy, K. Ennico and C. B. Olkin, *Icarus*, 2017, **287**, 207–217.
- 20 R. R. Hodges, *Geophys. Res. Lett.*, 2016, **43**, 6742–6748.
- 21 V. Formisano, S. Atreya, T. Encrenaz, N. Ignatiev and M. Giuranna, *Science*, 2004, **306**, 1758.
- 22 M. A. Barucci, F. Merlin, A. Guilbert, C. d. Bergh, A. Alvarez-Candal, O. Hainaut, A. Doressoundiram, C. Dumas, T. Owen and A. Coradini, *Astron. Astrophys.*, 2008, **479**, L13–L16.
- 23 C. A. Trujillo, M. E. Brown, D. L. Rabinowitz and T. R. Geballe, *Astrophys. J.*, 2005, **627**, 1057.
- 24 A. Delsanti, F. Merlin, A. Guilbert-Lepoutre, J. Bauer, B. Yang and K. J. Meech, *Astron. Astrophys.*, 2010, **520**, A40–A55.
- 25 D. P. Cruikshank, T. L. Roush, T. C. Owen, T. R. Geballe, C. de Bergh, B. Schmitt, R. H. Brown and M. J. Bartholomew, *Science*, 1993, **261**, 742–745.
- 26 R. H. Brown, D. P. Cruikshank, J. Veverka, P. Helfenstein and J. Eluszkiewicz, in *Neptune and Triton*, ed. D. P. Cruikshank, University of Arizona, Arizona, U.S.A., 1995, pp. 991–1030.
- 27 B. J. Holler, L. A. Young, W. M. Grundy and C. B. Olkin, *Icarus*, 2016, **267**, 255–266.
- 28 W. M. Grundy, L. A. Young, J. A. Stansberry, M. W. Buie, C. B. Olkin and E. F. Young, *Icarus*, 2010, **205**, 594–604.
- 29 W. M. Grundy, M. W. Buie and J. R. Spencer, *Astron. J.*, 2002, **124**, 2273.
- 30 M. E. Brown, A. J. Burgasser and W. C. Fraser, *Astrophys. J., Lett.*, 2011, **738**, L26–L30.
- 31 F. Merlin, A. Alvarez-Candal, A. Delsanti, S. Fornasier, M. A. Barucci, F. E. DeMeo, C. d. Bergh, A. Doressoundiram, E. Quirico and B. Schmitt, *Astron. J.*, 2009, **137**, 315.
- 32 E. L. Schaller and M. E. Brown, *Astrophys. J., Lett.*, 2007, **670**, L49–L51.
- 33 C. Morea Dalle Ore, M. A. Barucci, J. P. Emery, D. P. Cruikshank, L. V. Dalle Ore, F. Merlin, A. Alvarez-Candal, C. de Bergh, D. E. Trilling, D. Perna, S. Fornasier,

- R. M. E. Mastrapa and E. Dotto, *Astron. Astrophys.*, 2009, **501**, 349–357.
- 34 M. E. Brown, *Annu. Rev. Earth Planet. Sci.*, 2012, **40**, 467–494.
- 35 M. A. Barucci, C. M. D. Ore, A. Alvarez-Candal, C. D. Bergh, F. Merlin, C. Dumas and D. Cruikshank, *Astron. J.*, 2010, **140**, 2095.
- 36 H. B. Niemann, S. K. Atreya, S. J. Bauer, G. R. Carignan, J. E. Demick, R. L. Frost, D. Gautier, J. A. Haberman, D. N. Harpold, D. M. Hunten, G. Israel, J. I. Lunine, W. T. Kasprzak, T. C. Owen, M. Paulkovich, F. Raulin, E. Raaen and S. H. Way, *Nature*, 2005, **438**, 779–784.
- 37 O. Mousis, J. I. Lunine, A. G. Hayes and J. D. Hofgartner, *Icarus*, 2016, **270**, 37–40.
- 38 R. Samuelson, in *Solar System Ices*, ed. B. Schmitt, C. De Bergh and M. Festou, Springer Netherlands, Dordrecht, 1998, pp. 749–772.
- 39 M. J. Mumma, M. A. DiSanti, N. D. Russo, M. Fomenkova, K. Magee-Sauer, C. D. Kaminski and D. X. Xie, *Science*, 1996, **272**, 1310–1314.
- 40 M. J. Mumma, M. A. DiSanti, N. Dello Russo, K. Magee-Sauer, E. Gibb and R. Novak, *Adv. Space Res.*, 2003, **31**, 2563–2575.
- 41 E. L. Gibb, M. J. Mumma, N. Dello Russo, M. A. DiSanti and K. Magee-Sauer, *Icarus*, 2003, **165**, 391–406.
- 42 E. L. Gibb, B. P. Bonev, G. Villanueva, M. A. DiSanti, M. J. Mumma, E. Sudholt and Y. Radeva, *Astrophys. J.*, 2012, **750**, 102.
- 43 H. Kobayashi and H. Kawakita, *Astrophys. J.*, 2009, **703**, 121.
- 44 Y. L. Radeva, M. J. Mumma, G. L. Villanueva, B. P. Bonev, M. A. DiSanti, M. F. A'Hearn and N. Dello Russo, *Icarus*, 2013, **223**, 298–307.
- 45 P. Ehrenfreund and S. B. Charnley, *Annu. Rev. Astron. Astrophys.*, 2003, **38**, 427–483.
- 46 J. H. Lacy, J. S. Carr, N. J. Evans, II, F. Baas, J. M. Achtermann and J. F. Arens, *Astrophys. J.*, 1991, **376**, 556–560.
- 47 A. C. A. Boogert, W. A. Schutte, A. G. G. M. Tielens, D. C. B. Whittet, F. P. Helmich, P. Ehrenfreund, P. R. Wesselius, T. de Graauw and T. Prusti, *Astron. Astrophys.*, 1996, **315**, L377–L380.
- 48 E. L. Gibb, D. C. B. Whittet, A. C. A. Boogert and A. G. G. M. Tielens, *Astrophys. J., Suppl. Ser.*, 2004, **151**, 35–73.
- 49 K. I. Öberg, A. C. A. Boogert, K. M. Pontoppidan, G. A. Blake, N. J. Evans, F. Lahuis and E. F. v. Dishoeck, *Astrophys. J.*, 2008, **678**, 1032–1041.
- 50 A. C. A. Boogert, P. A. Gerakines and D. C. B. Whittet, *Annu. Rev. Astron. Astrophys.*, 2015, **53**, 541–581.
- 51 L. d'Hendecourt, L. Allamandola and J. Greenberg, *Astron. Astrophys.*, 1985, **152**, 130–150.
- 52 G. Strazzulla and R. E. Johnson, in *Comets in the Post-Halley Era*, ed. R. L. Newburn, Jr., M. Neugebauer and J. Rahe, Springer Netherlands, Dordrecht, 1991, pp. 243–275.
- 53 S. S. Prasad and S. P. Tarafdar, *Astrophys. J.*, 1983, **267**, 603–609.
- 54 L. A. Wall, D. W. Brown and R. R. Florin, *J. Phys. Chem.*, 1959, **63**, 1762–1769.
- 55 D. W. Brown, R. E. Florin and L. A. Wall, *J. Phys. Chem.*, 1962, **66**, 2602–2612.
- 56 B. Smaller and M. S. Matheson, *J. Chem. Phys.*, 1958, **28**, 1169–1178.
- 57 R. E. Florin, D. W. Brown and L. A. Wall, *J. Phys. Chem.*, 1962, **66**, 2672–2676.
- 58 H. Muto, K. Toriyama, K. Nunome and M. Iwasaki, *Radiat. Phys. Chem.*, 1982, **19**, 201–208.
- 59 D. R. Davis and W. F. Libby, *Science*, 1964, **144**, 991–992.
- 60 D. R. Davis, W. F. Libby and W. G. Meinschein, *J. Chem. Phys.*, 1966, **45**, 4481–4492.
- 61 R. I. Kaiser, R. M. Mahfouz and K. Roessler, *Nucl. Instrum. Methods Phys. Res., Sect. B*, 1992, **65**, 468–471.
- 62 R. I. Kaiser, J. Lauterwein, P. Müller and K. Roessler, *Nucl. Instrum. Methods Phys. Res., Sect. B*, 1992, **65**, 463–467.
- 63 R. I. Kaiser, G. Eich, A. Gabrysch and K. Roessler, *Astrophys. J.*, 1997, **484**, 487–498.
- 64 C. Lecluse, F. Robert, R. I. Kaiser, K. Roessler, C. T. Pillinger and M. Javoy, *Astron. Astrophys.*, 1998, **330**, 1175–1179.
- 65 R. I. Kaiser and K. Roessler, *Astrophys. J.*, 1998, **503**, 959–975.
- 66 G. A. Baratta, G. Leto and M. E. Palumbo, *Astron. Astrophys.*, 2002, **384**, 343–349.
- 67 G. A. Baratta, M. Domingo, G. Ferini, G. Leto, M. E. Palumbo, M. A. Satorre and G. Strazzulla, *Nucl. Instrum. Methods Phys. Res., Sect. B*, 2003, **209**, 283–287.
- 68 G. A. Baratta, R. Brunetto, G. Leto, M. E. Palumbo, F. Spinella and G. Strazzulla, *J. Raman Spectrosc.*, 2008, **39**, 211–219.
- 69 G. Ferini, G. A. Baratta and M. E. Palumbo, *Astron. Astrophys.*, 2004, **414**, 757–766.
- 70 R. Brunetto, M. A. Barucci, E. Dotto and G. Strazzulla, *Astrophys. J.*, 2006, **644**, 646–650.
- 71 A. Narita, M. Honda, N. Hirao, Y. Baba and T. Yaita, *Appl. Surf. Sci.*, 2008, **255**, 883–885.
- 72 A. L. F. de Barros, V. Bordalo, E. Seperuelo Duarte, E. F. da Silveira, A. Domaracka, H. Rothard and P. Boduch, *Astron. Astrophys.*, 2011, **531**, A160.
- 73 C. F. Mejía, A. L. F. de Barros, V. Bordalo, E. F. da Silveira, P. Boduch, A. Domaracka and H. Rothard, *Mon. Not. R. Astron. Soc.*, 2013, **433**, 2368–2379.
- 74 F. A. Vasconcelos, S. Pilling, W. R. M. Rocha, H. Rothard, P. Boduch and J. J. Ding, *Phys. Chem. Chem. Phys.*, 2017, **19**, 12845–12856.
- 75 C. J. Bennett, C. S. Jamieson, Y. Osumura and R. I. Kaiser, *Astrophys. J.*, 2006, **653**, 792–811.
- 76 J. He, K. Gao, G. Vidali, C. J. Bennett and R. I. Kaiser, *Astrophys. J.*, 2010, **721**, 1656.
- 77 M. Barberio, R. Vasta, P. Barone, G. Manico and F. Xu, *World J. Condens. Matter Phys.*, 2013, **3**, 14–20.
- 78 B. M. Jones and R. I. Kaiser, *J. Phys. Chem. Lett.*, 2013, **4**, 1965–1971.
- 79 P. Ausloos, R. E. Rebbert and S. G. Lias, *J. Chem. Phys.*, 1965, **42**, 540–548.

- 80 P. Gerakines, W. Schutte and P. Ehrenfreund, *Astron. Astrophys.*, 1996, **312**, 289–305.
- 81 H. Cottin, M. H. Moore and Y. Bénilan, *Astrophys. J.*, 2003, **590**, 874.
- 82 K. I. Öberg, E. F. v. Dishoeck, H. Linnartz and S. Andersson, *Astrophys. J.*, 2010, **718**, 832.
- 83 M.-Y. Lin, J.-I. Lo, H.-C. Lu, S.-L. Chou, Y.-C. Peng, B.-M. Cheng and J. F. Ogilvie, *J. Phys. Chem. A*, 2014, **118**, 3438.
- 84 J. B. Bossa, D. M. Paardekooper, K. Isokoski and H. Linnartz, *Phys. Chem. Chem. Phys.*, 2015, **17**, 17346–17354.
- 85 D. M. Paardekooper, J. B. Bossa, K. Isokoski and H. Linnartz, *Rev. Sci. Instrum.*, 2014, **85**, 104501.
- 86 B. M. Jones, R. I. Kaiser and G. Strazzulla, *Astrophys. J.*, 2014, **781**, 85.
- 87 B. M. Jones, R. I. Kaiser and G. Strazzulla, *Astrophys. J.*, 2014, **788**, 170.
- 88 M. J. Abplanalp, M. Förstel and R. I. Kaiser, *Chem. Phys. Lett.*, 2016, **644**, 79–98.
- 89 P. A. Gerakines and R. L. Hudson, *Astrophys. J., Lett.*, 2015, **805**, L20.
- 90 P. Groner, I. Stolkin and H. H. Gunthard, *J. Phys. E: Sci. Instrum.*, 1973, **6**, 122.
- 91 R. I. Kaiser, S. Maity and B. M. Jones, *Phys. Chem. Chem. Phys.*, 2014, **16**, 3399–3424.
- 92 S. Góbi, A. Bergantini and R. I. Kaiser, *Astrophys. J.*, 2016, **832**, 164.
- 93 A. Bergantini, P. Maksyutenko and R. I. Kaiser, *Astrophys. J.*, 2017, **841**, 96.
- 94 S. Góbi, A. Bergantini and R. I. Kaiser, *Astrophys. J.*, 2017, **838**, 84.
- 95 S. Góbi, M. Förstel, P. Maksyutenko and R. I. Kaiser, *Astrophys. J.*, 2017, **835**, 241.
- 96 R. I. Kaiser and P. Maksyutenko, *J. Phys. Chem. C*, 2015, **119**, 14653–14668.
- 97 D. Drouin, A. R. Couture, D. Joly, X. Tastet, V. Aimez and R. Gauvin, *Scanning*, 2007, **29**, 92–101.
- 98 M. Á. Satorre, M. Domingo, C. Millán, R. Luna, R. Vilaplana and C. Santonja, *Planet. Space Sci.*, 2008, **56**, 1748–1752.
- 99 A. I. Prokhorov and A. P. Isakina, *Phys. Status Solidi A*, 1983, **78**, 147–155.
- 100 P. Maksyutenko, L. G. Muzangwa, B. M. Jones and R. I. Kaiser, *Phys. Chem. Chem. Phys.*, 2015, **17**, 7514–7527.
- 101 M. H. Moore, R. L. Hudson and P. A. Gerakines, *Spectrochim. Acta, Part A*, 2001, **57**, 843–858.
- 102 G. A. Cruz-Diaz, G. M. Muñoz Caro, Y. J. Chen and T. S. Yih, *Astron. Astrophys.*, 2014, **562**, A120.
- 103 A. M. Turner, M. J. Abplanalp, S. Y. Chen, Y. T. Chen, A. H. H. Chang and R. I. Kaiser, *Phys. Chem. Chem. Phys.*, 2015, **17**, 27281–27291.
- 104 M. Förstel, P. Maksyutenko, A. M. Mebel and R. I. Kaiser, *Astrophys. J., Lett.*, 2016, **818**, L30.
- 105 S. Góbi, A. Bergantini, A. M. Turner and R. I. Kaiser, *J. Phys. Chem. A*, 2017, **121**, 3879–3890.
- 106 M. J. Abplanalp, A. Borsuk, B. M. Jones and R. I. Kaiser, *Astrophys. J.*, 2015, **814**, 45–61.
- 107 M. Förstel, P. Maksyutenko, B. M. Jones, B.-J. Sun, S.-H. Chen, A. H. H. Chang and R. I. Kaiser, *ChemPhysChem*, 2015, **16**, 3139–3142.
- 108 M. Förstel, Y. A. Tsegaw, P. Maksyutenko, A. M. Mebel, W. Sander and R. I. Kaiser, *ChemPhysChem*, 2016, **17**, 2726–2735.
- 109 A. M. Turner, M. J. Abplanalp and R. I. Kaiser, *Astrophys. J.*, 2016, **819**, 97.
- 110 M. Förstel, P. Maksyutenko, B. M. Jones, B. J. Sun, A. H. H. Chang and R. I. Kaiser, *Chem. Commun.*, 2016, **52**, 741–744.
- 111 M. J. Abplanalp, S. Gozem, A. I. Krylov, C. N. Shingledecker, E. Herbst and R. I. Kaiser, *Proc. Natl. Acad. Sci. U. S. A.*, 2016, **113**, 7727–7732.
- 112 G. Tarczay, M. Förstel, S. Góbi, P. Maksyutenko and R. I. Kaiser, *ChemPhysChem*, 2017, **18**, 882–889.
- 113 M. Förstel, P. Maksyutenko, B. M. Jones, B. J. Sun, H. C. Lee, A. H. H. Chang and R. I. Kaiser, *Astrophys. J.*, 2016, **820**, 117.
- 114 S. Maity, R. I. Kaiser and B. M. Jones, *Astrophys. J.*, 2014, **789**, 36.
- 115 S. Maity, R. I. Kaiser and B. M. Jones, *Faraday Discuss.*, 2014, **168**, 485.
- 116 R. I. Kaiser, S. Maity and B. M. Jones, *Angew. Chem.*, 2014, **127**, 197–202.
- 117 S. Maity, R. I. Kaiser and B. M. Jones, *Phys. Chem. Chem. Phys.*, 2015, **17**, 3081–3114.
- 118 G. Tarczay, M. Förstel, P. Maksyutenko and R. I. Kaiser, *Inorg. Chem.*, 2016, **55**, 8776–8785.
- 119 P. Maksyutenko, M. Förstel, P. Crandall, B.-J. Sun, M.-H. Wu, A. H. H. Chang and R. I. Kaiser, *Chem. Phys. Lett.*, 2016, **658**, 20–29.
- 120 M. J. Abplanalp and R. I. Kaiser, *Astrophys. J.*, 2017, **836**, 195.
- 121 M. J. Abplanalp and R. I. Kaiser, *Astrophys. J.*, 2016, **827**, 132.
- 122 W. A. Chupka and J. Berkowitz, *J. Chem. Phys.*, 1967, **47**, 2921–2933.
- 123 NIST Standard Reference Database Number 69, <http://webbook.nist.gov/chemistry/ie-ser/>, August 21, 2017.
- 124 N. Marcelino, J. Cernicharo, M. Agúndez, E. Roueff, M. Gerin, J. Martín-Pintado, R. Mauersberger and C. Thum, *Astrophys. J.*, 2007, **665**, L127.
- 125 J. M. C. Rawlings, D. A. Williams, S. Viti and C. Cecchi-Pestellini, *Mon. Not. R. Astron. Soc.*, 2013, **436**, L59–L63.
- 126 L. Zhou, T. Dahbia, R. Evelyne, H. Eric, W. Nadine, A. C. Callie, Y. Zhibo, P. S. Theodore and M. B. Veronica, *Astrophys. J.*, 2013, **765**, 80.
- 127 E. Dartois, G. M. M. Caro, D. Deboffle, G. Montagnac and L. d'Hendecourt, *Astron. Astrophys.*, 2005, **432**, 895–908.
- 128 S. Pilling, D. P. P. Andrade, E. F. da Silveira, H. Rothard, A. Domaracka and P. Boduch, *Mon. Not. R. Astron. Soc.*, 2012, **423**, 2209–2221.
- 129 T. B. Mahajan, J. E. Elsila, D. W. Deamer and R. N. Zare, *Origins Life Evol. Biospheres*, 2002, **33**, 17–35.
- 130 D. E. Woon and J.-Y. Park, *Icarus*, 2009, **202**, 642–655.

- 131 A. Belloche, H. S. Müller, K. M. Menten, P. Schilke and C. Comito, *Astron. Astrophys.*, 2013, **559**, 1–187.
- 132 S. Muller, F. Combes, M. Guélin, M. Gérin, S. Aalto, A. Beelen, J. H. Black, S. J. Curran, J. Darling, D. V-Trung, S. García-Burillo, C. Henkel, C. Horellou, S. Martín, I. Martí-Vidal, K. M. Menten, M. T. Murphy, J. Ott, T. Wiklind and M. A. Zwaan, *Astron. Astrophys.*, 2014, **566**, A112.
- 133 C. Vastel, C. Ceccarelli, B. Lefloch and R. Bachiller, *Astrophys. J., Lett.*, 2014, **795**, L2.
- 134 F. Goulay, D. L. Osborn, C. A. Taatjes, P. Zou, G. Meloni and S. R. Leone, *Phys. Chem. Chem. Phys.*, 2007, **9**, 4291–4300.
- 135 A. B. Vakhtin, D. E. Heard, I. W. M. Smith and S. R. Leone, *Chem. Phys. Lett.*, 2001, **344**, 317–324.
- 136 F. Zhang, Y. S. Kim, R. I. Kaiser, S. P. Krishtal and A. M. Mebel, *J. Phys. Chem. A*, 2009, **113**, 11167–11173.
- 137 F. Zhang, B. Jones, P. Maksyutenko, R. I. Kaiser, C. Chin, V. V. Kislov and A. M. Mebel, *J. Am. Chem. Soc.*, 2010, **132**, 2672–2683.
- 138 D. S. N. Parker, B. B. Dangi, R. I. Kaiser, A. Jamal, M. Ryazantsev and K. Morokuma, *J. Phys. Chem. A*, 2014, **118**, 12111–12119.
- 139 B. B. Dangi, D. S. N. Parker, T. Yang, R. I. Kaiser and A. M. Mebel, *Angew. Chem., Int. Ed.*, 2014, **53**, 4608–4613.
- 140 Y. S. Kim and R. I. Kaiser, *Astrophys. J., Suppl. Ser.*, 2009, **181**, 543.
- 141 V. Vuitton, R. V. Yelle, P. Lavvas and S. J. Klippenstein, *Astrophys. J.*, 2012, **744**, 11.
- 142 D. S. N. Parker, F. Zhang, Y. S. Kim, R. I. Kaiser, A. Landera, V. V. Kislov, A. M. Mebel and A. G. G. M. Tielens, *Proc. Natl. Acad. Sci. U. S. A.*, 2012, **109**, 53–58.
- 143 D. S. N. Parker, B. B. Dangi, R. I. Kaiser, A. Jamal, M. N. Ryazantsev, K. Morokuma, A. Korte and W. Sander, *J. Phys. Chem. A*, 2014, **118**, 2709–2718.
- 144 T. Yang, L. Muzangwa, R. I. Kaiser, A. Jamal and K. Morokuma, *Phys. Chem. Chem. Phys.*, 2015, **17**, 21564–21575.
- 145 A. Coustenis, A. Salama, B. Schulz, S. Ott, E. Lellouch, T. H. Encrenaz, D. Gautier and H. Feuchtgruber, *Icarus*, 2003, **161**, 383–403.
- 146 A. Coustenis, R. K. Achterberg, B. J. Conrath, D. E. Jennings, A. Marten, D. Gautier, C. A. Nixon, F. M. Flasar, N. A. Teanby, B. Bézard, R. E. Samuelson, R. C. Carlson, E. Lellouch, G. L. Bjoraker, P. N. Romani, F. W. Taylor, P. G. J. Irwin, T. Fouchet, A. Hubert, G. S. Orton, V. G. Kunde, S. Vinatier, J. Mondellini, M. M. Abbas and R. Courtin, *Icarus*, 2007, **189**, 35–62.
- 147 B. Bézard, P. Drossart, T. Encrenaz and H. Feuchtgruber, *Icarus*, 2001, **154**, 492–500.
- 148 J. Cernicharo, A. M. Heras, A. G. G. M. Tielens, J. R. Pardo, F. Herpin, M. Guélin and L. B. F. M. Waters, *Astrophys. J., Lett.*, 2001, **546**, L123–L126.
- 149 B. M. Jones, F. Zhang, R. I. Kaiser, A. Jamal, A. M. Mebel, M. A. Cordiner and S. B. Charnley, *Proc. Natl. Acad. Sci. U. S. A.*, 2011, **108**, 452–457.
- 150 F. Zhang, X. Gu and R. I. Kaiser, *J. Chem. Phys.*, 2008, **128**, 084315.
- 151 R. I. Kaiser, L. Vereecken, J. Peeters, H. F. Bettinger, P. v. R. Schleyer and H. F. Schaefer III, *Astron. Astrophys.*, 2003, **406**, 385–391.
- 152 H. F. Bettinger, P. v. R. Schleyer, H. F. Schaefer III, P. R. Schreiner, R. I. Kaiser and Y. T. Lee, *J. Chem. Phys.*, 2000, **113**, 4250–4264.
- 153 X. Gu, Y. Guo, F. Zhang, A. M. Mebel and R. I. Kaiser, *Chem. Phys. Lett.*, 2007, **436**, 7–14.
- 154 X. Gu, Y. Guo, A. M. Mebel and R. I. Kaiser, *Chem. Phys. Lett.*, 2007, **449**, 44–52.
- 155 P. P. Bera, R. Peverati, M. Head-Gordon and T. J. Lee, *Phys. Chem. Chem. Phys.*, 2015, **17**, 1859–1869.
- 156 F. Zhang, D. Parker, S. Kim, R. I. Kaiser and A. M. Mebel, *Astrophys. J.*, 2011, **728**, 141.
- 157 G. da Silva, *J. Phys. Chem. A*, 2014, **118**, 3967–3972.
- 158 J. Thapa, M. Spencer, N. G. Akhmedov and F. Goulay, *J. Phys. Chem. Lett.*, 2015, **6**, 4997–5001.
- 159 A. Landera, R. I. Kaiser and A. M. Mebel, *J. Chem. Phys.*, 2011, **134**, 024302.
- 160 F. Zhang, X. Gu, Y. Guo and R. I. Kaiser, *J. Org. Chem.*, 2007, **72**, 7597–7604.
- 161 M. Frenklach, A. Packard and R. Feeley, in *Comprehensive Chemical Kinetics*, ed. R. W. Carr, Elsevier, Amsterdam, 2007, ch. 6, vol. 42, pp. 243–291.
- 162 M. Frenklach, H. Wang and M. J. Rabinowitz, *Prog. Energy Combust. Sci.*, 1992, **18**, 47–73.
- 163 L. Zhou, S. Maity, M. Abplanalp, A. Turner and R. I. Kaiser, *Astrophys. J.*, 2014, **790**, 38–47.
- 164 Y. S. Kim, C. J. Bennett, C. Li-Hsieh, K. O. Brien and R. I. Kaiser, *Astrophys. J.*, 2010, **711**, 744–756.
- 165 A. N. Heays, A. D. Bosman and E. F. van Dishoeck, *Astron. Astrophys.*, 2017, **602**, A105.
- 166 S. Satyapal, G. W. Johnston, R. Bersohn and I. Oref, *J. Chem. Phys.*, 1990, **93**, 6398–6402.
- 167 R. Gorden, Jr. and P. Ausloos, *J. Res. Natl. Bur. Stand., Sect. A*, 1971, **75**, 141–146.
- 168 P. J. Ausloos and S. G. Lias, *Annu. Rev. Phys. Chem.*, 1971, **22**, 85–107.
- 169 R. I. Kaiser, *Chem. Rev.*, 2002, **102**, 1309–1358.
- 170 G. R. Gladstone, W. R. Pryor and S. A. Stern, *Icarus*, 2015, **246**, 279–284.
- 171 T. E. Cravens and D. F. Strobel, *Icarus*, 2015, **246**, 303–309.
- 172 L. Zhou, W. Zheng, R. I. Kaiser, A. Landera, A. M. Mebel, M. C. Liang and Y. L. Yung, *Astrophys. J.*, 2010, **718**, 1243.
- 173 R. I. Kaiser and K. Roessler, *Astrophys. J.*, 1997, **475**, 144–154.
- 174 M. H. Moore and R. L. Hudson, *Icarus*, 1998, **135**, 518–527.
- 175 J. Crovisier, K. Leech, D. Bockelée-Morvan, T. Y. Brooke, M. S. Hanner, B. Altieri, H. U. Keller and E. Lellouch, *Science*, 1997, **275**, 1904–1907.
- 176 M. H. Moore and R. L. Hudson, *Icarus*, 2003, **161**, 486–500.
- 177 Y.-J. Wu, H.-F. Chen, S.-J. Chuang and T.-P. Huang, *Astrophys. J.*, 2013, **768**, 83.
- 178 C. Chih-Hao, C. Sian-Cong, L. Meng-Chen, H. Tzu-Ping and W. Yu-Jong, *Astrophys. J., Suppl. Ser.*, 2016, **224**, 17.

- 179 Y.-J. Wu, C. Y. R. Wu, S.-L. Chou, M.-Y. Lin, H.-C. Lu, J.-I. Lo and B.-M. Cheng, *Astrophys. J.*, 2012, **746**, 175.
- 180 W. M. Grundy, B. Schmitt and E. Quirico, *Icarus*, 2002, **155**, 486–496.
- 181 H. G. Roe and W. M. Grundy, *Icarus*, 2012, **219**, 733–736.
- 182 W. M. Grundy, PhD thesis, University of Arizona, 1995.
- 183 B. J. Holler, L. A. Young, M. W. Buie, W. M. Grundy, J. E. Lyke, E. F. Young and H. G. Roe, *Icarus*, 2017, **284**, 394–406.
- 184 V. A. Krasnopolsky and D. P. Cruikshank, *J. Geophys. Res.: Planets*, 1995, **100**, 21271–21286.
- 185 C. J. Bennett, T. Hama, Y. S. Kim, M. Kawasaki and R. I. Kaiser, *Astrophys. J.*, 2011, **727**, 27.
- 186 Y. S. Kim and R. I. Kaiser, *Astrophys. J.*, 2010, **725**, 1002–1010.
- 187 C. J. Bennett and R. I. Kaiser, *Astrophys. J.*, 2007, **660**, 1289–1295.
- 188 C. Ennis, H. Yuan, S. Sibener and R. I. Kaiser, *Phys. Chem. Chem. Phys.*, 2011, **13**, 17870–17884.
- 189 M. H. M. Herman, *Mol. Phys.*, 1998, **94**, 829–838.
- 190 Y.-J. Wu, S.-J. Chuang, S.-C. Chen and T.-P. Huang, *Astrophys. J., Suppl. Ser.*, 2014, **212**, 7.
- 191 M. Hepp and M. Herman, *J. Mol. Spectrosc.*, 1999, **197**, 56–63.
- 192 A. Snelson, *J. Phys. Chem.*, 1970, **74**, 537–544.
- 193 J. Wormhoudt and K. E. McCurdy, *Chem. Phys. Lett.*, 1989, **156**, 47–50.
- 194 J. Pacansky and M. Dupuis, *J. Am. Chem. Soc.*, 1982, **104**, 415–421.
- 195 C. Brecher and R. S. Halford, *J. Chem. Phys.*, 1961, **35**, 1109–1117.
- 196 A. Brock, N. Minacamilde and C. Manzanares, *J. Phys. Chem.*, 1994, **98**, 4800–4808.
- 197 J. Comeford and J. H. Gould, *J. Mol. Spectrosc.*, 1961, **5**, 474–481.
- 198 R. Hudson, P. Gerakines and M. Moore, *Icarus*, 2014, **243**, 148–157.
- 199 M. E. Jacox, *J. Chem. Phys.*, 1962, **36**, 140–143.
- 200 C. Chapados and A. Cabana, *Can. J. Chem.*, 1972, **50**, 3521–3533.
- 201 D. A. Dows, *J. Chem. Phys.*, 1962, **36**, 2833–2835.
- 202 E. Rytter and D. M. Gruen, *Spectrochim. Acta, Part A*, 1979, **35**, 199–207.
- 203 J. H. Schachtschneider and R. G. Snyder, *Spectrochim. Acta*, 1963, **19**, 117–168.
- 204 S. Kondo and S. Saeki, *Spectrochim. Acta, Part A*, 1973, **29**, 735–751.
- 205 P. Calvani, A. Nucara, M. C. Salvasaggio and S. Lupi, *J. Chem. Phys.*, 1994, **101**, 20–24.
- 206 T. Momose, H. Hoshina, M. Fushitani and H. Katsuki, *Vib. Spectrosc.*, 2004, **34**, 95–108.
- 207 S. Bell, B. R. Drew, G. A. Guirgis and J. R. Durig, *J. Mol. Struct.*, 2000, **553**, 199–219.
- 208 S. B. Tejada and D. F. Eggers, *Spectrochim. Acta, Part A*, 1976, **32**, 1557–1562.